

https://dspace.org/

# Properties of composite nanomaterials for gas sensor applications

**Diantantu, Aime Diakanwa**

**2023-09**
University of the Witwatersrand, Johannesburg
https://hdl.handle.net/10539/42625
Diantantu, Aime Diakanwa. (2023). Properties of composite nanomaterials for gas sensor applications. [Master's dissertation, University of the Witwatersrand, Johannesburg].

Downloaded from a DSpace repository. https://dspace.org/




# Properties of composite nanomaterials for gas sensor applications

*Submitted by*

**Aime Diakanwa Diantantu**

**(346680)**

**Supervisor: Doctor Ibrahim Usman**

Johannesburg, 2023




# Properties of composite nanomaterials for gas sensor applications

*Submitted by*

**Aime Diakanwa Diantantu**

**(346680)**

A dissertation was presented to the Faculty of Sciences at the University of the Witwatersrand in Johannesburg, South Africa, to satisfy the requirements for the Master of Science degree.

**Supervisor: Doctor Ibrahim Usman**

Johannesburg, 2023

# DECLARATION

I declare that this dissertation titled *"Properties of composite nanomaterials for gas sensor applications"* is my own unaided research work, and external effort and work as cited and acknowledged in the references. There is no degree for which this written dissertation has been submitted.

Name: **Aime Diakanwa Diantantu**

Student Number: **346680**

Signature: ……  …….

Date: 13/09/2023……..

# DEDICATION

This project is devoted to:

My late parents: Diakanwa Pierre and Mafwene Elisabeth

My late elder brother: Diakanua Yizila.

My wife, Billy Ilunga Bulanda and my son, Elie Diakanwa Mafwene

My beloved Diakanwa's and Diantantu's families, and

My supportive close friends and Church of the Living God.

# ACKNOWLEDGEMENTS

For their assistance in making this study endeavour a success, I would like to thank the following.

To my supervisor Doctor Ibrahim Usman, thank you for your patience during every phase of my research adventure, support, and direction.

To Prof Nkazi, thank you for your advice and encouragement, this aided in giving direction and impetus to the project which led to its subsequent fruition.

To the staff in the following Schools of the Faculty of Science (Schools of Chemistry, Microbiology and Physics), I salute your overwhelming and timely support by way of:

- The Microscopy and Microanalysis Unit (MMU) staff for assisting with foremost training on the operation of the Transmission Electron Microscope and the subsequent analysis of Data collecting in this work. I would like to thank, Doctor Roy Forbes of the School of Chemistry for sharing his knowledge and expertise on X-ray Diffraction pattern analysis.
- I want to express my deepest appreciation to Professor Rudolph Erasmus for assistance with Raman Spectroscopy measurements and analysis.

To the Staff of the School of Chemical and Metallurgical Engineering, University of the Witwatersrand:

- I would like to thank, Mr. Motlatsi Phali for his assistance with granting access to his laboratory to conduct a suite of measurements with Fourier Transform Infrared spectroscopy (FTIR), Thermal Gravimetric Analysis (TGA) amongst others.
- Last but not least; I would like to thank Dr. Petra Dinham for assistance with the capturing of Scanning Electron Microscope images and their analysis.

# ABSTRACT

Sensors are- important devices nowadays that have been instrumental towards the development of the Internet of Things (IoT) amongst other recent technological innovations. They are used to detect and respond to some form of input or stimulus from the environment we are living in. There are different types of sensors in the market nowadays, depending on the materials used for their manufacture and their applications, namely position sensors, pressure sensors, gas sensors, etc. Gas sensors use semiconductors as materials. Metal oxides, conducting polymers, carbon nanotubes, graphene, and transition metal chalcogenides are some semiconductors materials used in gas sensors. Metal oxides are very good gas sensors materials due to their low cost, high stability, and sensitivity but their high operating temperature disqualify them. Conducting polymers are also good sensors materials due to their flexibility and low operating temperature but they are altered by humidity. To counteract humidity problem, conducting polymers need to be modified or doped with selected elements or molecules. In this project, cellulose was drugged with carbon nanotube (CNT) to create a mechanically and chemically stable structure, which can interact and sense many gases. The chemical and physical properties of cellulose make it a potential material for the development of conductive and potential sensing stuff. This led to the focus of this investigation, which is the development of mixed cellulose nanocrystal (CNC) – CNT materials for sensor application. The CNC was synthesized through the Tempo oxidation method, and various amounts of CNT were added into the CNC below the aggregation threshold of 2.5% using ultrasonication to form a CNC – CNT rectangular sheet. The developed mixed materials were characterized using Scanning Electron Microscopes (SEM) and Transmission Electron Microscope (TEM) to determine the morphology. Fourier Transform Infrared (FTIR), Raman Spectroscopy and X-ray Diffraction (XRD) were employed to investigate the structure of the final material, while TGA has shown similar degradation temperatures of CNC and CNC – CNT.

SEM images showed an interconnected network-like structure with a porous architecture assembled by curved thin sheets, and the increase in CNT resulted in aggregate formation within the CNC. TEM micrographs confirmed the structure of CNC, which was rod-like and artefactual dendrites particles, and the presence of CNT in the matrix, while FTIR confirmed the main functional groups of the mixed matrix sheet. The degree of graphitization and presence of disordered cellulose in the mixed materials were determined by Raman spectroscopy to vary between 0.98 and 1.2.

The XRD pattern has shown that the crystallinity index of the CNC – CNT composite is correlated to the increase in the concentration of CNT. However, the TGA data has shown that the CNC – CNT materials exhibited similar thermal behaviour, this is expected, since the concentrations of the composites have similar bonding structure and configuration compared to the pristine CNC. It is also evident that the increase in CNT content reduces the thermal degradation (reduced slope) of the CNC.

The research work has developed CNC – CNT materials for sensor applications. The composite has exhibited sensor response and thereby detected $H_2$, $CO_2$, $NO_2$ and Ar gases at room temperature through the changes in their electrical conductivities. The ability of CNC-CNT to respond to these gases at room temperature opens-up the possibility for its easy use in indoor and outdoor monitoring.

# TABLE OF CONTENTS

## Table of Contents

**DECLARATION** ..... **iii**
**DEDICATION** ..... **iv**
**ACKNOWLEDGEMENTS** ..... **v**
**ABSTRACT** ..... **vi**
**TABLE OF CONTENTS** ..... **viii**
**NOMENCLATURE** ..... **xiv**

**Chapter 1: Research background** ..... **1**
1.1. Introduction ..... 1
1.2. Problem statement ..... 2
1.3. Aims and objectives ..... 2
1.4. Dissertation outline ..... 3
**Chapter 2: Literature review** ..... **4**
2.1 Introduction ..... 4
2.2 Conductive Polymers ..... 5
2.3 carbon nanotubes ..... 6
2.4 Semiconducting metal oxide for sensor applications ..... 7
2.5 Gas sensors system ..... 8
2.5.1 Basic operating principles of Gas sensors ..... 9
2.5.2 Transport ..... 13
2.5.3 Sensor performance and characteristics ..... 13
2.6 Summary ..... 13
**CHAPTER 3: Experimental procedures and analytical techniques** ..... **15**
3.1 Introduction ..... 15
3.2 Materials ..... 15
3.3 Carbon nanotubes preparation ..... 15
3.4 Cellulose nanocrystal preparation ..... 16
3.4.1 Oxidation ..... 16
3.4.2 Filtration and Washing ..... 167
3.4.3 Sonification and Centrifugation ..... 167
3.5 Carbon nanotubes doped on cellulose nanocrystal ..... 17

3.5.1 CNC/CNT Composite Formation ..... 17
3.5.2 Sheet-Forming and Drying ..... 17
3.6 Characterization techniques ..... 18
3.6.1 Scanning electron microscopy (SEM) ..... 18
3.6.2 Transmission electron microscopy (TEM) ..... 18
3.6.3 Fourier transform infra-red spectroscopy (FTIR) ..... 19
3.6.4 Raman spectroscopy analysis ..... 20
3.6.5 X-ray diffraction analysis (XRD) ..... 21
3.6.6 Resistivity ..... 22
3.7 Summary ..... 22
**CHAPTER 4: Results and Discussions ..... 25**
4.1 Characterization of cellulose nanocrystal ..... 25
4.1.1 Scanning electron microscopy (SEM) ..... 25
4.1.2 Transmission electron microscopy (TEM) ..... 27
4.1.3 Fourier transform infra-red spectroscopy (FTIR) ..... 28
4.1.4 Raman spectra ..... 30
4.1.5 X-ray diffraction patterns ..... 31
4.1.6 Thermal gravimetric analysis (TGA) and Differential thermal analysis (DTA) ..... 33
4.2 Properties of carbon nanotubes doped on cellulose nanocrystal for sensor application 36
4.2.1 Introduction ..... 36
4.2.2 Conductivity analysis ..... 37
4.2.3 Proposed structure of the sensor device ..... 40
4.3 Summary ..... 38
**CHAPTER 5: CONCLUSIONS AND RECOMMENDATIONS ..... 42**
**REFERENCES ..... 43**
**APPENDIX ..... 51**
A.1 CNC ..... 51
A.1.1 Raman ..... 51
A.1.2 FTIR ..... 55
A.1.3 XRD ..... 57
A.1.4 TEM ..... 59
A.1.5 SEM ..... 60
A.2 CNT ..... 63
A.2.1 SEM ..... 63
A.3 CNC doped with CNT in Wt% ..... 64

A.3.1 Raman .....64
A3.2 FTIR .....75
A.3.3 XRD .....78
A.3.4 TGA and DTA .....80
A.3.5 TEM .....82
A.3.6 SEM .....85

**List of Figures**

Figure 1: Synthesis routes .....5
Figure 2: CNTs structures .....6
Figure 3: Energy bands .....8
Figure 4: Sensing system .....10
Figure 5: Schematic of the Chemical Vapour Deposition Reactor.....16
Figure 6: Key components of SEM instrument .....18
Figure 7: Key components of TEM instrument .....19
Figure 8: Schematic diagram of FTIR spectroscopy .....20
Figure 9: Raman Spectrometer set-up for room temperature measurements .....21
Figure 10: XRD Bruker D2 PHASER with sample holder and interior view .....22
Figure 11: Multimeter for measuring resistivity of sample .....23
Figure 12: SEM images of TEMPO-oxidized cellulose sheet after oxidation time of (a) 6 hours (b) 24 hours (c) 72 and (d) 96 hours. .....26
Figure 13: SEM images of TEMPO-oxidized cellulose sheet mixed with (a) 0% CNT, (b) 0.5% CNT, (c) 1% CNT, (d) 1.5% CNT, (e) 2% CNT and (f) 2.5% CNT .....27
Figure 14: TEM images of TEMPO-oxidized cellulose sheet mixed with (a) 0% CNT, (b) 0.5% CNT, (c) 1% CNT, (d) 1.5% CNT, (e) 2% CNT and (f) 2.5% CNT .....28
Figure 15: FTIR images of TEMPO-oxidized cellulose sheet after oxidation time of (a) 6 hours (b) 24 hours and (c) 72 hours. .....29
Figure 16: FTIR images of TEMPO-oxidized cellulose sheet mixed with (a) 0% CNT, (b) 0.5% CNT, (c) 1% CNT, (d) 1.5% CNT, (e) 2% CNT and (f) 2.5% CNT .....30
Figure 17: Raman spectra of CNC with CNT 0%, 0.5%, 1%, 1.5%, 2% and 2.5%.....31
Figure 18: XRD spectra of CNC with CNT 0%, 0.5%, 1%, 1.5%, 2% and 2.5%.....33
Figure 19: TGA and DSC of CNT sample.....34
Figure 20: TGA and DSC of CNC sample .....34
Figure 21: TGA of CNT, CNC-CNT 0, 0.5, 1, 1.5, 2 and 2.5% samples.....35
Figure 22: DTA of CNT, CNC, CNC-CNT 0.5, 1, 1.5, 2 and 2.5% samples.....35
Figure 23: Conductivity behaviour with CNT content of the sensor.....38
Figure 24: Gas sensing range.....38
Figure 25: Sensing stability with time .....39
Figure 26: Sensing Capacity .....39

Figure 27: proposed sensing device (a) of the structure of the template system, and (b) front view of the sensing device .....41

## List of Tables

Table 1: Classification of solid-state gas sensors ..... 11
Table 2: Advantages of semiconducting sensors ..... 12
Table 3: Comparative study of advantages and drawbacks of sensors based upon transduction principle. ..... 12
Table 4: $I_D/I_G$ ratio of CNC – CNT samples ..... 31
Table 5: The crystallinity index of the synthesized CNC compared to some published investigation ..... 32

# NOMENCLATURE

| | |
|---|---|
| Ar: | Argon gas |
| C – C: | Carbon – Carbon bond |
| C – H: | Carbon – Hydrogen bond |
| C – O: | Carbon – Oxygen bond or Carbon monoxide |
| C – O – C: | Carbon – Oxygen – Carbon bond or Carbon dioxide |
| CNC: | Cellulose nanocrystal |
| CNC – CNT: | Cellulose nanocrystal doped with Carbon nanotube |
| CNC – 0% CNT: | Cellulose nanocrystal doped with 0% of Carbon nanotube. |
| CNC – 0.5% CNT: | Cellulose nanocrystal doped with 0.5% of Carbon nanotube. |
| CNC – 1% CNT: | Cellulose nanocrystal doped with 1% of Carbon nanotube. |
| CNC – 1.5% CNT: | Cellulose nanocrystal doped with 1.5% of Carbon nanotube. |
| CNC – 2% CNT: | Cellulose nanocrystal doped with 2% of Carbon nanotube. |
| CNC – 2.5% CNT: | Cellulose nanocrystal doped with 2.5% of Carbon nanotube. |
| CNT: | Carbon nanotube |
| $CO_2$: | Carbon dioxide gas |
| CVD: | Chemical vapour deposition |
| D: | First peak at Raman band |
| DNA: | Deoxyribonucleic acid |
| DSC | Differential scanning calorimetry |
| DTA | Differential thermal analysis |
| FTIR: | Fourier Transform Infrared |
| G: | Second peak at Raman band |
| G*: | Third peak at Raman band |

| | |
|---|---|
| GO | Graphene oxide |
| $H_2$: | Hydrogen gas |
| HCl: | Hydrochloric acid |
| IR: | Infrared |
| $I_D$: | Intensity at band D Raman |
| $I_G$: | Intensity at band G Raman |
| MMU: | Microscopy and Microanalysis unit |
| MWCNT: | Multi walled Carbon nanotube |
| MWNT: | Multi walled nanotube |
| $N_2$ : | Nitrogen gas |
| NaBr: | Sodium bromide |
| NaOCl: | Sodium hypochlorite |
| NaOH: | Sodium hydroxide |
| OH: | Hydroxide |
| O – H: | Oxygen – Hydrogen bond or Hydroxyl |
| pH: | Potential of hydrogen or power of hydrogen |
| SEM: | Scanning electron microscopy |
| SWNT: | Single walled nanotube |
| SWCNT: | Single walled carbon nanotube |
| TCNF: | Thin carbon nanofibers |
| TEM: | Transmission electron microscopy |
| TEMPO: | Chemical compound |
| TGA: | Thermal gravimetric analysis |
| TO-NFC: | Tempo nanofibrillated cellulose |
| Wt. %: | Weight percentage |

| | |
|---|---|
| XRD: | X-ray Diffraction |

# Chapter 1: Research background

## 1.1. Introduction

Because of its biocompatibility and hydrophobicity, cellulose is a natural component that draws interest from researchers for the creation of innovative materials. When compared to the mother cellulose, the cellulose that has been doped with elements or molecules exhibits different and useful physicochemical and mechanical properties (Costa et al., 2021; Tudoroiu et al., 2021). Inorganic nanoparticles such as oxides of metals and graphene, carbon nanotubes, graphene and conducting polymers can be added to cellulose to enhance their functionality. The metal oxide nanomaterial-based sensors suffer from high operating temperatures, low sensitivity and high fabrication costs. These properties enhance their limited feasibility in sensor application particularly in the low and moderate temperature regimes. On the other hand, Cellulose type gas sensors can operate at room temperature with a dynamic sensing range between -10 to 80 °C (Johnson, B. and Kaushal, T., 2004).

Graphene oxide (GO) is a material-based gas sensor which can be used alone or blended with other materials for good performance. The operating temperature range is between 25 and 250 $^{o}$C which is higher than that of a cellulose-based sensor (Malik et al., 2020). Conducting polymers are also used as sensor materials. Their application as sensors is limited by their complexity in fabrication. Additionally, they are unstable due to their susceptibility to irreversible oxidation and ultraviolet related degradation (Nikolic et al., 2020).

Over the past few decades, intense research interest has been stimulated by the development in the design and enhancement of gas sensors. This has been driven in part by the evolution of nanomaterials with diverse and tuneable functional properties as well as the advancements in nanotechnology-based fabrication methods or devices. Nano-scale materials embedded in the sensing material have been reported d by numerous groups and in copious amounts of literature (Malik et al, 2020). To detect different concentrations of $NO_2$, a single wall carbon nanotube (SWCNT) based sensor, prepared by blending hydroxypropyl-cellulose and SWCNT was used by Karthigeyan et al. (2008). The low operating temperature made this sensor better than metal oxide nanomaterial-based sensors.

The degree of electrical conductivity, ON–OFF ratio of electro-optical switching behaviour and electrochemical redox properties are highly dependent on the morphological structures of cellulosic materials (Lapka et al., 2021; Li et al., 2021; Zhao et al., 2021). The stimuli-response relation makes the cellulosic materials viable sensor for various applications; therefore, to enhance its sensor capacity, (Guo and Zhang, 2021; Olvera and Monaghan, 2021; Palencia et al., 2021; Xu et al., 2021). Researchers demonstrate the gas sensing potential of cellulose materials embedded with nanoparticles such as tin dioxide, copper oxide and zinc oxide, which can assist for the development of innovative cellulose-based gas sensors (Hittini et al., 2020; Ivanova et al., 2020; Rahman et al., 2021; Yang et al., 2020; Zhou et al., 2020).

## 1.2. Problem statement

The use of cellulose-based materials as sensors is essential for reducing the negative effects of excessive hazardous gas consumption on the environment and human health (Li et al., 2021; Mahapatra et al., 2021; Phasuksom et al., 2021; Rivadeneyra et al., 2021; Ummartyotin and Manuspiya, 2015). In some instances, these gases though toxic in small concentrations are likely to be undetected by oxide-based sensors. Therefore, undetected gases pose huge concerns not only to the environment but also in their propensity to lead to serious illnesses or health hazards. Therefore, developing a simple and cheaper gas sensor system can aid in monitoring gases at low concentrations and standard conditions, in this project, we surmise that the application of a cellulose nanocrystal-carbon nanotube composite provides a cost friendly pathway towards the development of a sensor with the following functionalities or performance benchmarks:

- low operating temperature,
- good selectivity to a wide variety or range of gases,
- good sensitivity to low gas concentration and
- Lastly, easier to fabricate and deploy relative to the above derivatives of nanomaterials discussed in section 1.1.

## 1.3. Aims and objectives

The purpose of this study was to create a gas sensor system and test its sensitivity to various gases. This was achieved through the following objectives:

- To Synthesize CNC – CNT mixed nanomaterials and assess their morphology, chemical and physical structures, thermal behaviour and crystallinity status;
- To investigate the effect of CNTs concentrations (0, 0.5, 1.0, 1.5, 2.0 and 2.5 %) on the sensing behaviours of the mixed nanomaterials.
- To investigate the effect of gases (argon, nitrogen, carbon dioxide and hydrogen) on the sensing behaviours of the mixed nanomaterials;
- To investigate the effect of exposure time (5, 10, 15, 20, 25, 30 and 35 seconds) on the sensing capacity of the mixed nanomaterials;
- To propose a sensor device structure based on the sensing behaviour of the mixed nanomaterials.

## 1.4. Dissertation Outline

Background information on the research topics, problem statement, and hypotheses are provided in the introduction chapter. In order to place the upcoming research within the pre-existing theoretical paradigms and underline areas where more research is necessary, Chapter 2 summarizes pertinent literature and covers the investigations done up to date in relation with the focus of this investigation. In chapter 3, the research methodology is explained and justified. The data collection techniques covered the synthesis methods, characterization, and the tests used to evaluate the developed sensor with a focus on the population parameters and scope of the study. The results and discussion of the characterization of CNC and CNT materials and the sensor behaviours are reported in Chapter 4, along with the descriptive statistics and statistical analysis's conclusions, which is then followed by a summary in Chapter 5 that incorporates the research's observations, discussions, and any possible suggestions for additional research.

# Chapter 2: Literature review

## 2.1 Introduction

Nanocellulose has attracted a lot of study interest due to its variety of uses in the domains of material science, biomedical engineering, and sensing applications (Khalid et al., 2021; Subhedar et al., 2021; Varshney et al., 2021; Wu et al., 2021). These applications are due to its renewable nature, anisotropic shape, exceptional mechanical behaviour, excellent biocompatibility, tailorable surface chemistry, and good optical properties (Fareez et al., 2021; Guan et al., 2021; Lv et al., 2021; Motaung, 2021; Nivethithaa and Baskar, 2021). These materials' adaptability is determined by the cellulose's chemistry and nature, which can coexist with both hydrophilic and hydrophobic species. Additionally, it can be altered to covalently include the proper chemicals and host active optical nanoparticles (Ross et al., 2010).

The electrical, mechanical, and thermal characteristics of carbon nanotubes (CNT) are distinctive. Numerous researchers have looked at various reactions for covalently grafting CNTs to polymer due to the potential improvement of electrical properties of polymer via the homogenous distribution of CNTs. The use of CNT-polymer composites as functional materials for organic transistor devices, gas sensors, biosensors, and chemical vapour sensors has increased recently. CNT-polymer composites provide many characteristics for quantitative, selective, and sensitive analyte molecule detection in sensor applications. The CNTs in the composites function as a conducting network and as self-detection molecules by giving and taking electrons (Yun & Kim, 2010). SWCNT has been used in cellulose in order to improve the sensitivity to humidity, gas and vapours within a wide range (Han et al., 2012). The reason being in this project MWCNT was employed on cellulose paper for sensing several gasses such as $CO_2$, $N_2$, Ar, CO and $H_2$.

The interaction of the target gas with the sensor materials determines the gas sensing selectivity, which is defined as a surface-controlled process in which the reactive sites' sizes, porosity, surface states, and oxygen content in the cellulose all affect the sensing mechanism. (Rahman et al., 2021; Cao et al., 2021). Cao et al. (2021) investigation showed a fast response time for gas sensors with an average time of 20 seconds, which met the requirement of the sensor response time.

## 2.2 Conductive Polymers

Polymers are poor electron conductive materials (Wang et al., 2019). To enhance their electrical conductivity, suitable choice of dopants and their concentrations are required. The mobility of the charged flaws in the conjugated framework serves as their conduction mechanism (Padvi et al., 2021). Additionally, phonon-activated electron transport and multiple trap and release mechanisms can assist in enhancing the mobility of the charge carriers in these polymers. Conductive polymers are generally not thermoplastics but can have high electrical conductivity with different mechanical properties compared to other commercial polymers (John and Thomas, 2003).

Cellulose-based electro-conductive composites can be prepared by adding electroactive materials to the cellulose material due to the hydrophilic compatibility of both materials. The addition of inorganic nanoparticles through doping, blending or coating allows the formation of an architectural structure within the cellulose matrix. The co-network structure formed can be tested for its electrical conductivity (Durfresne and Vignon, 2000; Wu et al., 2016). Figure 1 shows the distinct routes of synthesis of the cellulose-based conductive composite.

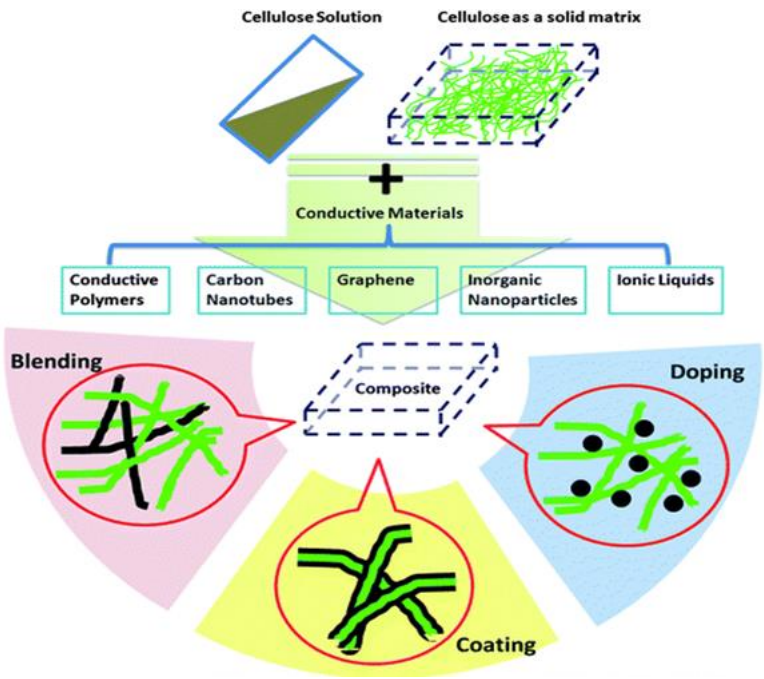



*Figure 1: Synthesis routes* ***(Durfresne and Vignon, 2000)***

Polymer-doped nanoparticles exhibit superior qualities over alternative gas sensors at room temperature operation, provide good mechanical properties and with cost-effective and simple route of preparation. Therefore, the improvement of their long-term stability, selectivity and reversibility can make them commercially competitive (Padvi et al., 2021). Other possibilities are to coat or blend the nanomaterial (which is not what we did).

## 2.3 Carbon nanotubes

Carbon nanotubes (CNTs) are nanomaterials that can be fabricated with tuneable–electrical conductivity of its lattice structure. The way the graphene sheet is rolled to create the tube determines whether it will be metallic (armchair) or a semiconductor (zigzag), which will affect its electrical properties (Padvi, 2021; Pei et al., 2010). Carbon nanotubes come in a variety of varieties, mostly classified as single-walled (SWNT) or multi-walled nanotubes (MWNT), as seen in Figure 2. While MWNTs are made up of numerous concentric rolled out graphene layers, SWNTs are formed of a single layer of graphene sheet that has been flawlessly rolled into a cylindrical tube (Siro and Placket, 2010).

Due to their high surface-to-volume ratio, highly electrically conductive CNTs may one day serve as a very affordable alternative to metal wires, which are frequently utilized in gas sensing applications. Carbon nanotubes are promising gas sensing materials, due to their specific surface area and unique electrical properties with low noise (Yun & Kim, 2010; Padvi, 2021). Based on the gas's interaction with the sensing element and its adsorption and desorption, the CNTs have a low response and recovery rate, though.

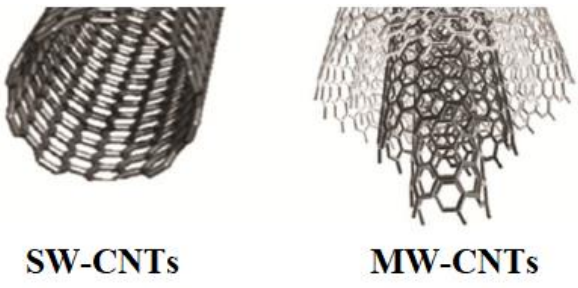



*Figure 2: CNTs structures (Siro and Placket, 2010)*

## 2.4 Semiconducting metal oxides for sensor applications

Semiconducting nanoparticles based on metallic oxides show unique excellent qualities of optical, electrical, thermal and catalytic properties. For that reason, semiconductors have attracted significant interest in the fabrication of various electrochemical sensors. There are chemo-resistance sensors, in which the sensing element is a semiconducting material sandwiched between two metallic electrodes. They exhibit excellent electron and phonon confinement sensitivity, higher response-recovery time and strong adsorption ability due to their chemical composition as made from transition or post-transition metals with oxygen (Bassey, 2014). Bassey (2014) found that ballistic transport, coulomb blockade effects and energy band model characterize their electronic behaviours. The electronic band structure is represented by the dispersion of the electron energy with its momentum. Therefore, based on quantum mechanical principles we can identify regions for which the electrons occupancy is permitted in the ground and excited states and regions for which the electrons or holes are restricted. These three band zones describe the energy states (valence band, conduction and band gap) as prescribed by the Pauli-Exclusion Principle, atomic coordination and lastly on the respective electronic structure of the atoms that participate in the bonding process. The illustration of these energy bands is seen in Figure 3.

The valence band represents the highest region of electron energy, while the conduction band presents a region of energy sufficient to liberate the electron. The band gap zone is the area of energy that is in between the valence band and the conduction band.

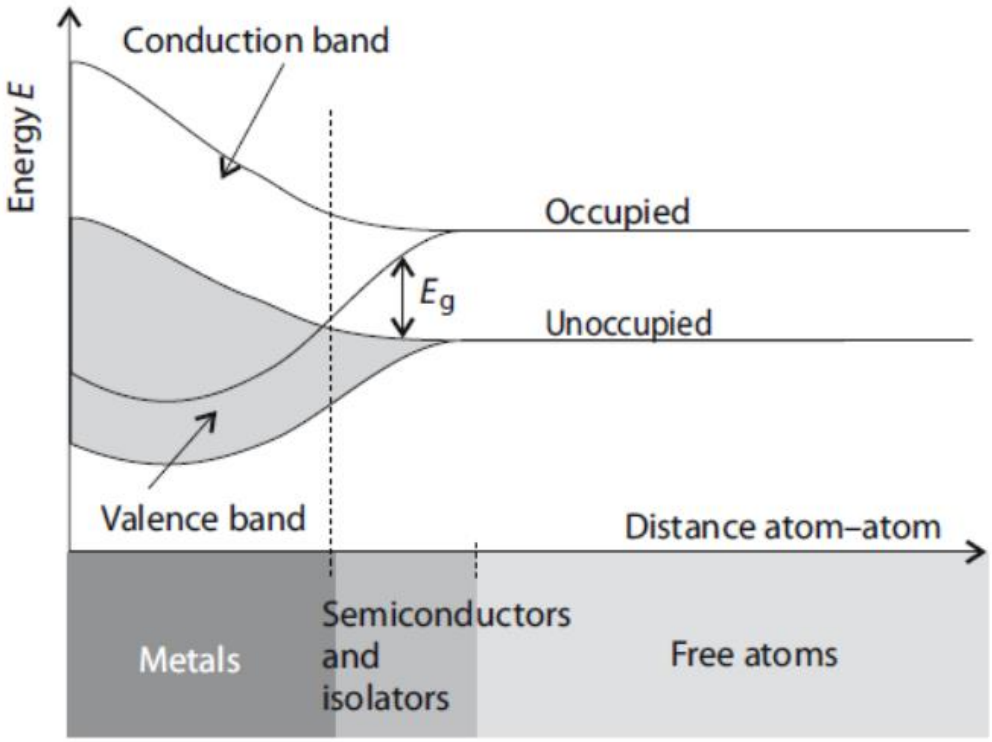



*Figure 3: Energy bands (Bassey, 2014).*

Padvi et al. (2021) found that metal sulphides are better gas sensors when compared to their counterparts' metal oxides. Based on the presence of sulphur, alternative sensors should be investigated. The presence of gas on the sensing element influenced the material's conductivity, which enable gas detection. Currently, metal oxides are the most used in gas sensing process (Padvi et al., 2021)

## 2.5 Gas sensors system

Gas detections play a vital role in the healthy living through the identification of harmful or toxic gases. Therefore, providing an affordable sensor for chemical practices can alleviate toxic effects in our daily life (Padvi et al., 2021).

Gases can be classified into four types:

- flammable gases such as hydrogen, methane ...,
- toxic (carbon monoxide, carbon dioxide, hydrogen sulphide …),
- asphyxiant (low oxygen concentration makes the environment unsuitable for respiration.

- Inert gases such as Argon, Helium etc.

Excess exposure to nitrogen leads to deficiency of oxygen and this may lead to harmful effects such as suffocation. Hence it is imperative that the type of gas and its concentration as well as its dynamical changes need to be monitored over time.

The sensing properties of the nanomaterials depend on the gas system. This is a critical factor that affects the effectiveness of gas detection. In environmental monitoring, industrial pollution, medical testing, defence, and military operations, the use and development of gas sensors are at highly essential (Yang et al. 2021). When a gas molecule must be in close proximity to the active layer for a gas sensor system to function, the detection method may involve a chemical reaction or physical adsorption of the gaseous molecules on the surface, which causes changes in the electrical responses. Other times, the presence of gas will have an impact on the optical nanostructure resonance with the dielectric characteristics of the gas sensors. (Liu et al. 2011). The sensing mechanism in semiconductors relies on perturbations of surface conductivity induced by the interaction between target gases and the surface of the semiconductor. A gas sensor's performance is determined by a number of factors, including sensor responsiveness, sensitivity, selectivity, stability, response, and recovery time. When the dangerous concentration of the target gas is reached, the wearable sensors should be able to operate accurately at room temperature with excellent sensing performance (with improved sensitivity, detection limit, and response time), and deliver the anticipated response to the users in real-time (Tanguy et al. 2022). Data can be retrieved nearby the sensor to identify damage (Reshmy et al. 2020).

### 2.5.1 Basic operating principles of gas sensors

Chemical sensors such as gas sensors work by oxidizing or reducing the gas species at the electrode of the sensing device. The sensing element's surface-level interactions with the gas molecules change its physical characteristics. Sensing capacity, or the capability to offer an observation of a feature of the physical world in the form of measurement data, is determined by the level of interaction or electrochemical detection... For most of the solid-state gas sensors, the major used property is the change in the electrical conductivity that can be transduced in work function or alternative energy by the gas – solid interaction (Padvi et al., 2021; Bassey,

2014). The measurands depend on the working mechanism of the sensor, which can be conductometric, photo-acoustic, thermal conductivity and cantilever for the electrochemical, optical, calorimetric and mass-sensitive based sensors, respectively (Padvi et al., 202; Bassey, 2014; Korotcenkov, 2011). Beside the working mechanism, the reliability of the sensor depends on its accuracy, stability, and time and frequency responses (Padvi et al., 2021).

The sensor operates in sequences of events as described in Figure 4. The receptor interacts with the gas molecules, and the generated change in physico-chemical information is translated into chemical energy measured by the transducer as electrical quantity. It is anticipated that semiconductor materials would have a porous crystal structure to aid in the adsorption of gas molecules. This makes it easier for gases to diffuse and receive across it. (Padvi et al., 2021).

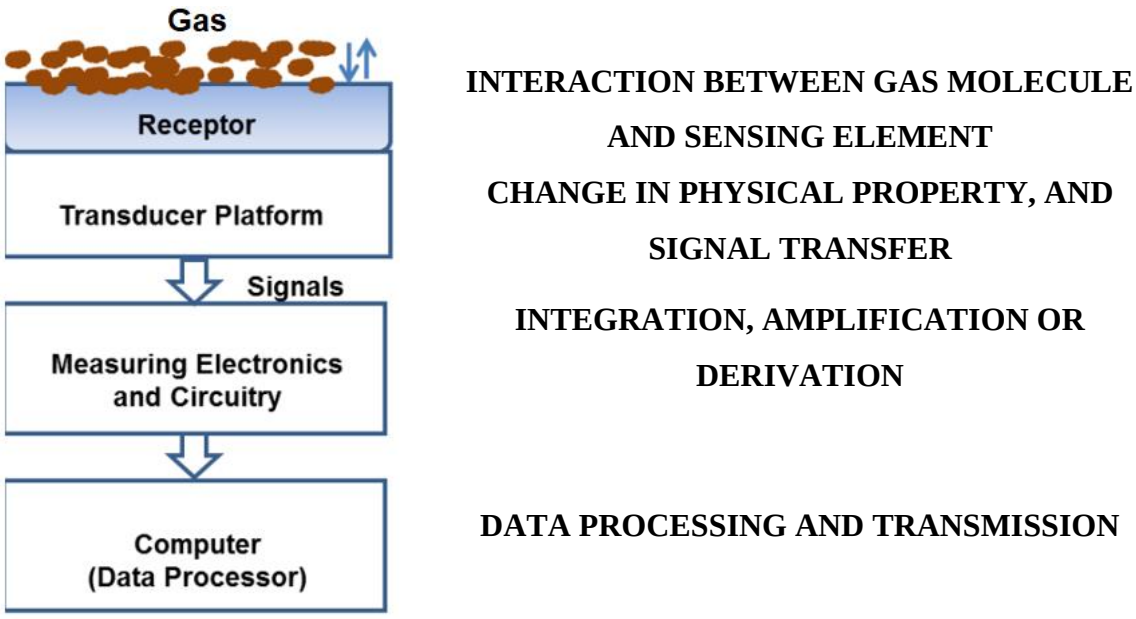



*Figure 4: Sensing system (Padvi et al., 2021; Bassey, 2014)*

Solid-state gas sensing material in general can be organic or inorganic in which the sensing element is deposited as thin or thick films on a non-conducting support. Because of its inexpensive cost, wide range of gas detection, and straightforward construction, chemo-resistor sensors are frequently employed for the detection of combustible and dangerous gases. Materials for solid-state gas sensors can be categorized in Table 1.

*Table 1: Classification of solid-state gas sensors (Padvi et al., 2021)*

| | **Types of sensing process** | **Working Principle** |
|---|---|---|
| Solid State Sensors | Chemiresistive | Change in material resistance should be noticed when the gas interacts with semiconducting material |
| | Chemical field effect transistor | The change of the target analyte concentration due to the presence of gas corresponds to a change in the current through the transistor |
| | Calorimetric | Temperature differences should be noticed when the oxidation process takes place. The temperature change depends on the concentration of gas. |
| | Potentiometric | The gas concentration affects the potential differential between the working electrode and the reference electrode. |
| | Amperometry | The diffusion current of an ionic conductor depends on the gas concentration. |

The advantages and drawbacks of solid-state gas sensing materials are enumerated, in Table 2

*Table 2: Advantages of semiconducting sensors (Padvi et al., 2021)*

| **Advantages** | **Drawbacks** |
|---|---|
| Inexpensive to manufacture | Non-targeted gas may be adsorbed and false the detection. |
| simplicity and scalability | The simplicity depends on the relationship between response and gas concentration |
| Designed for low or high gas concentration | Individual gas calibration may lead to increasing sensor cost |
| | Can be unstable and inaccurate at high relative humidity and varying temperature. |

Different gas detection techniques are used such as optical, electrochemical and thermal. Their advantages and transduction principles are given in Table 3.

*Table 3: Comparative study of advantages and drawbacks of sensors based upon transduction principle (Padvi et al., 2021).*

| Sensor Type | Advantage | Drawback | Transduction principle |
|---|---|---|---|
| Optical | The absence of oxygen eases the workability of the sensor. Not disturbed by the presence of electromagnetic interference. Monitoring and control area are very wide. | Affected by light interference. | Absorption, photoluminescence, fluorescence, refractive index and light scattering |
| Electrochemical | Low concentrations of toxic gases are relatively detected. Wide range of gases can be identified. | Failures modes are not notice except if advanced monitoring technique is used. | Voltometric and potentiometric |
| Catalytic | Simple to use and measures the flammability of gases | Easily poisoned by lead, chlorine and silicones | Conductivity |

| | | | |
|---|---|---|---|
| Infra-red | No observable failure modes. Used in inert atmospheres and/or physical techniques only | Monitoring is slow and more user expertise required | |
| Thermal | Simple to construct. Simple to operate without oxygen. | Reacts due to the heating wire. | Thermometric |

### 2.5.2 Transport

The chemical and physical structures of the sensor material and the electron transport should be well understood for a well-designed gas sensor. The electronic transport in a sensing system depends on the shapes and the amount of microstructural (pores and interfacial boundaries). These should be well designed for better management of the potential barrier between the air (pore) and semiconductor interface. Bassey (2014) found also that the transport is challenged by the trapping-detrapping effect caused by the change in energy and the morphological disorder. Therefore, the transport mechanism should account for surface diffusion, pore-boundary diffusion and bulk-diffusion.

### 2.5.3 Sensor performance and characteristics

The sensor signal can be measured in the form of conductance, which depends on the gas amount around the sensing element. The stability of the sensor signal at equilibrium is required. The response efficiency or sensing capacity is measured by the ratio of the change in conductivity over the initial conductivity in the air environment. Changes in a material's optical and dielectric properties are additional characteristics that can be used to depict the sensing process. This can be determined by measuring the capacitance of the dielectric after the analyte gas has been absorbed. By monitoring these changes one can be able to establish the response, sensitivity and selectivity of the sensor material upon exposure to diverse gases and for a variety of concentrations. A well-designed sensor should have higher sensitivity for change in capacitance on contact with a very small amount of the gas. If the same material of sensor is used, it should provide a change in conductivity for different gases (it should be selective), be reproducible, cost effective, low power consumer, have low response and recovery time, and display negligible error (Padvi et al., 2021).

## 2.6 Summary of Chapter 2

The electronic behaviour of the CNTs in a composite material to donate or accept electrons places it as a potential sensor material. Therefore, characterisation for quantitative, selective, and sensitive analyte molecule detection are required prior to the development of sensor device for commercialisation. Previous investigations discussed in Chapter 2 showed that SWCNT and MWCNT improve the sensitivity capacity and response time to humidity, gas and vapours. The way the sensing substance and the sensor interact is a key aspect in determining how well a detection works. The wearable sensors should be capable to operate accurately at various working or living environmental conditions with high sensing performance.

# CHAPTER 3: EXPERIMENTAL PROCEDURES AND ANALYTICAL TECHNIQUES

## 3.1 Introduction

This chapter presents the methodology used in fabrication of the CNC composite and the process of doping with CNTs at various concentrations. The process of developing CNC was through TEMPO oxidation route, and thereafter dopants of d CNT with concentrations in the range (X ,….Z %) was carried out to form the CNC composite.. The control of material properties necessitates the pre-screening through characterization for structural, morphological, thermal and chemical properties. In this respect,

The synthesized materials were characterized by several techniques; these are Raman spectroscopy, scanning electron microscope (SEM), transmission electron microscope (TEM), X-ray diffraction (XRD), Fourier transform infrared spectroscopy (FTIR), Thermogravimetric analysis (TGA) and derivative thermogravimetry (DTA). Lastly, we present the method used to determine the sensing capacity of the doped and pristine CNS. The sensing capacity was measured from the changes in the electrical conductivity of the sample before and after exposure to the analyte gas.

## 3.2 Materials

Micro-cellulose paper developed in 2018 provided by SAPPI was used as a cellulose source, distilled water, 2,2,6,6-Tetramethylpiperidine-1-oxy (TEMPO), NaBr, NaOCl solution (13-15%), NaOH pellets, HCl (32%), methanol and MWCNTs (at 95% purity).

## 3.3 Carbon nanotubes preparation

Figure 3: shows a vertically oriented chemical vapour deposition (CVD) reactor used to create CNT. The CNT was created at 800$^{o}$C using ferrocene as both a catalyst and a carbon source (Le et al., 2021). A small amount of the catalyst, ferrocene, was placed inside the vaporiser, and the setup was connected and sealed with vacuum grease. A schematic of the CVD system is shown in Figure 5. Nitrogen was pumped through the system to flush out contaminants and determine any vacuum leaks. The system was then passed through with argon and acetylene

acting as carrier gases, and the ferrocene was vaporised and carried to the reactor where the CNT was formed. The cyclone solid carbon product of CNT was collected and characterized for morphology using a scanning electron microscope (SEM) and transmission electron microscope (TEM).

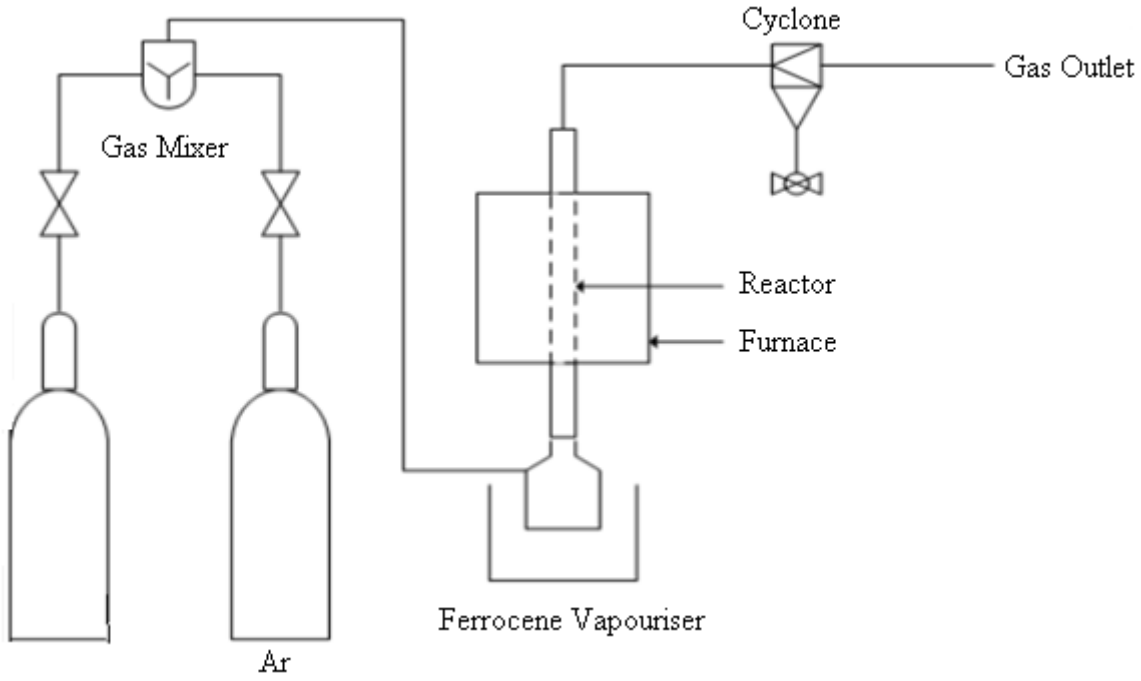



*Figure 5: Schematic of the Chemical Vapour Deposition Reactor*

## 3.4 Cellulose nanocrystal preparation

### 3.4.1 Oxidation

A mass of 2 g of micro-cellulose paper was shredded and dissolved in 400 ml of distilled water (i.e. at a consistency of 0.5% w/w) and left to stand overnight. A mass of 33 mg of TEMPO and 330 mg of NaBr were dissolved in the solution using a magnetic stirrer at 700 rpm. The oxidation was initiated with the addition of 20 mL of NaOCl. The pH of the solution was maintained between 10-11 by using the required amount of NaOH or HCl. The oxidation was

allowed to run for a certain period and then terminated using 10 mL of methanol. The solution was then neutralized (by lowering pH to 7) using 0.1 mol HCl.

### 3.4.2 Filtration and Washing

After oxidation, the solution was filtered using a normal filtration system and a vacuum pump. The dispersion was washed with a total volume of 1.2 L of distilled water to remove TEMPO and any remaining salt.

### 3.4.3 Sonication and Centrifugation

The CNC was redissolved in distilled water and sonicated for 20 minutes (using Heilscher ultrasound technology, UP200s) at one cycle and an amplitude percentage of 50. In an ice bath, sonication was performed. Centrifuged at 10,000 rpm for 10 minutes, the resultant solution. To avoid any fungal assaults, the recovered CNC gel was then chilled.

## 3.5 Carbon nanotubes doped on cellulose nanocrystal

### 3.5.1 CNC/CNT Composite Formation

A mass of 50 mg CNC gel was prepared under an oxidation condition for 96 hours and dissolved in distilled water. MWCNTs were added to the solution at a weight ratio ranging from 0.2% to 1% in increments of 0.2%. The mixture was then sonicated for 30 minutes using the same equipment and conditions as in the previous sub-section. The process was followed by centrifugation at 10 000 rpm to recover the CNC/CNT gel which was also refrigerated at minus 5 $^{o}$C for similar reasons.

### 3.5.2 Sheet-Forming and Drying

CNC (without CNTs) was dried at an ambient temperature of 22$^{o}$C. The CNC/CNT mixture was dried in an oven at 22 $^{o}$C, 40 $^{o}$C, 60 $^{o}$C, and 80 $^{o}$C for 24 hours. A glass surface was used for casting the films/sheets.

The formed sheets were then analyzed using SEM to determine the surface morphology, additionally, FTIR was used to study the degree of oxidation and, subsequent determination of the electrical resistance of the resultant cellulose or composite sheets cast on glass.

## 3.6 Characterization techniques

### 3.6.1 Scanning electron microscope (SEM)

The surface morphology was recorded with Scanning Electron Microscope (Model: S-4300, Japan). The incident electron beam traverses through a series of lenses, and it can interact on the specimen surface through reflection, for which the reflected electron beam is collected by detectors. The intensity of the transferred electron signal is encoded in a colour scheme to represent the strength of the detected signal. The conditions for SEM sample characteristics are that it must be conductive to minimise space charge which is associated with charging, and it may lead to image artefacts that provide incorrect analytical interpretation and poor image quality/resolution. Samples were mounted on metal stubs in a coater unit and placed at higher energy electrons between 2 to 1000 keV. The schematic diagram of key components of SEM used in this work is shown in Figure 6.

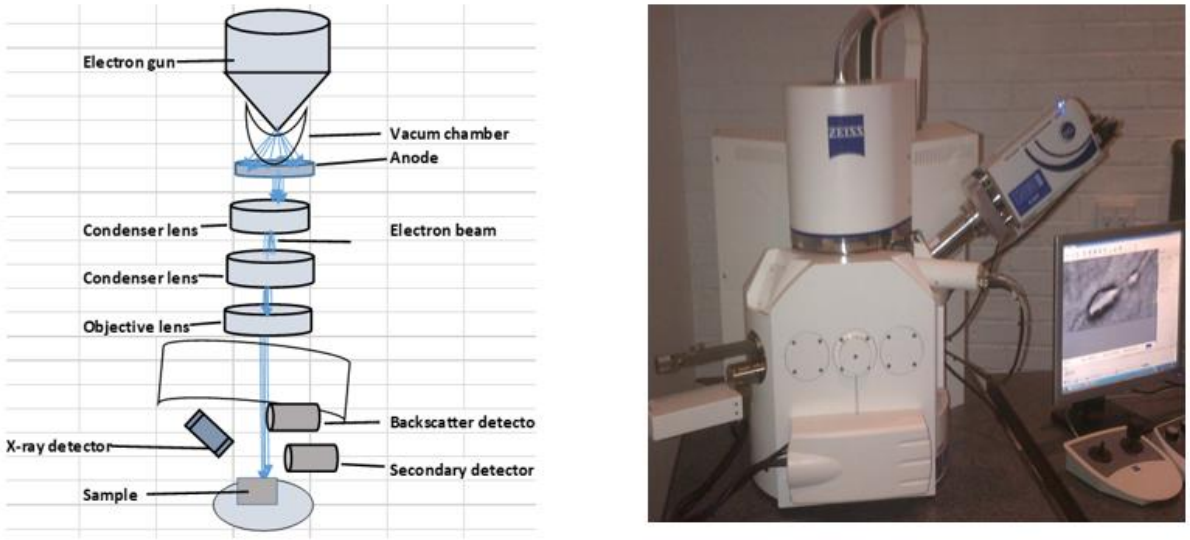



*Figure 6: Key components of SEM instrument* ***(Skoog et al., 2014)***

### 3.6.2 Transmission electron microscope (TEM)

TEM works on the same fundamental laws that govern the operation of light microscopes except that it achieves more magnification than what light microscopes achieve because the light is restricted by its wavelength whereas TEM uses electrons. The wavelength of light is approximately 600 nm and the wavelength of an electron is 6 pm. The shorter wavelength gives higher resolution or magnification. The probe used by a TEM instrument originates from the

electrons (Microscopemaster.com, 2015). TEM analysis was used to visualize the change in the morphology of the nano cellulose fibre sample. In this study, TEM measurements were done on a Jeol model 1200EX instrument operating at 80 kV. Electrons are easily deflected and accelerated using an external field and potential, respectively. The electrons are transmitted or scattered through the material. The non-uniform distribution of electrons contained the detailed structure of the sample. The TEM consists of the following critical components that lead to the formation of an image (Figure 7):

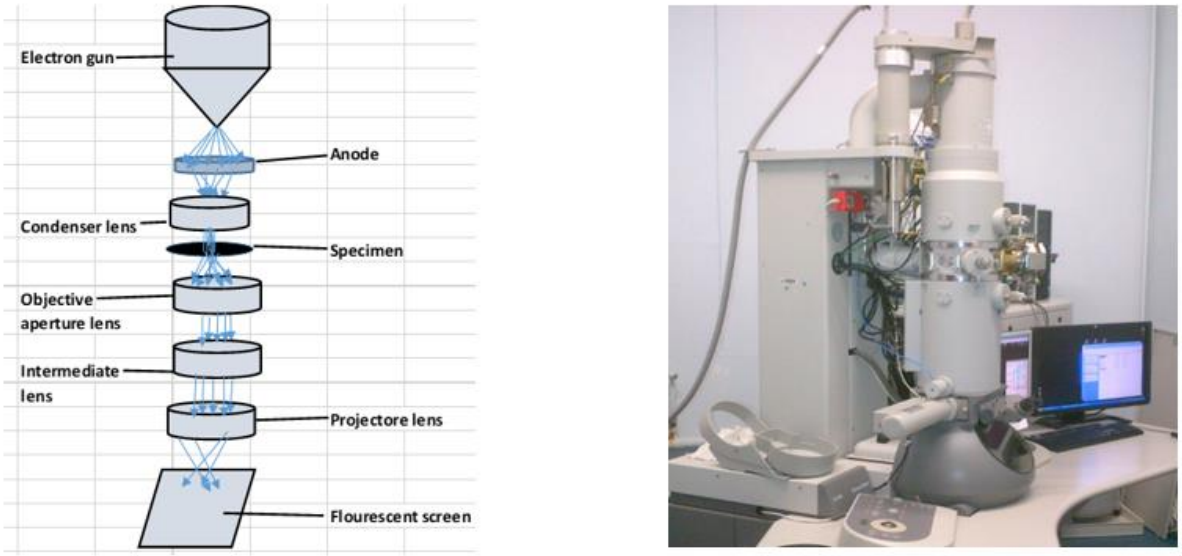



*Figure 7: Key components of TEM instrument* ***(Skoog et al., 2014)***

## 3.6.3 Fourier transform infrared spectroscopy (FTIR)

In this technique, the infrared beam after leaving the interferometer passes through an optically dense crystal with a higher reflective index. After its interaction with the sample, the infrared spectrum is obtained. The total reaction time of the cellulose with oxidizing agents was six hours. The concentrations (concentrations) of the oxidizing sodium hypochlorite (NaOCl) and the catalyst sodium bromide (NaBr) were also doubled and halved. The FTIR spectra of all cellulose nanofibres obtained were determined and analyzed. The energy absorbed by the organic groups and subsequent vibrations, stretching, rotation, and bending of functional groups was recorded at specific wavenumbers against absorbance. The scans were performed in the vicinity of 650 and 4000 $cm^{-1}$ at a degree of 4 $cm^{-1}$. A schematic diagram of an FTIR instrument is shown in Figure 8.

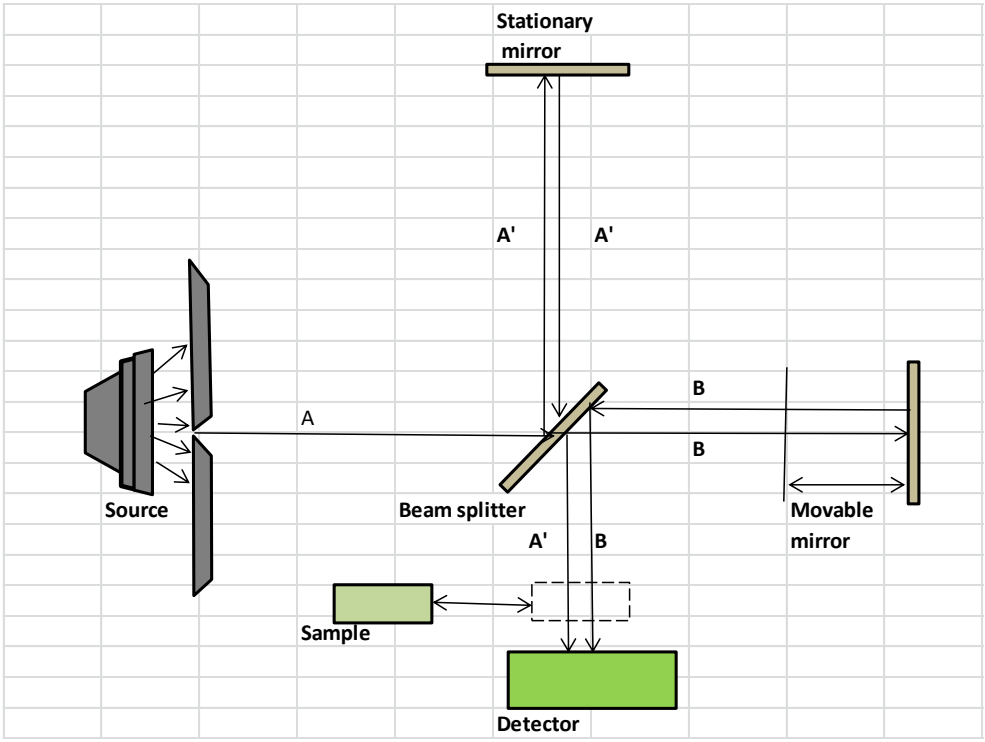



*Figure 8: Schematic diagram of FTIR spectroscopy* ***(Skoog et al., 2014)***

## 3.6.4 Raman spectroscopy

Raman spectroscopic analysis assists in assessing the degree of graphitization and the structural properties of materials. This project used the Jobin-Yvon T6400 micro-Raman spectrometer (Figure 9), which is equipped with an $Ar^+$ ion laser excitation operating at an excitation wavelength of 514.5 nm.

Liquid nitrogen was used to cool the charge-coupled device (CCD) detector before any acquisition of the Raman spectra with the spectrometer. The standard silicon sample was used to calibrate the energy axis at 521 ± 0.5 $cm^{-1}$. At room temperature, all measurements were completed.

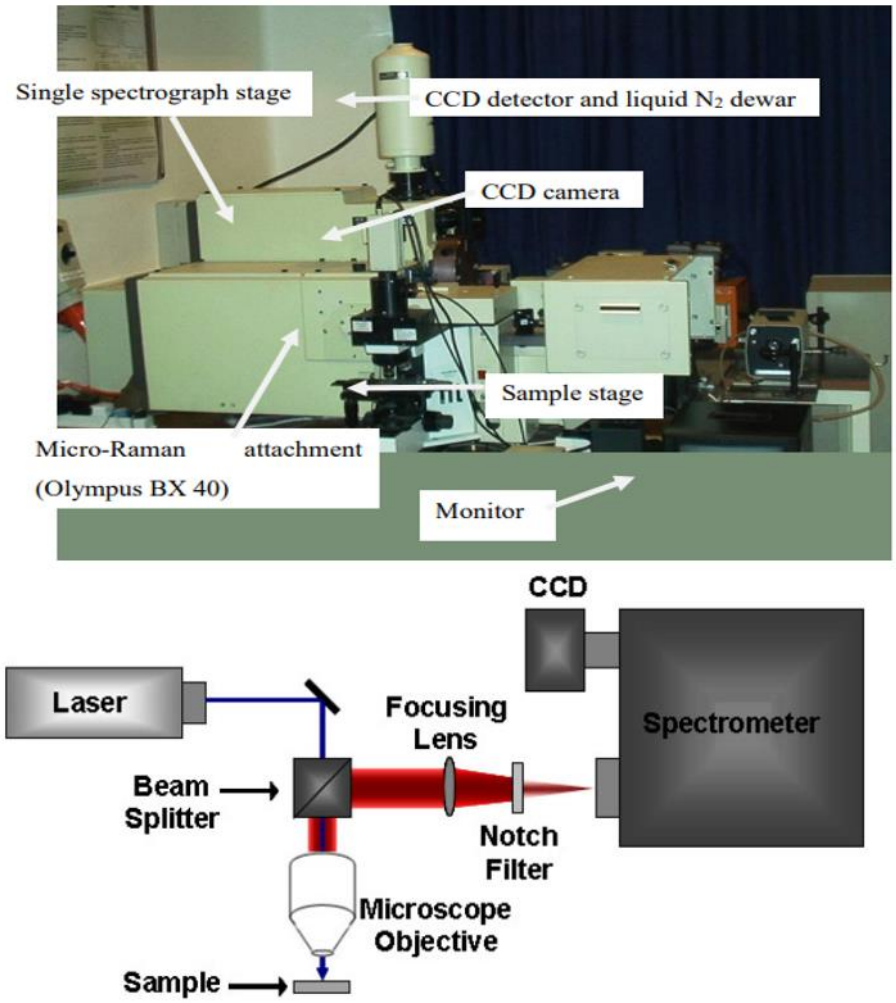



*Figure 9: Raman Spectrometer set-up for room temperature measurements* ***(Usman, 2018).***

### 3.6.5 X-ray diffraction (XRD)

Figure 10 shows an X-ray diffractometer (XRD) setup, Bruker 2 PHASER with Co-Kα (1.789Å) located in the School of Chemistry. Powder X-ray diffraction is a non-destructive characterization technique, to investigate the structural information, the structural strain, and the microstructure of materials. XRD analysis of the nano crystalline cellulose has shown two diffraction peaks associated with the degree corresponding to the following Miller indices (200) and (110). At a diffraction angle of about 19.1°, 20.0°and 20.9°, the amorphous portion's intensity was assessed as being the lowest 2θ = 18.0°, and the highest intensity bands located near 2θ = 26.0° (Ghaemi et al., 2018)

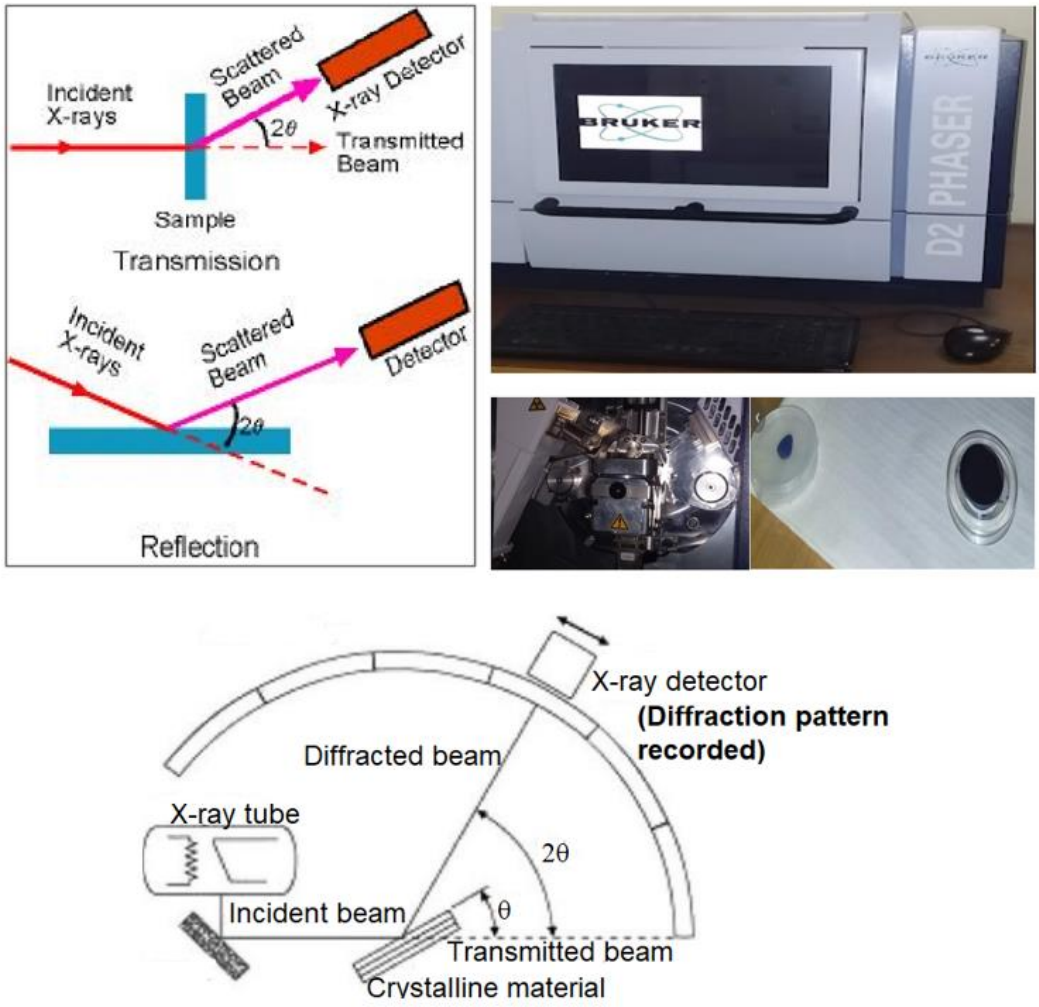



*Figure 10: XRD Bruker D2 PHASER with sample holder and interior view* ***(Wits CHEM XRD Lab).***

### 3.6.6 Resistivity

All the samples that were used for electrical conductivity measurement were completely dried overnight in the oven at 50 ºC under the temperature-ambient. The multimeter (Figure 11) outputted the electrical resistance values for a 2- probe configuration. The same measurement procedure was carried out for all samples and their readings were recorded for the same geometrical configuration. As a result, the resistance R and conductance G of a uniform cross-sectional conductor can be calculated as follows:

$$R = \rho \frac{\ell}{A} \qquad (3.1)$$

$$G = \sigma \frac{A}{\ell} \qquad (3.2)$$

where $\ell$ is the sensor's length in metres (m), A is the cross-sectional area of the conductor in square meters ($m^2$), σ (sigma) is the electrical conductivity expressed in Siemens per meter

($S \cdot m^{-1}$), and ρ (rho) is the material's electrical resistivity (also known as specific electrical resistance) measured in ohmmeter (Ω·m). Resistance and conductivity are inversely proportional ($\rho = 1/\sigma$). Four measurements were made for each sample and the average was taken.



*Figure 11: Multimeter for measuring resistivity of the sample*

**Characterization of the sensor active layer**

To determine the sensing system's abilities, the CNC-CNTs system was placed in the gaseous environment while the conductivity was measured. The conductivity was measured after every 5 seconds. The sensor capacity was calculated from the expression of equation (3.3).

$$S\ (\%) = \frac{\sigma_I - \sigma_F}{\sigma_I} \times 100 \qquad (3.3)$$

Where $\sigma_I$ *and* $\sigma_F$ are initial and final conductivities.

## 3.7 Summary of chapter 3

In this chapter, we have presented the principles of the suite of analytical techniques for the characterization of the cellulose samples in their pristine and composite format. A combination of spectroscopic techniques has been used to examine the structural and morphological characteristics of the candidate materials. Lastly, the suitability of the developed materials for sensing applications has been examined by monitoring the changes in their electrical properties in the presence and absence of the gaseous compounds. The sensing mechanisms of the developed nanomaterials can be thoroughly understood by the correlation of the morphology,

the chemical and physical properties, which have been adequately measured from the experimental setups used in this project.

# CHAPTER 4: RESULTS AND DISCUSSION

Chapter 4 presents a discussion on the results of CNC – CNTs obtained from the SEM, TEM, FTIR, Raman, TGA and DTA studies. These characterization techniques have provided information on the surface morphology, the chemical bonding and IR active functional groups embedded in the nanomaterials. Additionally, the structural properties and the thermal stability of the resulting CNC-CNT composites have been evaluated from the Raman and X-ray diffraction as well as the TGA and DTA methods. The developed samples were tested using Ar, $CO_2$, $H_2$ and N gases to assess their sensing capacities, and possible correlations between the physical and chemical properties with the sensing behaviours or response.

## 4.1 Characterization of cellulose nanocrystal

### 4.1.1 Scanning electron microscopy (SEM)

The nanocomposite sheets' surface morphology was examined using SEM. Variations in oxidation time caused changes in the surface morphology of the produced sheets. (Pandi et al., 2021). Oxidation is necessary to increase the number of active sites. As oxidation time was increased, individualized cellulose fibers were easily identifiable on the surface of the sheets. In addition, pores started forming on the surface of the sheets after 48 hours of oxidation, the quantity and size of pores increased as oxidation time was increased from 48, 72 to 96 hours. The increase in pore size and number also had a part in increasing the transparency of the sheets. The pore formation is understood to be an indication of the presence of surface absorbed oxygen ions. The cellulose fibers would have the same surface charge and would reject one another electrostatically if carboxylate linkages weren't present on their surface (Mohammed et al. 2022; Moser, 2019). Therefore, an increase in carboxylate content would thus lead to an increase in the pore size and pore density as seen in Figure 12. The maximum oxidation time of 96 hours resulted in the most individualization of fibers.

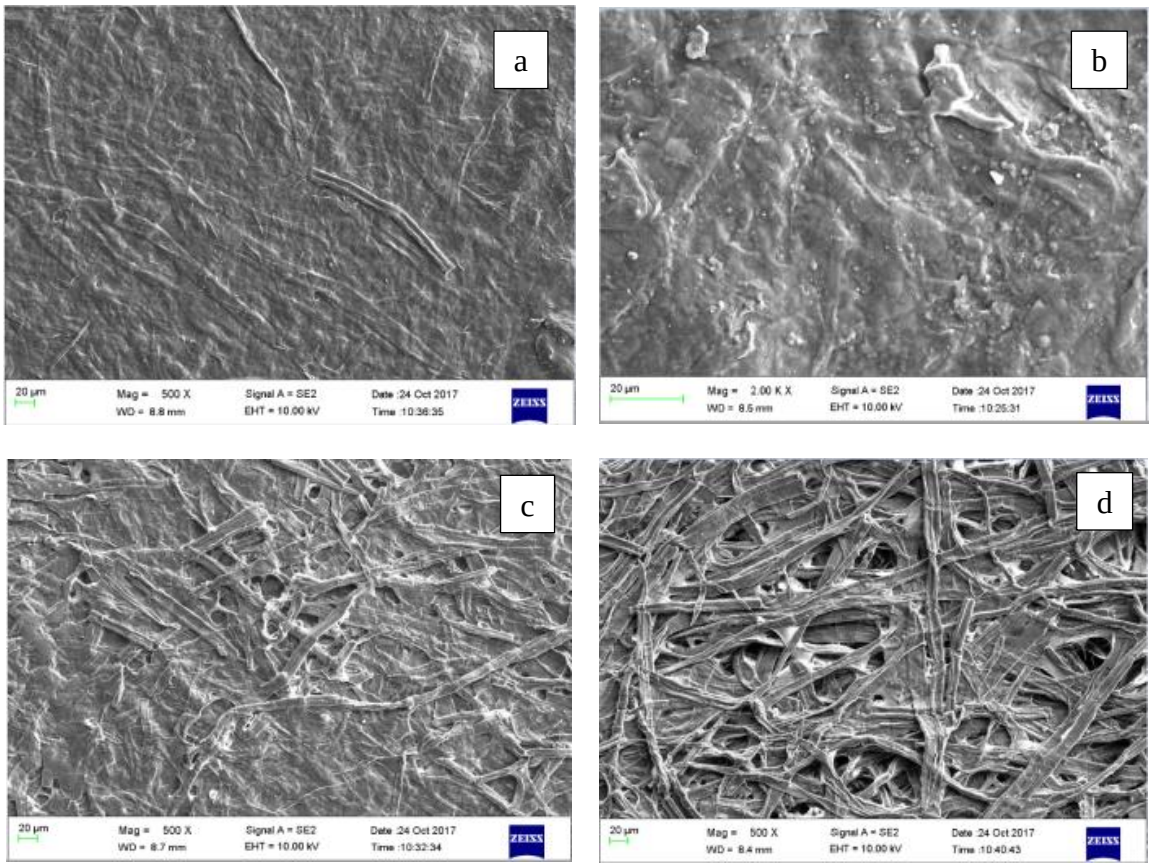



*Figure 12: SEM images of TEMPO-oxidized cellulose sheet after oxidation time of (a) 6 hours (b) 24 hours (c) 72 and (d) 96 hours.*

Figure 13 displays the SEM images of cellulose nanocomposite consisting of (a) 0% CNT, (b) 0.5% CNT, (c) 1% CNT, (d) 1.5% CNT, (e) 2% CNT and (f) 2.5% CNT, the cellulose used in the fabrication of the composite sheet was oxidized for 96 hours. The same amount of cellulose was used in the formation of the composite. The SEM images of Figure 13 show a network of homogenous interconnected tubular structure, which form a porous architecture of thin curved sheets. These images agree with those observed in the investigation of Nepomuceno et al. (2021) and Liu et al. (2015). The images showed that increasing the CNT content from 0.5 to 2.5% resulted in an aggregation of CNT (as seen in Figure 11 (f)). This effect may be due to the interaction of CNT particles (London dispersion forces) (Pandi et al., 2021) with each other at specific sites on the oxidized cellulose surface. Higher concentrations of CNT could not be forced through the CNC pore through the blending process' usage of ultrasonic energy.

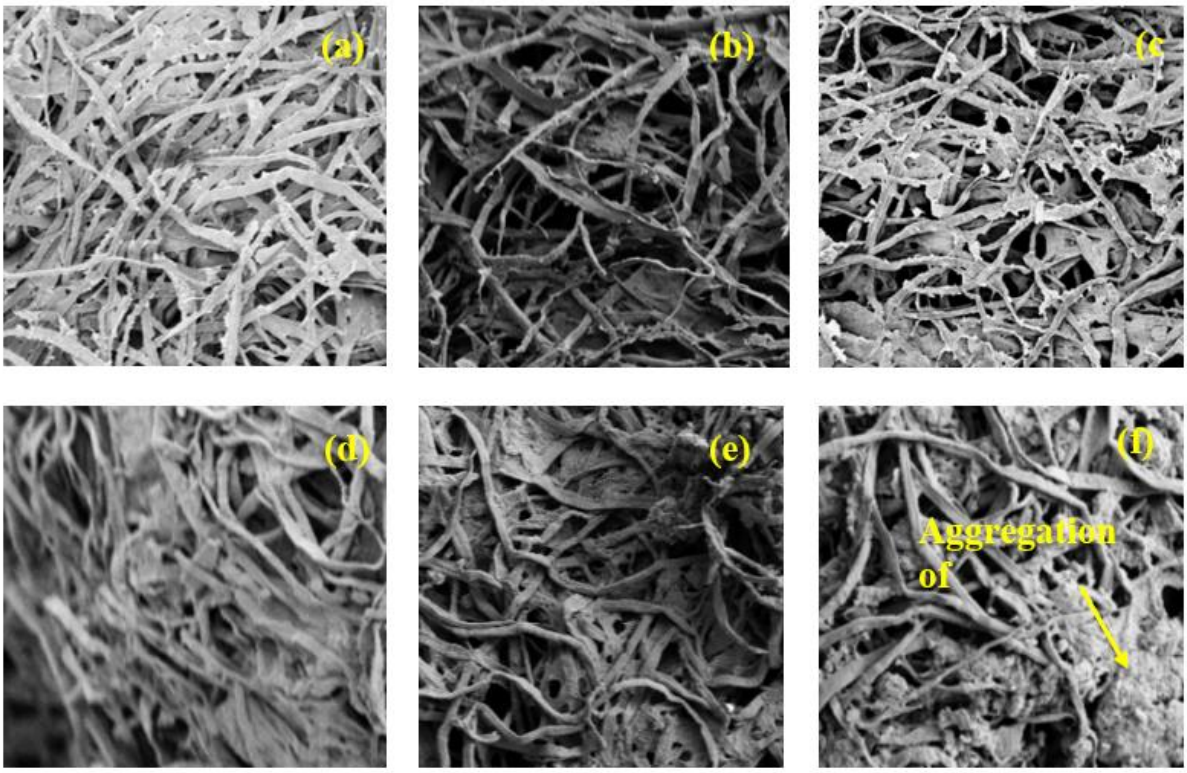



*Figure 13: SEM images of TEMPO-oxidized cellulose sheet mixed with (a) 0% CNT, (b) 0.5% CNT, (c) 1% CNT, (d) 1.5% CNT, (e) 2% CNT and (f) 2.5% CNT*

### 4.1.2 Transmission electron microscopy (TEM)

Kaushik et al. (2015) claimed that the cellulose source and the way of preparation affect the CNC's morphology. TEM micrographs of the CNC - CNT samples are shown in Figure 14. It is seen that the tubular length and width vary between 20 – 70 nm and 5 – 10 nm, respectively. The presence and increase in the concentrations of CNT evident in Figures 14 (b) to (f). The observed shape of CNC is rod-like, and the images shows the presence of artifactual dendritic particles. This is consistent with the outcomes mentioned by Corletto et al. (2022).

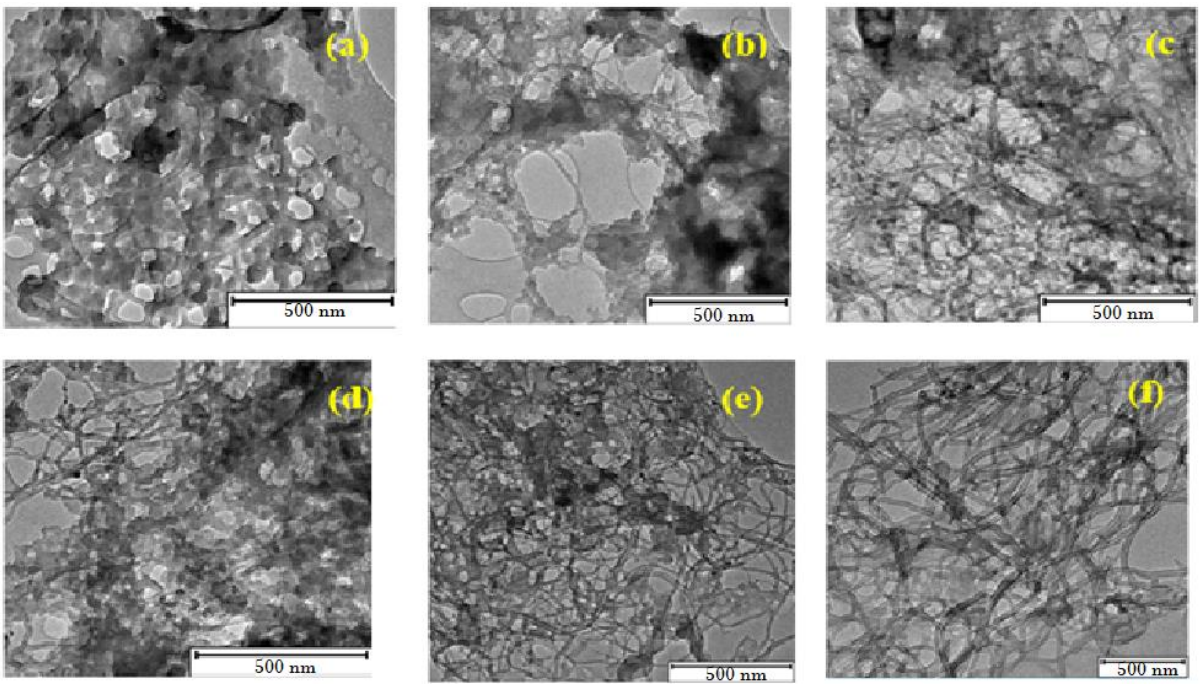



*Figure 14: TEM images of TEMPO-oxidized cellulose sheet mixed with (a) 0% CNT, (b) 0.5% CNT, (c) 1% CNT, (d) 1.5% CNT, (e) 2% CNT and (f) 2.5% CNT*

### 4.1.3 Fourier transform infrared spectroscopy (FTIR)

Fourier Transform Infrared (FTIR) analysis was used to determine the degree of oxidation on each sample determined from the ratio of the relative intensity of the target functional groups. During TEMPO-mediated oxidation, the C6 hydroxyl group is selectively converted to a carboxylate functional group. FTIR analysis indicates the functional groups or bonds corresponding to the infra-red active molecules in the sample. The functional group of interest, in this case, is the OH (hydroxyl) bond; the signature of this chemical bond is the absorption dips at wave numbers between 3200 and 3600 $cm^{-1}$. In the IR spectra of cellulose and CNC - CNT samples, the presence of this functional group can be identified by a dip in the percentage transmittance in the above-mentioned region. Figure 15 (a) shows the IR spectra of the untreated micro-cellulose paper. The percentage transmittance of the OH bond in untreated micro-cellulose paper is 94.56 % (FTIR instrument error was 0.5 $cm^{-1}$ (Wits CHMT FTIR Lab)) which correspond to the instrument error obtained by Smith et al. (2011), Esonye et al. (2019) and Schanofski et al. (2023). After an oxidation time of 48 hours, the percentage transmittance increases to 94.64% as can be seen in Figure 15 (b). An increase in oxidation time to 72 hours results in the percentage transmittance increasing to 97.84%, see Figure 15

(c). The increase in percentage transmittance indicates that the quantity of OH bonds in the cellulose molecule decreases as the oxidation time is increased; hus the degree of oxidation increases with an increase in oxidation time.

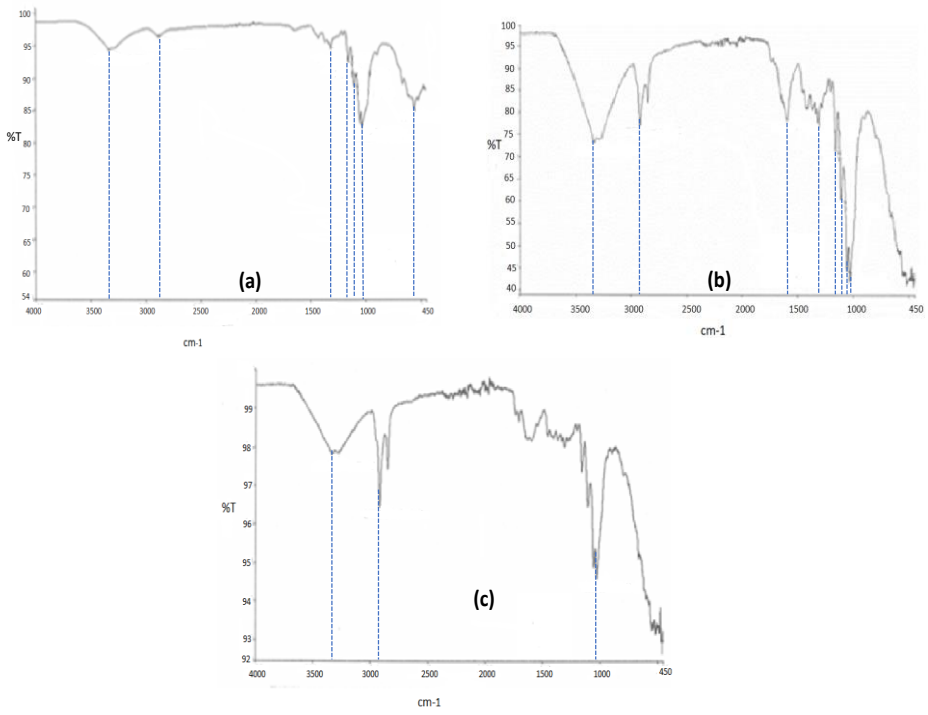



*Figure 15: FTIR images of TEMPO-oxidized cellulose sheet after oxidation time of (a) 6 hours (b) 24 hours and (c) 72 hours*

Figure 15 compares the FTIR spectra of CNC and the CNC-CNTs. The absorption peaks at 3325, 2892, 2140, 1952, 1301, 1036 and 539 $cm^{-1}$ were attributed to the O-H stretching of hydrogen bonds, the C-H stretching vibration, the C-O of the aromatic ring, the C-O-C pyranose ring skeleton, and the C-O-C stretching, respectively. This FTIR spectrum matches the spectra pattern of cellulose materials synthesized by Pandi et al. (2021) and Verma et al. (2021).

Figure 16 showed an FTIR peak at 3325 $cm^{-1}$ in all CNC–CNT materials, which confirmed the O-H stretching vibration of intra and intermolecular hydrogen bond interaction within the CNC. Low intense peaks were observed at 2892 and 2140 $cm^{-1}$ in all the spectra, which correspond to the symmetrical stretching vibration of the C-H group and ester linkage of the carboxylic group, respectively that is in line with the work of Gupta et al. (2021). The peak of the O-H bending of the absorbed water was observed at 1952 $cm^{-1}$. A low intense peak characteristic of lignin was observed at 1301 $cm^{-1}$, which showed that lignin was not significant

in the CNC. The vibration of ether groups (C–O–C) and the rocking vibration of C–H bonds were observed at 1036 and 539 $cm^{-1}$. The FTIR patterns confirmed the structure of CNC, which was not modified by the addition of CNT. Gupta et al. (2021) also observed similar patterns.

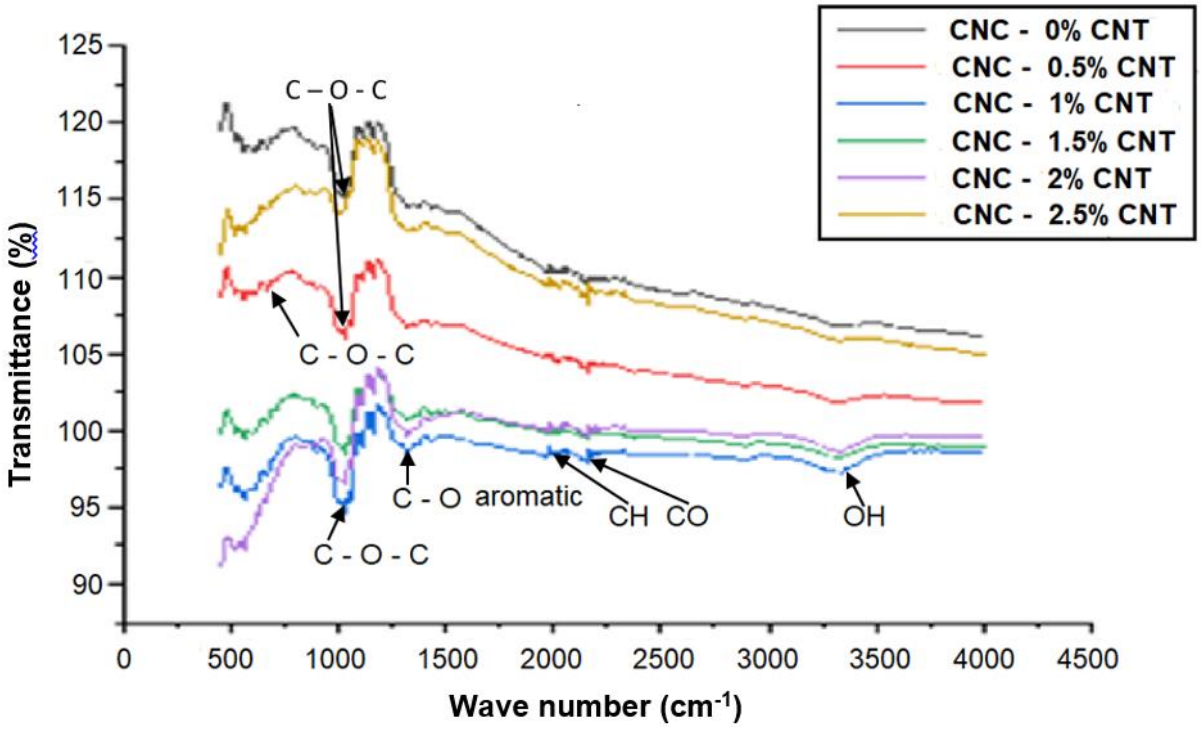



*Figure 16: FTIR images of TEMPO-oxidized cellulose sheet mixed with (a) 0% CNT, (b) 0.5% CNT, (c) 1% CNT, (d) 1.5% CNT, (e) 2% CNT and (f) 2.5% CNT*

### 4.1.4 Raman spectra

The Raman spectra of CNC-CNT materials displayed mainly three characteristic bands in the region of 1100 – 1800 $cm^{-1}$ of that two are for the CNT carbon (D and G). The disordered carbon and graphite characteristics in the synthesized materials were represented by the Raman bands at 1351 cm1 and 1583 cm1, respectively, demonstrating the degree of graphitization by the ratio of carbon D to G intensities (ID/IG). The D peak is elevated in the mixed materials due to the presence of disordered cellulose. Table 4 displays the ID/IG ratio. The Raman spectrum for the CNC - CNT (Figure 17) with major peaks at 1583 and 1351 $cm^{-1}$, which is a characteristic of the CNT G-band and D-band, respectively showed similar behaviour as per the investigation of Corletto et al. (2022). The presence of CNTs in the mixed materials was confirmed through Raman, which presents the signal of the scanned materials over the peak of interest. The CNTs Raman spectral peak at 1583 $cm^{-1}$ is due to the C−C $sp^2$ graphene's bond stretching vibrational mode. Therefore, the G-band peak confirmed the presence of CNTs.

*Table 4: ID/IG ratio of CNC – CNT samples*

| % CNT | D band ($cm^{-1}$) | G band ($cm^{-1}$) | $I_D/I_G$ ratio |
|---|---|---|---|
| 0 | 447 | 492 | 0.908 |
| 0.5 | 786 | 661 | 1.189 |
| 1 | 925 | 826 | 1.120 |
| 1.5 | 855 | 678 | 1.261 |
| 2 | 897 | 785 | 1.142 |
| 2.5 | 673 | 557 | 1.208 |

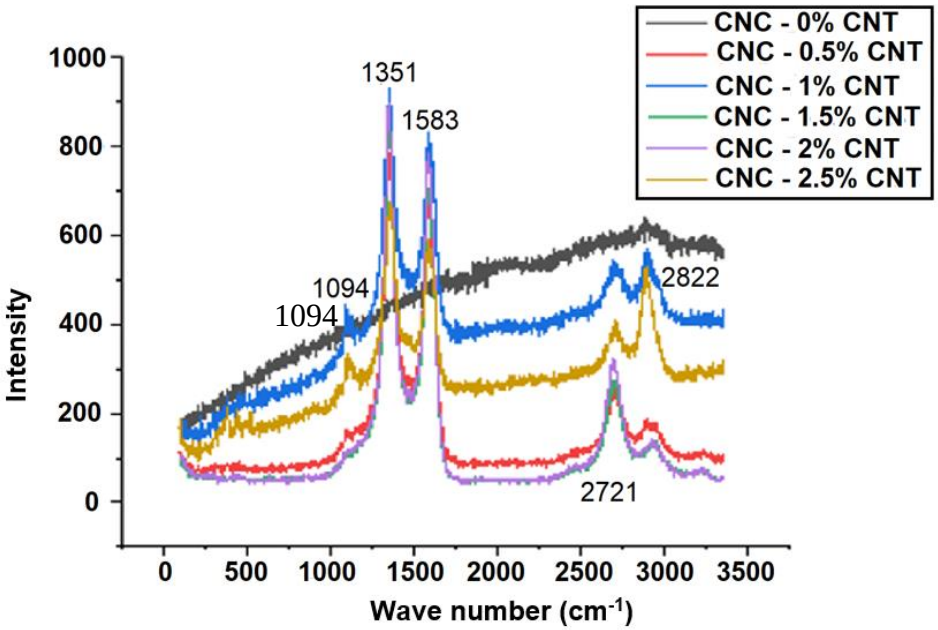



*Figure 17: Raman spectra of CNC with CNT 0%, 0.5%, 1%, 1.5%, 2% and 2.5%*

### 4.1.5 X-ray diffraction patterns

The XRD pattern of samples presented in Figure 18 (with A = 2 - theta) showed mainly three peaks at 18.2º, 26.6º and 40.5º. These patterns are consistent with the results for cellulose measured by Yan et al. (2013), Kim et al. (2006), Li and Sheng (2009). The increase in CNT does not affect the structural phases of the CNC as evident from the XRD patterns of Figure 18. This implies that the addition of CNT does not really modify the bonding configuration and the interaction of ionic species within the CNC structure.

The crystallinity index of the CNC–CNT materials (Table 5) decrease with increasing concentration of CNT, and this is attributed to 71.5. Our results corroborate the observations of Zhu et al. (2022), Song et al. (2019), Neto et al. (2013) and Salajkova (2012).

The crystallinity index of the CNC samples was analyzed by Bruker D4 X-ray diffractometer. The crystallinity index (CI) was calculated from $\mathbf{CI = (I_{200} - I_{am}) \times 100 / I_{200}}$

Where $I_{200}$ was the intensity of 200 peak ($I_{200}$) between $2\theta = 22 – 23°$ and $I_{am}$ was the minimum intensity between the peaks at 200 and 110 ($I_{am}$) $2\theta = 18–19°$.

*Table 5: The crystallinity index of the synthesized CNC compared to some published investigation*

| **CNC materials** | **Production method** | **Crystallinity index** | **References** |
|---|---|---|---|
| CNC – 0% CNT | Tempo mediation | 78.3 | This investigation |
| CNC – 0.5% CNT | Tempo mediation | 70.6 | This investigation |
| CNC – 1% CNT | Tempo mediation | 72.5 | This investigation |
| CNC – 1.5% CNT | Tempo mediation | 72.7 | This investigation |
| CNC – 2% CNT | Tempo mediation | 68.5 | This investigation |
| CNC – 2.5% CNT | Tempo mediation | 66.2 | This investigation |
| CNC from Calotropis procera | Acid Hydrolysis | 68.7 | Song et al. (2019) |
| CNC from Soya hulls | Acid Hydrolysis | 71.5 | Neto et al. (2013) |
| TO-NFC | Tempo mediation | 66 | Salajkova et al. (2012) |
| CNC 3Hrs | Tempo mediation | 79 | Salajkova et al. (2012) |
| CNC 5Hrs | Tempo mediation | 80 | Salajkova et al. (2012) |
| CNC 7Hrs | Tempo mediation | 78 | Salajkova et al. (2012) |
| CNC | Tempo mediation | 83.4 | Zhu et al. (2022) |
| CCNC | Tempo mediation | 71.9 | Zhu et al. (2022) |
| TCNF | Tempo mediation | 59.3 | Zhu et al. (2022) |

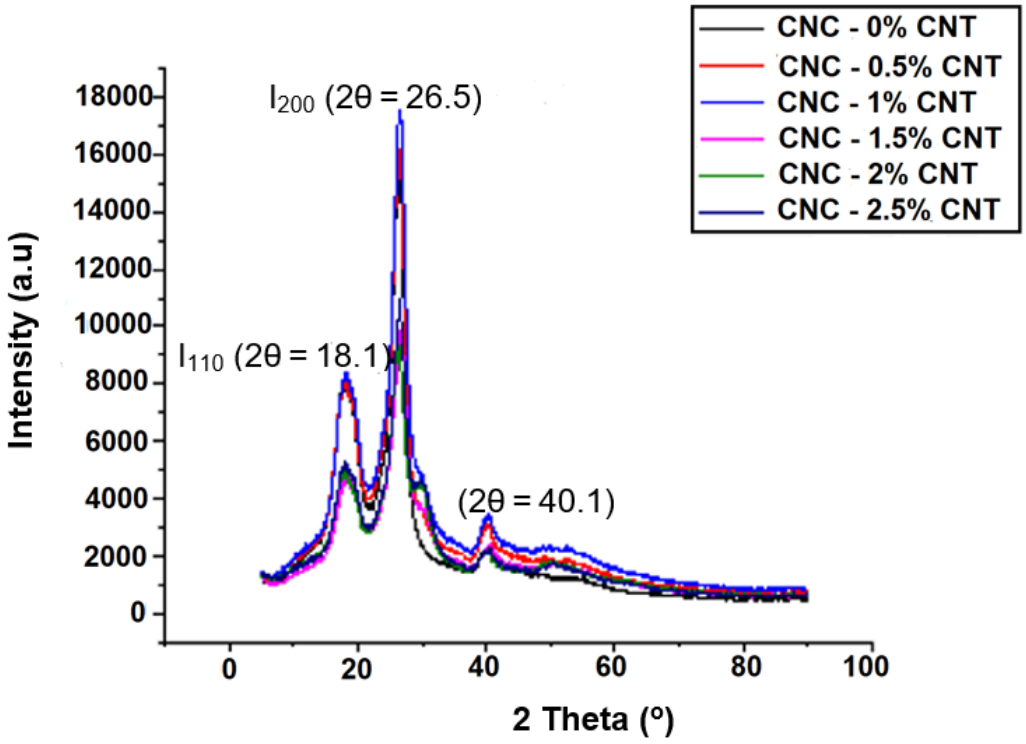



*Figure 18: XRD spectra of CNC with CNT 0%, 0.5%, 1%, 1.5%, 2% and 2.5%*

### 4.1.6 Thermogravimetric analysis (TGA) and derivative gravimetry (DTA)

The TGA curve of CNT in Figure 19 showed a degradation from 185 $^{o}$C to 475 $^{o}$C with a degradation slope of 0.02931 %/$^{o}$C, which agrees with the TGA as per the investigation of Hoang et al. (2019). However, the TGA of the CNC curve seen in Figure 20 showed a sharp degradation from 250 to 350 $^{o}$C with a degradation slope of 0.85 %/ $^{o}$C. The degradation profile of CNC resembles the degradation as per the investigation of Shariatnia et al. (2020) and Dehesa et al. (2020). The CNC- CNT TGA graph (Figure 21) demonstrated the weight losses and rates of degradation while heating in a nitrogen atmosphere. The temperature increase causes the cellulose glycosyl units to depolymerize, dehydrate, and decompose, which results in the abrupt deterioration slopes as per the investigation by Dehesa et al. (2020) and Dumanh et al. (2012). When the CNT amount increased from 0.5 to 2.5 %, the degradation slope decreased as seen in the TGA graph of CNC – CNT. Figures 20, 21 and 22 showed that the differential thermal behaviour of the synthesized materials have similar thermal behaviour as the pure CNC. This is due to the volatile content of CNC compared to CNT.

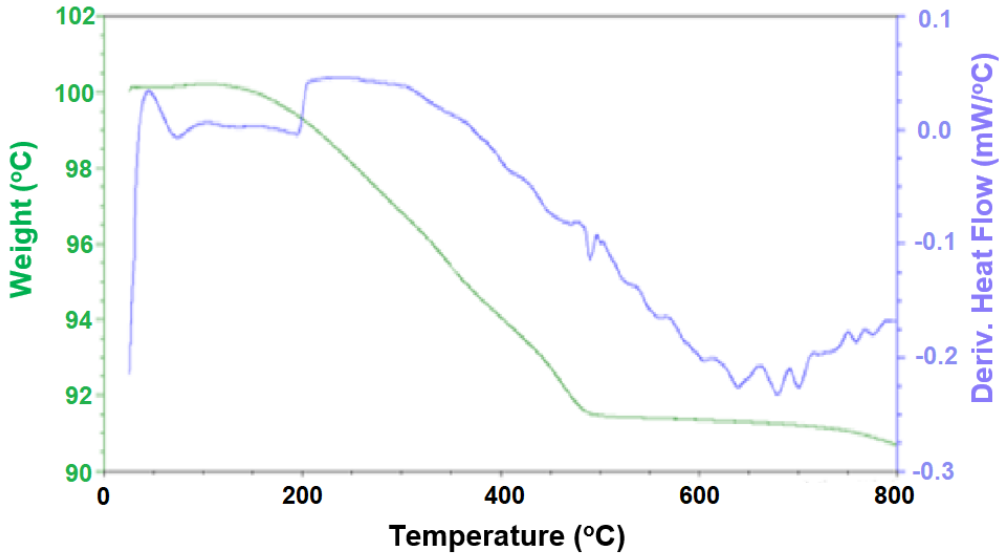



*Figure 19: TGA and DSC of CNT sample*

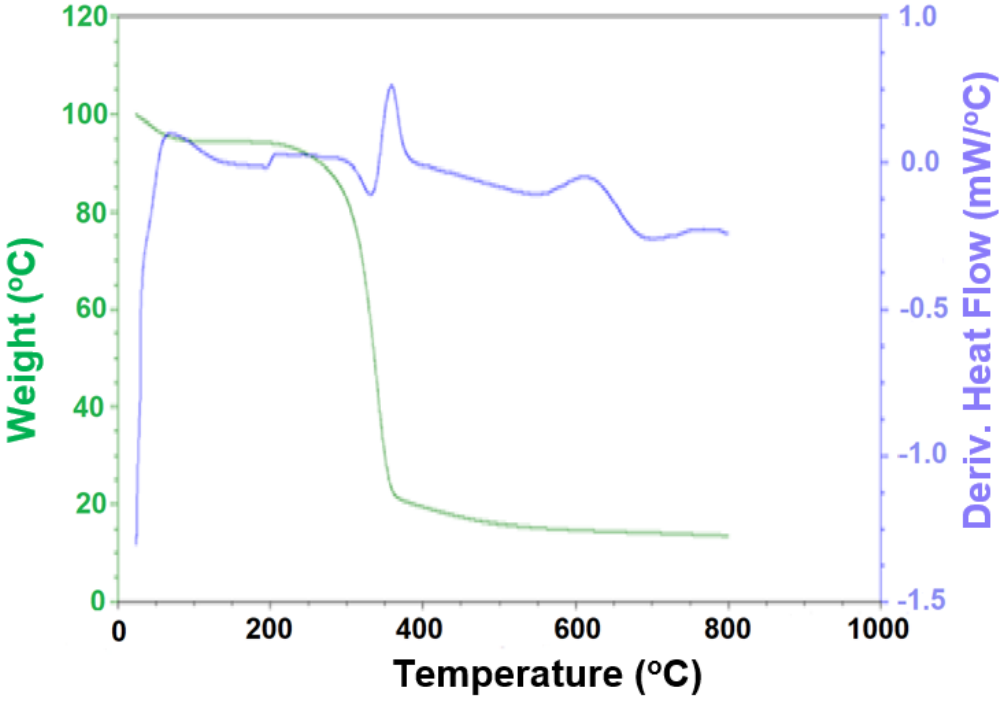



*Figure 20: TGA and DSC of CNC sample*

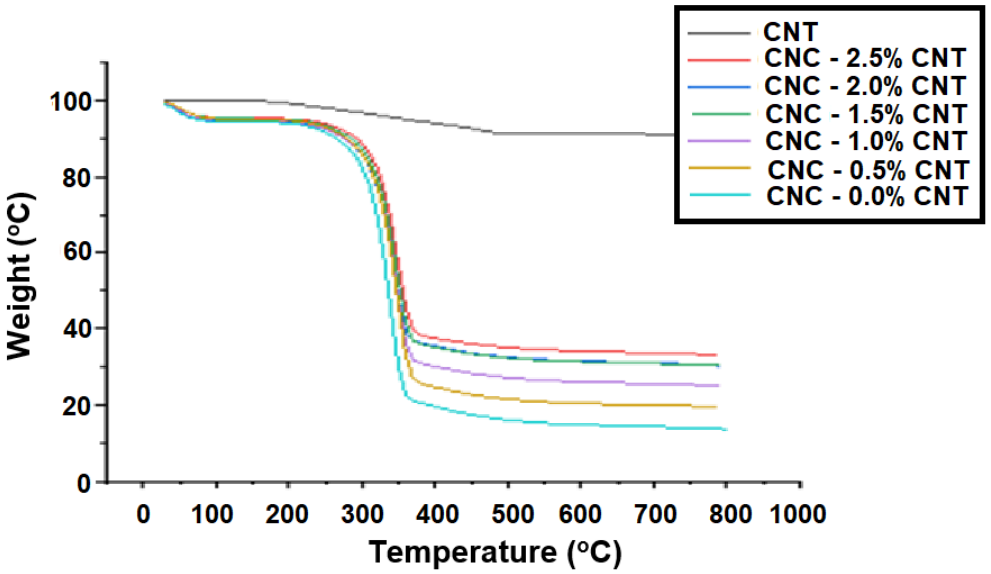



*Figure 21: TGA of CNT, CNC-CNT 0, 0.5, 1, 1.5, 2 and 2.5% samples*

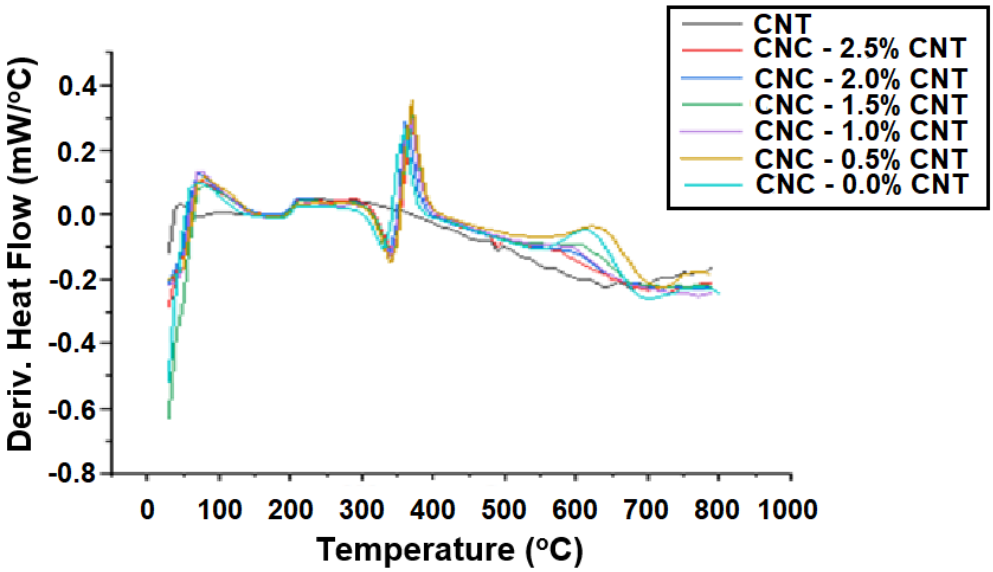



*Figure 22: DTA of CNT, CNC, CNC-CNT 0.5, 1, 1.5, 2 and 2.5% samples*

## 4.2 Properties of carbon nanotubes doped on cellulose nanocrystal for sensor application

### 4.2.1 Introduction

The materials developed in this investigation used the same amount of cellulose for various nanomaterials added in the template as a gas sensing agent. The sensing response depends on the CNTs distribution on the template and was more controlled by the amount of CNTs on the template because the 0% CNT displayed poor response. The homogeneous distribution of CNTs on the template was achieved using ultrasonication, which enhanced the diffusion of CNTs on the CNC-CNTs system. The observed uniform colour of each amount added of CNTs on the template was an indication of the homogeneity across the surface, but this does not exclude further homogeneity tests if facilities are available. As discussed above, the sensing response changed with various amounts of CNTs as observed. It is important to remember that the TEMPO oxidation was a procedure used to transform the microcellulose material into the cellulose nanocrystal. Therefore, the CNC molecule could not be denatured by this method. The modified CNC displayed significant potential for several applications due to the hydroxyl functional groups present on the surface, resulting in the creation of diverse materials with flexible properties, as discussed by Fareez et al (2021).

It should be noted that the FTIR as known is used to detect different functional groups, which did not show any difference before and after the gas exposure. The availability of an integrated online FTIR facility that could be used to test insitu the changes in functional groups of the CNC-CNTs sensors in the presence of the gases could have further enhanced our understanding of the sensing mechanism from the correlation between the FTIR spectra and the conductivity behaviour. However, this was not available during the tenure of the project.

Before the Raman assessment of the 2D peak line shape, a linear background was determined and subtracted. The focus here was to assess the level of crystallinity and the significance of the disordered structure through the $I_D/I_G$ ratio. The D and G peaks were associated with CNTs and not with the crystalline material CNC. These showed that the CNC was used to accommodate the amorphous materials, which played the most in the sensing response.

The TGA degradation of CNC resulted in chars as remnant material besides CNTs after heating at different temperatures, while CNTs were stable.

The conductivity analysis in this investigation assessed the ability of the CNC - CNT material to detect a gas in order to incorporate it as the active layer in a sensing device. Developing a simple gas sensor could assist in providing a device that could prevent humans from the toxicity of gas in our environment. Therefore, a series of gases constituting nitrogen, argon, hydrogen and carbon dioxide were investigated due to their intrinsic properties such as inertness, flammability and toxicity.

## 4.2.2 Conductivity analysis

The changes in electrical conductivity for a sensor material of constant dimensions (Constant length and width) as a function of CNT amount using different selected gas are discussed in subsections herein.

### 4.2.2.1 Effect of the amount of CNT on gas sensing

The increase in CNT has a positive effect on the conductivity of synthesized materials as function of CNT amount using different selected gas as seen in Figure 23. The increased conductivities, in general, were seen from inert to toxic gas, in which the smaller to the highest were nitrogen, argon, hydrogen and carbon dioxide, respectively. Jiang et al. (2019) observed a similar pattern of conductivity responses against the amount of MWNT embedded in CNC (Podsiadły et al., 2022). The mixed material CNC – CNT has potential conductivity behaviour which is due to the interaction between both materials. Zhai et al. (2021) explained how CNC could play a key role in stabilizing CNT, which enhanced the electrical conductivity and the sensing performance of mixed materials. Corletto et al. (2022) found that CNC produced through acid hydrolysis allowed better dispersion of CNT and improved the conductivity of the material. They also discovered that the various hydrophilic substrates of CNC and CNT may conduct electricity at great resolution. Zhu et al. (2019) discovered that CNT is the best conductor filler for the creation of stain sensors, which was consistent with the results of this experiment. They also found that the dispersion of CNT had a great effect on the physical and chemical properties of the mixed materials due to the strong van der Waals interaction. As per Corletto et al. (2022) investigation, Zhu et al. (2019) explained the dispersion mechanism, which is caused by the hydrophobic part of CNC with the hydrophobic surface of the CNT.

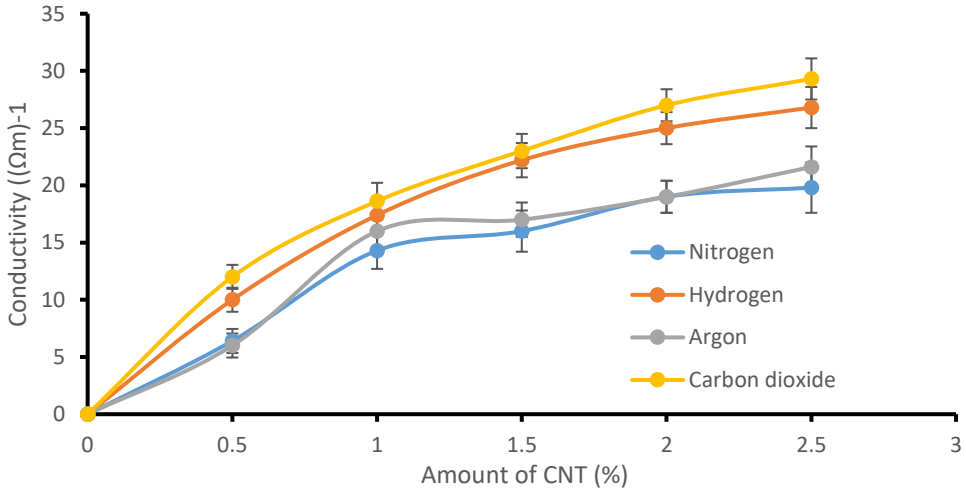



*Figure 23: Conductivity behaviour with CNT content of the sensor*

### 4.2.2.2 Selectivity of the gas sensor

The results illustrating the selectivity of the flammable and toxic gases that were investigated in this work are presented in Figure 24, for the pristine and composited samples. It is evident from the Figure that an exposed CNC – CNT sheet/ surface with 0.5% CNT shows significant changes in the conductivity after exposure to $H_2$ and $CO_2$. The difference in the conductivity between selected materials can determine the range of detection limits for these gases through a choice of critical electrical conductivity of the sensor device.

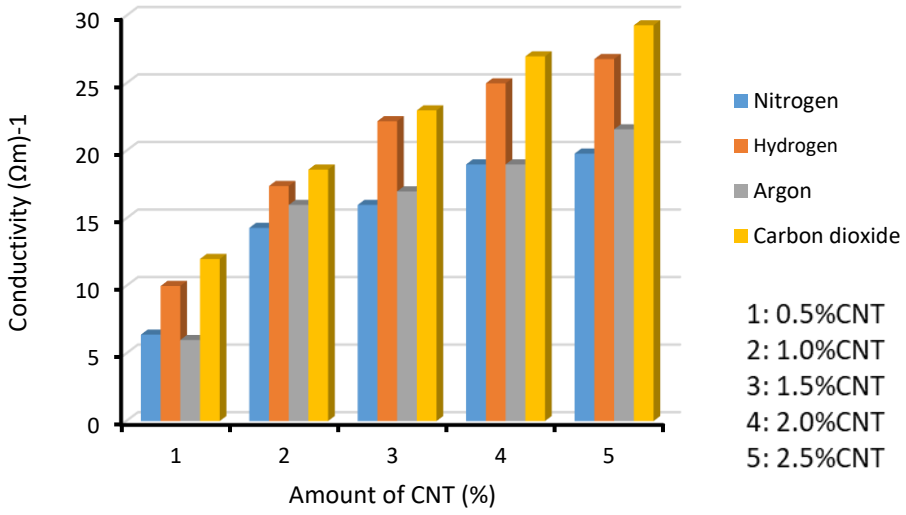



*Figure 24: Gas sensing range*

### 4.2.2.3 Stability of the gas sensor

Figure 25 showed the response time and stability of the 2.5% CNT composite materials upon exposure to $N_2$, $H_2$, Ar and $CO_2$. All the measurements were done at room temperature. It is clear that after 10 seconds of exposure to all of these gases, the conductivity remains constant; this saturation is explained by the fact that only a small volume of gas is needed to cover the sensor system's surface. The change in conductivity between 0 to 5 seconds showed the higher speed of the synthesized materials in sensing the selected gas. The difference in conductivities could be well seen with the graph of the sensing capacity (Figure 26).

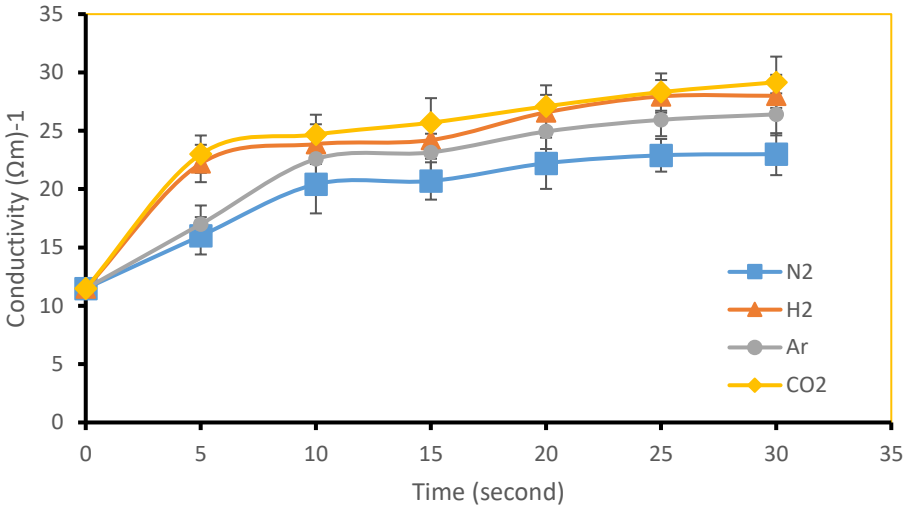



*Figure 25: Sensing stability with time*

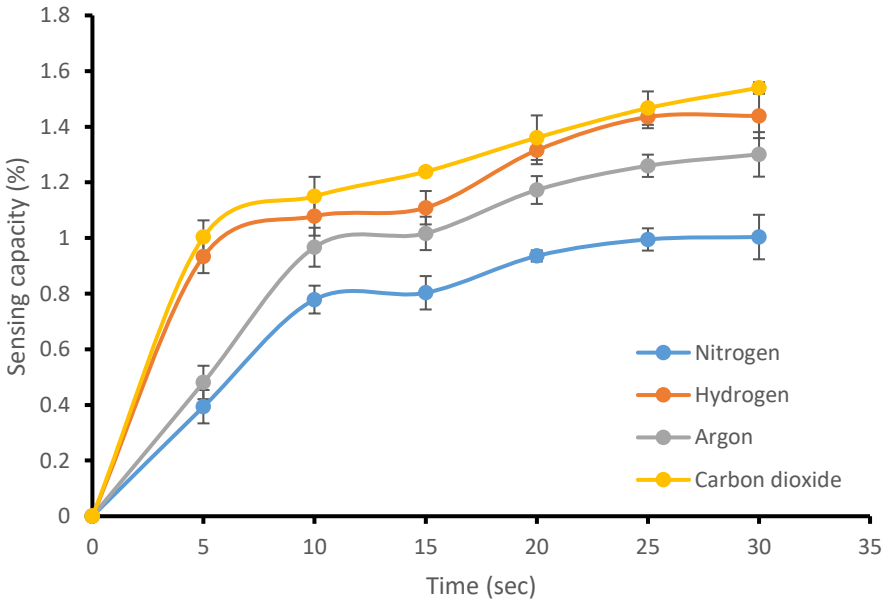
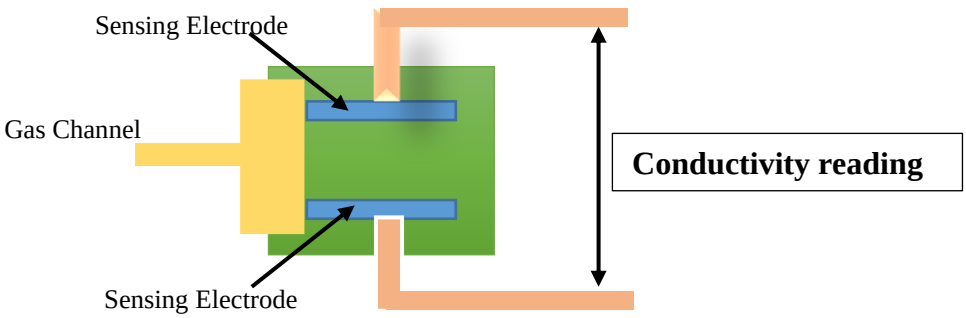



*Figure 26: Sensing Capacity*

The sensing behaviour varied with the temperature at which the sensor system works. Assessing the thermal stability of CNTs as supported by Mwakikunga et al. (2013), the impact of temperature on the sensing of CNC-CNTs was not the main topic of this work. According to their analysis, several materials lost their sensing capabilities compared to their initial capacities at the conclusion of the sensing test, which should impair the sensor's ability to recover. They found that the recovery is almost nearly perfectly proportional to the response time. At higher temperatures, the materials exhibit worse increases in sensing and recovery properties, this may be due to the vibrational and rotational motions of the particles. They conclude that sensors that operate at room temperature are more attractive as most of the time the environment is around room temperature. It recommended that winter temperatures should be investigated in the future to establish if the amount of CNTs in the CNC should be reduced. However, this investigation has explored as a proof of concept the utility of CNC – CNTs composite as an active material for sensor applications of select gases. On the temperature range of these composites, reference should be given to the DTA results which have shown that thermal decomposition occurs at 0.02931 %/$^{o}$C, making it rather difficult to operate these materials in sensors beyond these temperatures.

### 4.2.3 Proposed structure of the sensor device

The success in changing the conductivities when the synthesized materials are exposed to selected gases can enable a simple assembly of CNC – CNT connected with a conductivity meter and alarm (Figure 27). The alarm can be set from the conductivities of 15 $(\Omega m)^{-1}$ and 22 $(\Omega m)^{-1}$ for nitrogen/Argon and Hydrogen/ carbon, respectively. The device should be composed of a metal sheet holding the CNC – CNT at both ends, connected to the mini-conductivity meter in which an incorporated alarm could ring when the reading exceeds the set acceptable conductivity. Figure 27 provides an overview of the proposed devise.



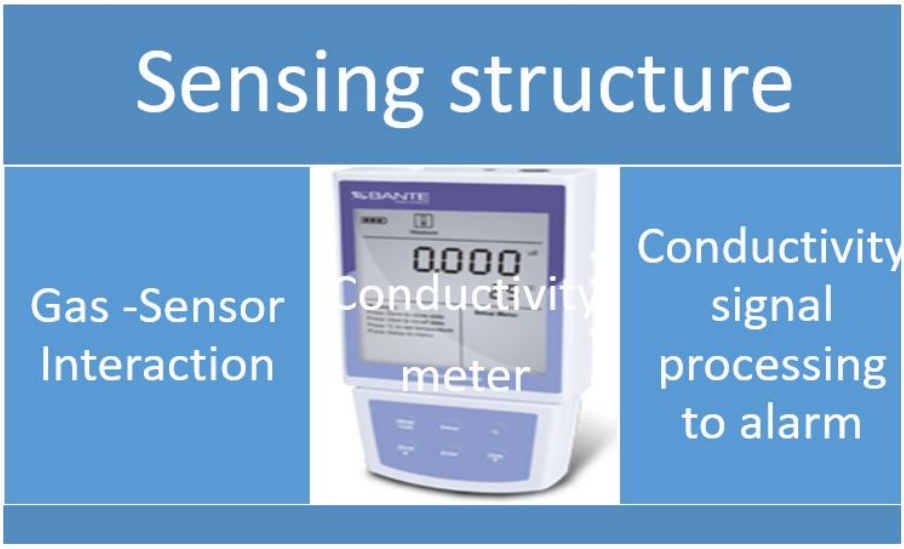



*Figure 27: proposed sensing device (a) of the structure of the template system, and (b) front view of the sensing device*

## 4.3 Summary of Chapter 4

This chapter showed how the analytical techniques used support the sensing behaviours of the CNC – CNTs samples. The nanomaterials could be used for the sensing of inert and toxic gases, and have a better sensing response time, which is 10 seconds. This project confirms previous investigations such as the work done by Mwakikunga et al. (2013) on the ability of nanomaterials to detect gases. The ratio of the difference between the resistances in the presence and absence of gases or the ratio of the difference between the conductivities in the presence and absence of gases was used to calculate the changes in the sensing responses of nanomaterials in the presence of specific gases. Mwakikunga et al. (2013) suggested that the sensing responses depend on the temperature at which the sensor is exposed. They found that the temperature and the response are inversely proportional (Response = ($R_{\text{presence of gas}}/R_{\text{absence of gas}}$) Exp ($E_{\text{absence of gas}} - E_{\text{presence of gas}}$)/ $K_B T$). This could depend on the materials used in the sensing device as the thermal stability range of the materials can affect the temperature behaviour and the sensing response. CNTs are thermally stable materials, which could be stable at sensing gases at different human operating temperatures. Future work should investigate the sensing response at low (winter) and high (summer) temperatures; and the effect of reusing the sensing device (number of cycle and possibly the cleaning process).

# CHAPTER 5: CONCLUSIONS AND RECOMMENDATIONS

The focus of this investigation was to develop a gas sensor system and test its sensing capacity through selected gas. The CNC – CNT materials were developed with excellent conductivity response, which makes them potential gas sensors. The mixed materials were characterized to assess their morphology, crystallinity, thermal and chemical structures. The characterization results showed the mixed materials resembled CNC. CNT was well dispersed within CNC through their hydrophilic sides. CNT was found to be the most suitable conductive fillers for the development of CNC - CNT sensors. The sensing test showed that the conductivities were almost stable after 10 seconds, and gases could be detected even from 0.5% CNT with a remarkable change in conductivities with an increased amount of CNT and type of gas used (inert, flammable and toxic). It was found that the alarm connected with the conductivity meter should be set at 15 and 22 $(\Omega m)^{-1}$ for inert and flammable/ toxic gases, respectively with a positive response between 10 to 30 seconds. Future work should investigate the effect of the environment (such as humidity conditions, which assist in investigating the in-depth charge-transport phenomena during the sensing process) and temperature at which the device is exposed.

# REFERENCES


Bartlett, P.N., 1990. Modified electrode surface in amperometric biosensors. *Medical and Biological Engineering and Computing*, *28*(3), pp.B10-B17.

Bassey, E.E., 2014. Development and characterisation of metal oxide gas sensors (Doctoral dissertation, Auckland University of Technology).

Brédas, J.L. and Silbey, R. eds., 2012. *Conjugated polymers: the novel science and technology of highly conducting and nonlinear optically active materials*. Springer Science & Business Media.

Cao, S., Wu, Z., Sun, Q., Zhang, W., Beysen, S., Wang, S., Shaymurat, T., Zhang, M. and Duan, H., 2021. Gas sensing properties of cotton-based carbon fibers and ZnO/carbon fibers regulated by changing carbonization temperatures. Sensors and Actuators B: Chemical, 337, p.129818.

Chen, W., Yu, H., Liu, Y., Chen, P., Zhang, M. and Hai, Y., 2011. Individualization of cellulose nanofibers from wood using high-intensity ultrasonication combined with chemical pretreatments. *Carbohydrate Polymers*, *83*(4), pp.1804-1811.

Corletto, A., Hosseinmardi, A., Annamalai, P.K., Martin, D.J. and Shapter, J.G., 2022. High-Resolution R2R-Compatible Printing of Carbon Nanotube Conductive Patterns Enabled by Cellulose Nanocrystals. ACS Applied Nano Materials.

Costa, C., Medronho, B., Lindman, B., Edlund, H. and Norgren, M., 2021. Cellulose as a Natural Emulsifier: From Nanocelluloses to Macromolecules. In Cellulose. IntechOpen.

Dehesa, A.A., Luzi, F., Puglia, D., Lizundia, E., Armentano, I. and Torre, L., 2020. Effect of SWCNT Content and Water Vapor Adsorption on the Electrical Properties of Cellulose Nanocrystal-Based Nanohybrids. The Journal of Physical Chemistry C, 124(27), pp.14901-14910.

Dufresne, A., Dupeyre, D. and Vignon, M.R., 2000. Cellulose microfibrils from potato tuber cells: processing and characterization of starch–cellulose microfibril composites. *Journal of applied polymer science*, *76*(14), pp.2080-2092.

Esonye, C., Onukwuli, O.D. and Ofoefule, A.U., 2019. Optimization of methyl ester production from Prunus Amygdalus seed oil using response surface methodology and Artificial Neural Networks. Renewable energy, 130, pp.61-72.

Fareez, I.M., Der Jiun, O. and Seng, W.Y., 2021. Nanocellulose: Chemical, Thermal, and Optical Properties. *Nanocellulose and Its Composites for Water Treatment Applications*, p.11.

Garnett, S. and Fried, I., 2001, July. Factors impending the industrial use of nanomaterials and nano-technology. In *Proceedings of the Int. Conference*.

Guan, Q.F., Yang, H.B., Han, Z.M., Ling, Z.C., Yin, C.H., Yang, K.P., Zhao, Y.X. and Yu, S.H., 2021. Sustainable Cellulose-Nanofiber-Based Hydrogels. *ACS nano*.

Guo, Q. and Zhang, X., 2021. A review of mechanochromic polymers and composites: From material design strategy to advanced electronics application. *Composites Part B: Engineering*, *227*, p.109434.

Gupta, V., Ramakanth, D., Verma, C., Maji, P.K. and Gaikwad, K.K., 2021. Isolation and characterization of cellulose nanocrystals from amla (Phyllanthus emblica) pomace. Biomass Conversion and Biorefinery, pp.1-12.

Han, J.W., Kim, B., Li, J. and Meyyappan, M., 2012. Carbon nanotube based humidity sensor on cellulose paper. *The Journal of Physical Chemistry C*, *116*(41), pp.22094-22097

Herrick, F.W., Casebier, R.L., Hamilton, J.K. and Sandberg, K.R., 1983, January. Microfibrillated cellulose: morphology and accessibility. In *J. Appl. Polym. Sci.: Appl. Polym. Symp.;(United States)* (Vol. 37, No. CONF-8205234-Vol. 2). ITT Rayonier Inc., Shelton, WA.

Hittini, W., Abu-Hani, A.F., Reddy, N. and Mahmoud, S.T., 2020. Cellulose-Copper Oxide hybrid nanocomposites membranes for H 2 S gas detection at low temperatures. *Scientific reports*, *10*(1), pp.1-9.

Ivanova, A., Frka-Petesic, B., Paul, A., Wagner, T., Jumabekov, A.N., Vilk, Y., Weber, J., Schmedt auf der Günne, J., Vignolini, S., Tiemann, M. and Fattakhova-Rohlfing, D., 2020. Cellulose nanocrystal-templated tin dioxide thin films for gas sensing. ACS applied materials & interfaces, 12(11), pp.12639-12647.

Jiang, M., Seney, R., Bayliss, P.C. and Kitchens, C.L., 2019. Carbon nanotube and cellulose nanocrystal hybrid films. Molecules, 24(14), p.2662.

John, M.J. and Thomas, S., 2008. Biofibres and biocomposites. *Carbohydrate polymers*, *71*(3), pp.343-364.

Ioelovich, M. and Figovsky, O., 2008. Nano-cellulose as promising biocarrier. In *Advanced Materials Research* (Vol. 47, pp. 1286-1289).

Karthigeyan, A., Minami, N. and Iakoubovskii, K., 2008. Highly sensitive, room-temperature gas sensors prepared from cellulose derivative assisted dispersions of single-wall carbon nanotubes. *Japanese journal of applied physics*, *47*(9R), p.7440.

Kaushik, M., Fraschini, C., Chauve, G., Putaux, J.L. and Moores, A., 2015. Transmission electron microscopy for the characterization of cellulose nanocrystals. The transmission electron microscope-theory and applications, pp.130-163.

Khalid, M.Y., Al Rashid, A., Arif, Z.U., Ahmed, W. and Arshad, H., 2021. Recent advances in nanocellulose-based different biomaterials: types, properties, and emerging applications. *Journal of Materials Research and Technology*, *14*, pp.2601-2623.

Korotcenkov, G. ed., 2011. *Chemical Sensors: Comprehensive Sensor Technologies Volume 6: Chemical Sensors Applications* (Vol. 6). Momentum Press.

Lakard, B., Ploux, L., Anselme, K., Lallemand, F., Lakard, S., Nardin, M. and Hihn, J.Y., 2009. Effect of ultrasounds on the electrochemical synthesis of polypyrrole, application to the adhesion and growth of biological cells. *Bioelectrochemistry*, *75*(2), pp.148-157.

Lapka, T., Kopecký, D., Mazúr, P., Prokeš, J., Ulbrich, P., Dendisová, M., Sedlačík, M. and Hassouna, F., 2021. Elaboration and properties of nanofibrillated cellulose composites with polypyrrole nanotubes or their carbonized analogs. *Synthetic Metals*, *278*, p.116806.

Le, G.T., Mala, P., Ratchahat, S. and Charinpanitkul, T., 2021. Bio-based production of carbon nanotubes via co-pyrolysis of eucalyptus oil and ferrocene. Journal of Analytical and Applied Pyrolysis, 158, p.105257.

Li, Z., Wang, J., Xu, Y., Shen, M., Duan, C., Dai, L. and Ni, Y., 2021. Green and sustainable cellulose-derived humidity sensors: A review. *Carbohydrate Polymers*, *270*, p.118385.

Liu, Q., Chen, C., Pan, F. and Zhang, J., 2015. Highly efficient oxygen reduction on porous nitrogen-doped nanocarbons directly synthesized from cellulose nanocrystals and urea. Electrochimica Acta, 170, pp.234-241.

Liu, N., Tang, M.L., Hentschel, M., Giessen, H. and Alivisatos, A.P., 2011. Nanoantenna enhanced gas sensing in a single tailored nanofocus. *Nature materials*, *10*(8), pp.631-636.

Lv, P., Lu, X., Wang, L. and Feng, W., 2021. Nanocellulose-Based Functional Materials: From Chiral Photonics to Soft Actuator and Energy Storage. *Advanced Functional Materials*, *31*(45), p.2104991.

Mahapatra, S., Srivastava, V.R. and Chandra, P., 2021. Nanobioengineered Sensing Technologies Based on Cellulose Matrices for Detection of Small Molecules, Macromolecules, and Cells. *Biosensors*, *11*(6), p.168.

Malik, R., Tomer, V.K., Mishra, Y.K. and Lin, L., 2020. Functional gas sensing nanomaterials: A panoramic view. *Applied Physics Reviews*, *7*(2), p.021301.

Mohammed, M., Rahman, R., Mohammed, A.M., Adam, T., Betar, B.O., Osman, A.F. and Dahham, O.S., 2022. Surface treatment to improve water repellence and compatibility of natural fiber with polymer matrix: Recent advancement. Polymer Testing, p.107707.

Moser, C., 2019. Manufacturing and Characterization of Cellulose Nanofibers. Doctoral Thesis in Fibre and Polymer Science School of Engineering Sciences in Chemistry, Biotechnology and Health KTH Royal Institute of Technology Stockholm, Sweden.

Motaung, T.E., 2021. Recent applications and innovations of cellulose-based materials: A critical review. *Cellulose Chemistry and Technology*, *55*(1-2), pp.1-12.

Mwakikunga, B.W., Motshekga, S., Sikhwivhilu, L., Moodley, M., Scriba, M., Malgas, G., Simo, A., Sone, B., Maaza, M. and Ray, S.S., 2013. A classification and ranking system on the H2 gas sensing capabilities of nanomaterials based on proposed coefficients of sensor performance and sensor efficiency equations. Sensors and Actuators B: Chemical, 184, pp.170-178.

Nepomuceno, N.C., Seixas, A.A.A., Medeiros, E.S. and Mélo, T.J.A., 2021. Evaluation of conductivity of nanostructured polyaniline/cellulose nanocrystals (PANI/CNC) obtained via in situ polymerization. Journal of Solid State Chemistry, 302, p.122372.

Nikolic, M.V., Milovanovic, V., Vasiljevic, Z.Z. and Stamenkovic, Z., 2020. Semiconductor gas sensors: Materials, technology, design, and application. *Sensors*, *20*(22), p.6694.

Nivethithaa, S. and Baskar, R., 2021, November. Functional characteristics of nanocellulose and its potential applications. In *AIP Conference Proceedings* (Vol. 2387, No. 1, p. 090006). AIP Publishing LLC.

Olvera, D. and Monaghan, M.G., 2021. Electroactive material-based biosensors for detection and drug delivery. *Advanced Drug Delivery Reviews*, *170*, pp.396-424.

Padvi et al, M.N., Moholkar, A.V., Prasad, S.R. and Prasad, N.R., 2021. A critical review on design and development of gas sensing materials. *Engineered Science*, *15*, pp.20-37.

Palencia, M., Espinosa-Duque, A., Otálora, A. and García-Quintero, A., 2021. Cellulose-based stimuli-responsive hydrogels. In *Plant and Algal Hydrogels for Drug Delivery and Regenerative Medicine* (pp. 423-470). Woodhead Publishing.

Pandi, N., Sonawane, S.H. and Kishore, K.A., 2021. Synthesis of cellulose nanocrystals (CNCs) from cotton using ultrasound-assisted acid hydrolysis. Ultrasonics sonochemistry, 70, p.105353.

Pei, A., Zhou, Q. and Berglund, L.A., 2010. Functionalized cellulose nanocrystals as biobased nucleation agents in poly (l-lactide)(PLLA)–Crystallization and mechanical property effects. *Composites Science and Technology*, *70*(5), pp.815-821.

Phasuksom, K., Ouajai, W.P. and Sirivat, A., 2021. Graphene oxide/doped polyindole/hydroxypropyl cellulose coated on interdigitated electrode as methanol sensor. *Microchemical Journal*, *171*, p.106889.

Podsiadły, B., Walter, P., Kamiński, M., Skalski, A. and Słoma, M., 2022. Electrically Conductive Nanocomposite Fibers for Flexible and Structural Electronics. Applied Sciences, 12(3), p.941.

Rahman, N.S.A., Greish, Y.E., Mahmoud, S.T., Qamhieh, N.N., El-Maghraby, H.F. and Zeze, D., 2021. Fabrication and characterization of cellulose acetate-based nanofibers and nanofilms for H2S gas sensing application. *Carbohydrate Polymers*, *258*, p.117643.

Reshmy, R., Philip, E., Paul, S.A., Madhavan, A., Sindhu, R., Binod, P., Pandey, A. and Sirohi, R., 2020. Nanocellulose-based products for sustainable applications-recent trends and possibilities. *Reviews in Environmental Science and Bio/Technology*, *19*(4), pp.779-806.

Rivadeneyra, A., Marín-Sánchez, A., Wicklein, B., Salmerón, J.F., Castillo, E., Bobinger, M. and Salinas-Castillo, A., 2021. Cellulose nanofibers as substrate for flexible and biodegradable moisture sensors. *Composites Science and Technology*, *208*, p.108738.

Rosa, M.F., Medeiros, E.S., Malmonge, J.A., Gregorski, K.S., Wood, D.F., Mattoso, L.H.C., Glenn, G., Orts, W.J. and Imam, S.H., 2010. Cellulose nanowhiskers from coconut husk fibers: Effect of preparation conditions on their thermal and morphological behavior. *Carbohydrate polymers*, *81*(1), pp.83-92.

Salajková, M., Berglund, L.A. and Zhou, Q., 2012. Hydrophobic cellulose nanocrystals modified with quaternary ammonium salts. Journal of Materials Chemistry, 22(37), pp.19798-19805.

Schanofski, M., Koch, L. and Schmidt, B.C., 2023. CO2 quantification in silicate glasses using μ-ATR FTIR spectroscopy. American Mineralogist, 108(7), pp.1346-1356.

Schmidt, C.E., Shastri, V.R., Vacanti, J.P. and Langer, R., 1997. Stimulation of neurite outgrowth using an electrically conducting polymer. *Proceedings of the National Academy of Sciences*, *94*(17), pp.8948-8953.

Shariatnia, S., Kumar, A.V., Kaynan, O. and Asadi, A., 2020. Hybrid cellulose nanocrystal-bonded carbon nanotubes/carbon fiber polymer composites for structural applications. ACS Applied Nano Materials, 3(6), pp.5421-5436.

Siró, I. and Plackett, D., 2010. Microfibrillated cellulose and new nanocomposite materials: a review. *Cellulose*, *17*(3), pp.459-494.

Smith, T.E.L., Wooster, M.J., Tattaris, M. and Griffith, D.W.T., 2011. Absolute accuracy and sensitivity analysis of OP-FTIR retrievals of CO 2, CH 4 and CO over concentrations representative of" clean air" and" polluted plumes". Atmospheric Measurement Techniques, 4(1), pp.97-116.

Song, K., Zhu, X., Zhu, W. and Li, X., 2019. Preparation and characterization of cellulose nanocrystal extracted from Calotropis procera biomass. Bioresources and Bioprocessing, 6(1), pp.1-8.

Subhedar, A., Bhadauria, S., Ahankari, S. and Kargarzadeh, H., 2021. Nanocellulose in biomedical and biosensing applications: A review. *International Journal of Biological Macromolecules*, *166*, pp.587-600.

Tudoroiu, E.E., Dinu-Pîrvu, C.E., Albu Kaya, M.G., Popa, L., Anuța, V., Prisada, R.M. and Ghica, M.V., 2021. An Overview of Cellulose Derivatives-Based Dressings for Wound-Healing Management. Pharmaceuticals, 14(12), p.1215.

Ummartyotin, S. and Manuspiya, H., 2015. A critical review on cellulose: from fundamental to an approach on sensor technology. *Renewable and Sustainable Energy Reviews*, *41*, pp.402-412.

Varshney, S., Mishra, N. and Gupta, M.K., 2021. Progress in nanocellulose and its polymer based composites: A review on processing, characterization, and applications. *Polymer Composites*.

Verma, C., Chhajed, M., Gupta, P., Roy, S. and Maji, P.K., 2021. Isolation of cellulose nanocrystals from different waste bio-mass collating their liquid crystal ordering with morphological exploration. International Journal of Biological Macromolecules, 175, pp.242-253.

Vetelino, J. and Reghu, A., 2017. *Introduction to sensors*. CRC press.

Wang, H.N., Meng, X., Dong, L.Z., Chen, Y., Li, S.L. and Lan, Y.Q., 2019. Coordination polymer-based conductive materials: ionic conductivity vs. electronic conductivity. *Journal of Materials Chemistry A*, *7*(42), pp.24059-24091.

Wu, C., Egawa, S., Kanno, T., Kurita, H., Wang, Z., Iida, E. and Narita, F., 2021. Nanocellulose reinforced silkworm silk fibers for application to biodegradable polymers. *Materials & Design*, *202*, p.109537.

Wu, Z.Y., Liang, H.W., Chen, L.F., Hu, B.C. and Yu, S.H., 2016. Bacterial cellulose: a robust platform for design of three dimensional carbon-based functional nanomaterials. *Accounts of chemical research*, *49*(1), pp.96-105.

Xu, Q., Gao, X., Zhao, S., Liu, Y.N., Zhang, D., Zhou, K., Khanbareh, H., Chen, W., Zhang, Y. and Bowen, C., 2021. Construction of Bio-Piezoelectric Platforms: From Structures and Synthesis to Applications. *Advanced Materials*, p.2008452.

Yang, J., Zhu, Z., Feng, J., Xue, M., Meng, Z., Qiu, L. and Mbola, N.M., 2020. Dimethyl sulfoxide infiltrated photonic crystals for gas sensing. *Microchemical Journal*, *157*, p.105074.

Yang, Z., Cao, W., Peng, C., Wang, T., Li, B., Ma, H., Su, Y., Zhou, Z., Yang, J. and Zeng, M., 2021. Construction, Application and Verification of a Novel Formaldehyde Gas Sensor

System Based on Ni-Doped SnO 2 Nanoparticles. *IEEE Sensors Journal*, *21*(9), pp.11023-11030.

Yun, S. and Kim, J., 2010. Multi-walled carbon nanotubes–cellulose paper for a chemical vapor sensor. *Sensors and Actuators B: Chemical*, *150*(1), pp.308-313

Zhai, J., Zhang, Y., Cui, C., Li, A., Wang, W., Guo, R., Qin, W., Ren, E., Xiao, H. and Zhou, M., 2021. Flexible Waterborne Polyurethane/Cellulose Nanocrystal Composite Aerogels by Integrating Graphene and Carbon Nanotubes for a Highly Sensitive Pressure Sensor. ACS Sustainable Chemistry & Engineering, 9(42), pp.14029-14039.

Zhao, Z., Xia, K., Hou, Y., Zhang, Q., Ye, Z. and Lu, J., 2021. Designing flexible, smart and self-sustainable supercapacitors for portable/wearable electronics: from conductive polymers. *Chemical Society Reviews*.

Zhou, W.D., Dastan, D., Yin, X.T., Nie, S., Wu, S., Wang, Q. and Li, J., 2020. Optimization of gas sensing properties of n-SnO 2/p-x CuO sensors for homogenous gases and the sensing mechanism. *Journal of Materials Science: Materials in Electronics*, *31*(21), pp.18412-18426.

Zhu, G., Giraldo Isaza, L., Huang, B. and Dufresne, A., 2022. Multifunctional Nanocellulose/Carbon Nanotube Composite Aerogels for High-Efficiency Electromagnetic Interference Shielding. ACS Sustainable Chemistry & Engineering.

Zhu, L., Zhou, X., Liu, Y. and Fu, Q., 2019. Highly sensitive, ultrastretchable strain sensors prepared by pumping hybrid fillers of carbon nanotubes/cellulose nanocrystal into electrospun polyurethane membranes. ACS applied materials & interfaces, 11(13), pp.12968-12

# APPENDIX

## A.1 CNC

### A.1.1 Raman

CNC at PH7

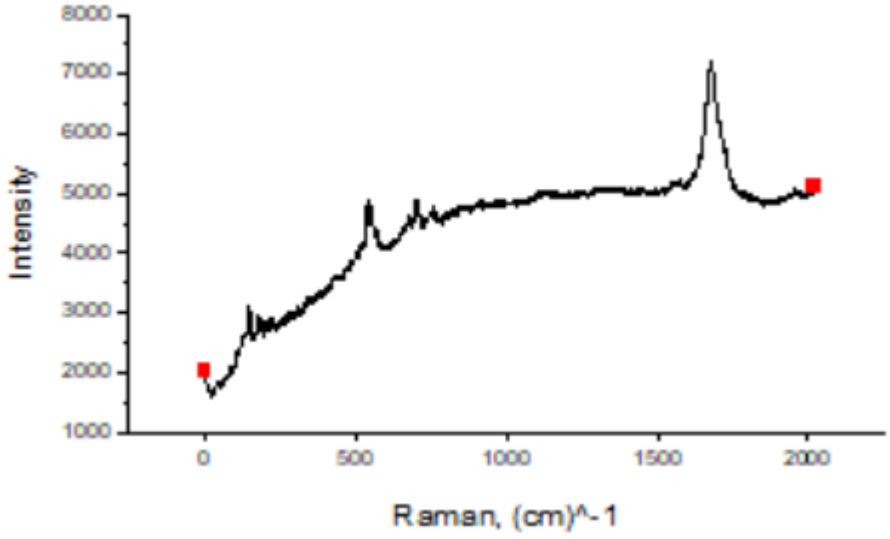



**Figure A.1.1.1.a CNC with 1 Tempo at PH7 a-b**

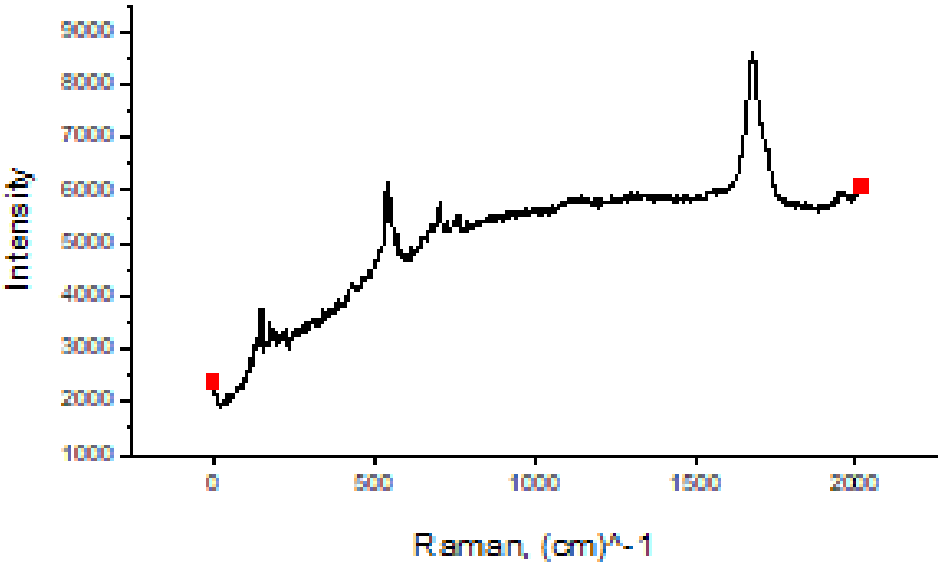



**Figure A.1.1.1.b CNC with 1 Tempo at PH7 c-d**

CNC Tempo 0.5

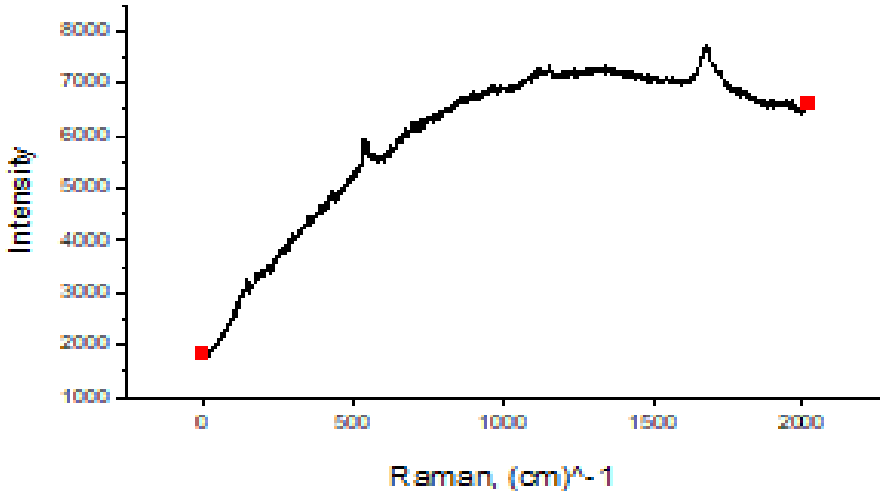



**Figure A.1.1.2 CNC with 0.5 Tempo at PH10**

CNC PH10 Tempo 1.25

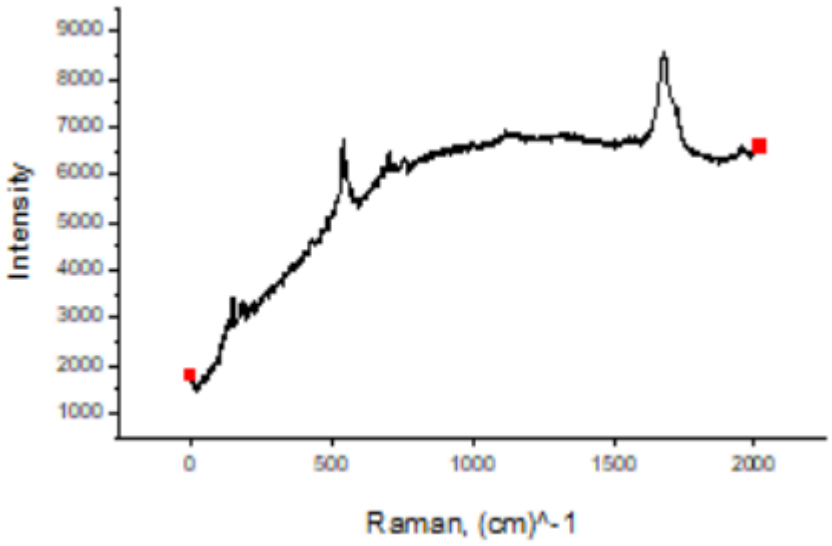



**Figure A.1.1.3 CNC with 1.25 Tempo at PH10**

CNC PH 10 Tempo 1.5

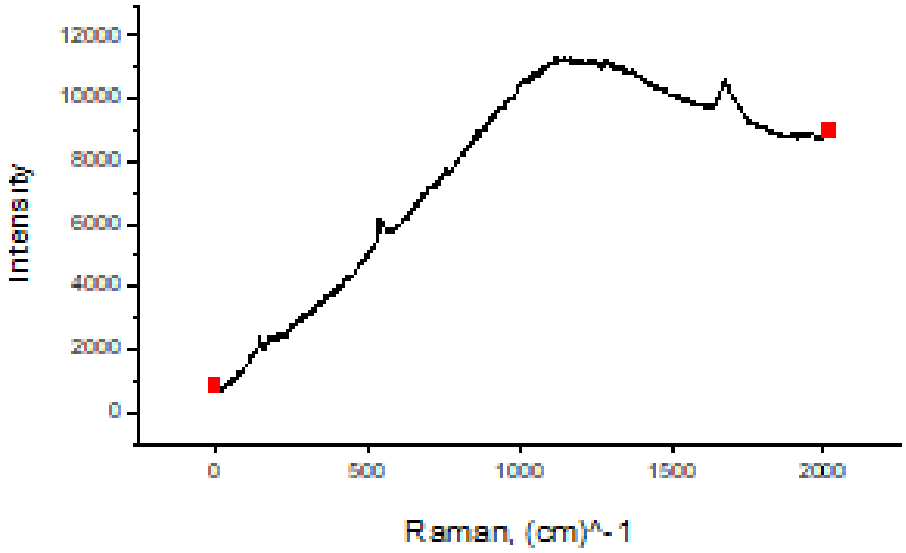



**Figure A.1.1.4 CNC with 1.5 Tempo at PH10**

CNC-CNT 0 % -a-b

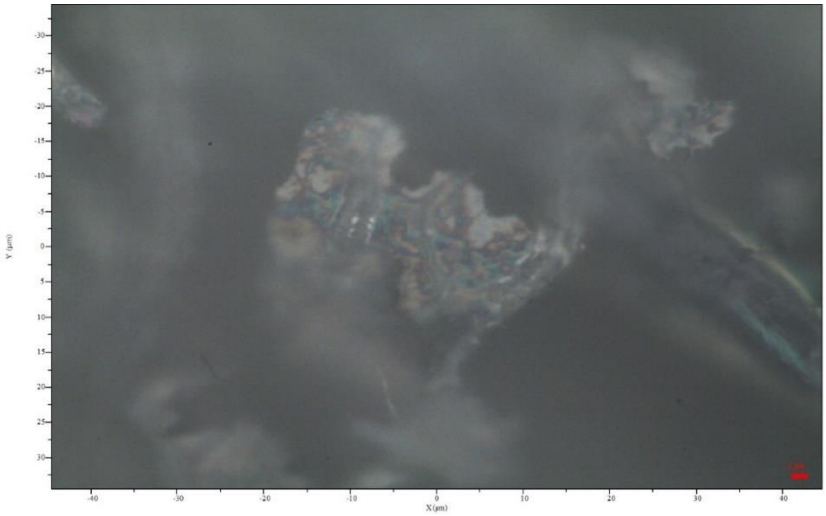


**Figure A.1.1.5.a Image of CNC with CNT O% a-b**

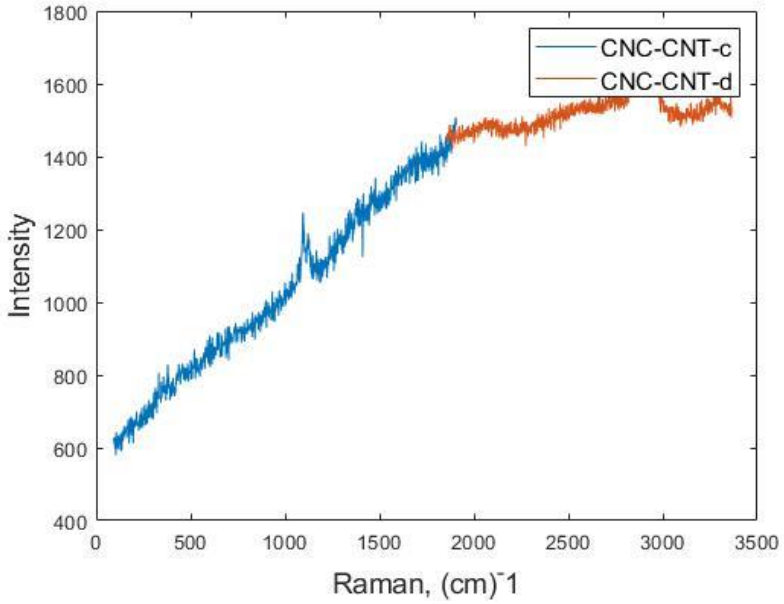



**Figure A.1.1.5.b CNC with CNT O% c-d**

CNC-CNT 0 per -c-d

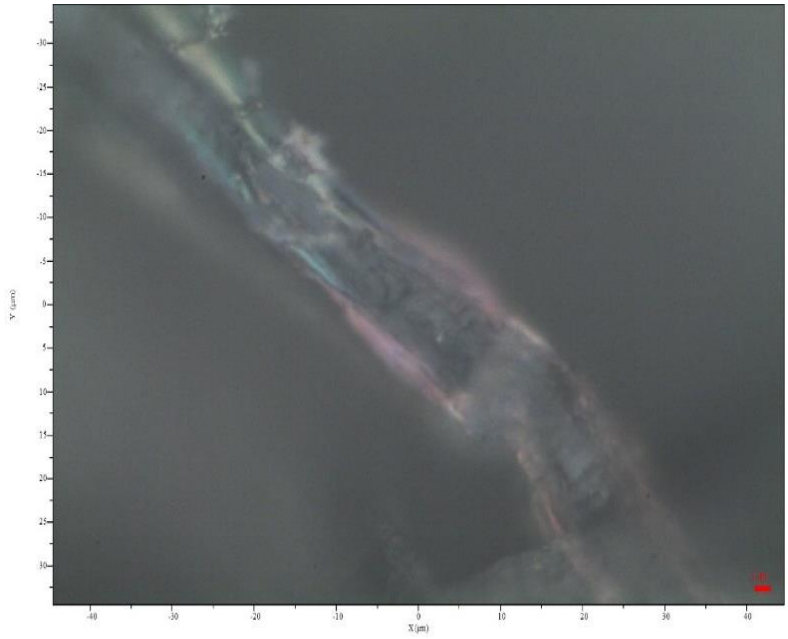


**Figure A.1.1.5.c Image of CNC with CNT O% c-d**

## A.1.2 FTIR

CNC at PH7 Tempo 1

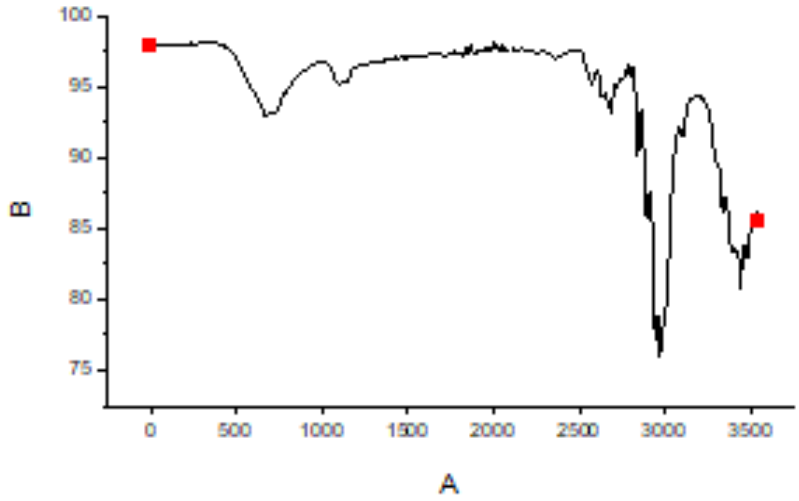



**Figure A.1.2.1 CNC with CNT 0% at PH7**

CNC 0.5 Tempo at PH10

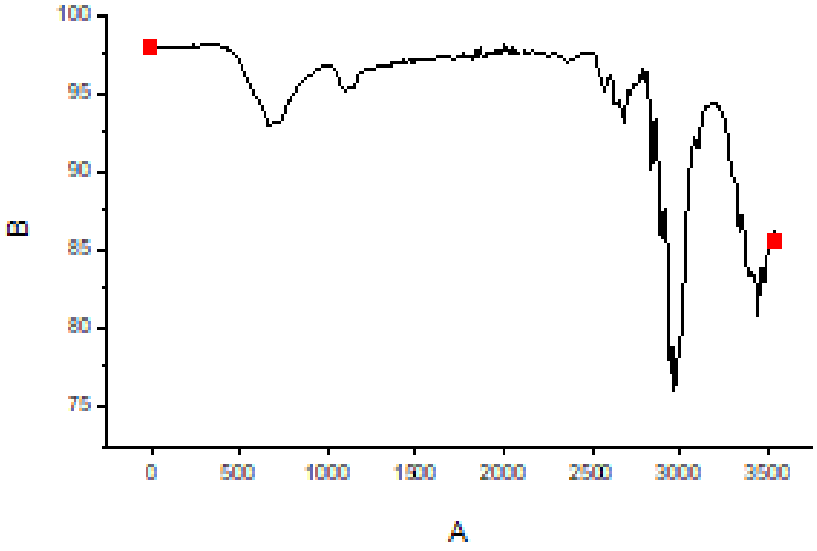



**Figure A.1.2.2 CNC with CNT 0% at PH10 (0.5 Tempo)**

CNC with 1.25 Tempo at PH10

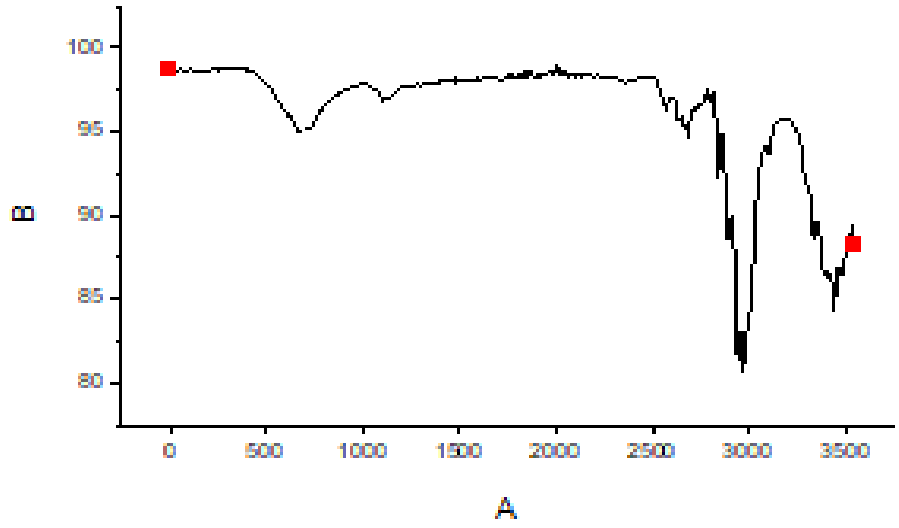



**Figure A.1.2.3 CNC with CNT 0% at PH10 (1.25 Tempo)**

Tempo 1.5

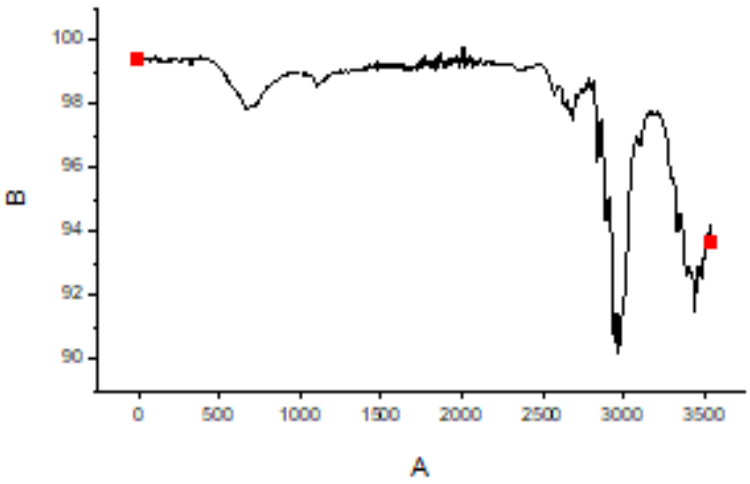



**Figure A.1.2.4 CNC with CNT 0% at PH10 (1.5 Tempo)**

## A.1.3 XRD

CNC Tempo 0.5 at PH10

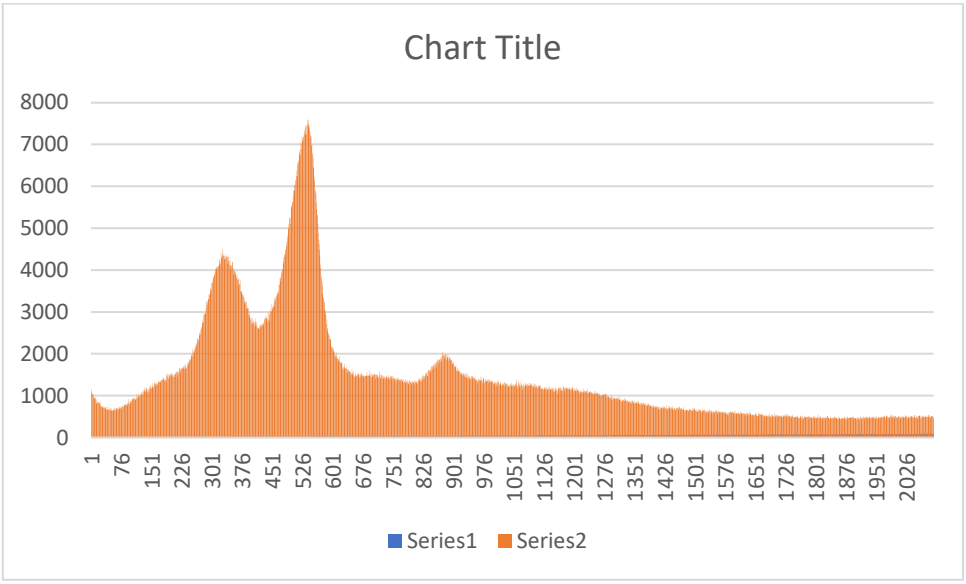



**Figure A.1.3.1 CNC with CNT 0% at PH10 (0.5 Tempo)**

CNC Tempo 1.25

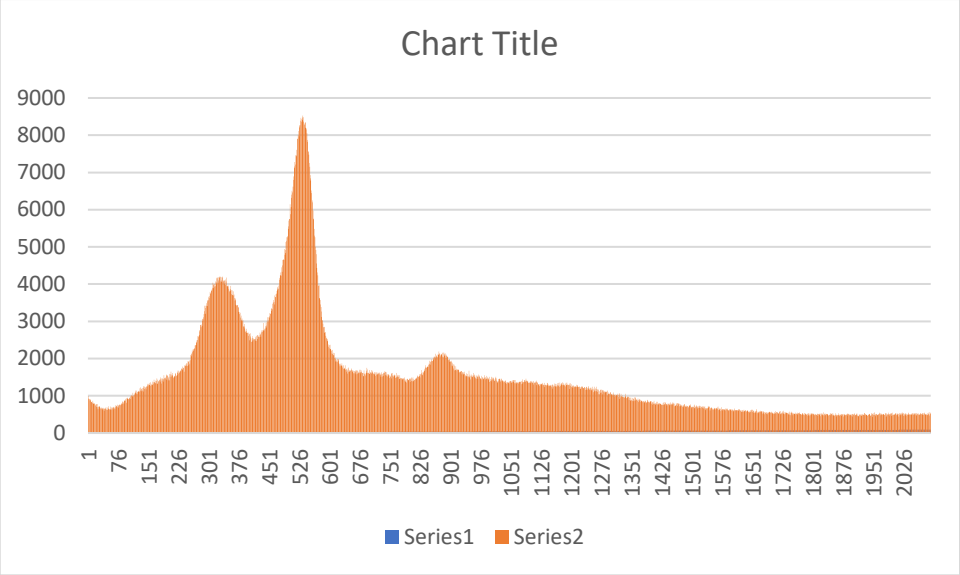



**Figure A.1.3.2 CNC with CNT 0% at PH10 (1.25 Tempo)**

CNC Tempo 1.5

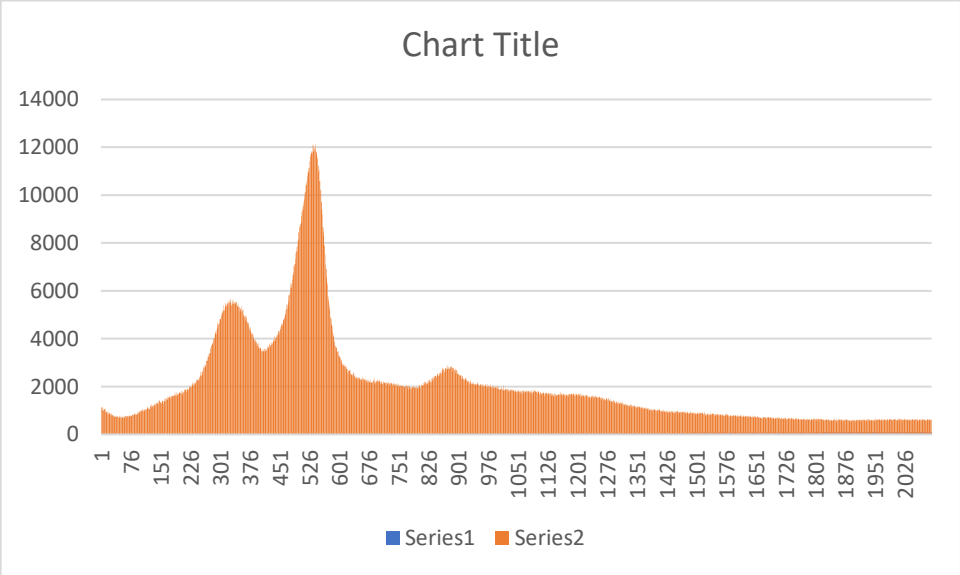



**Figure A.1.3.3 CNC with CNT 0% at PH10 (1.5 Tempo)**

CNC at PH7

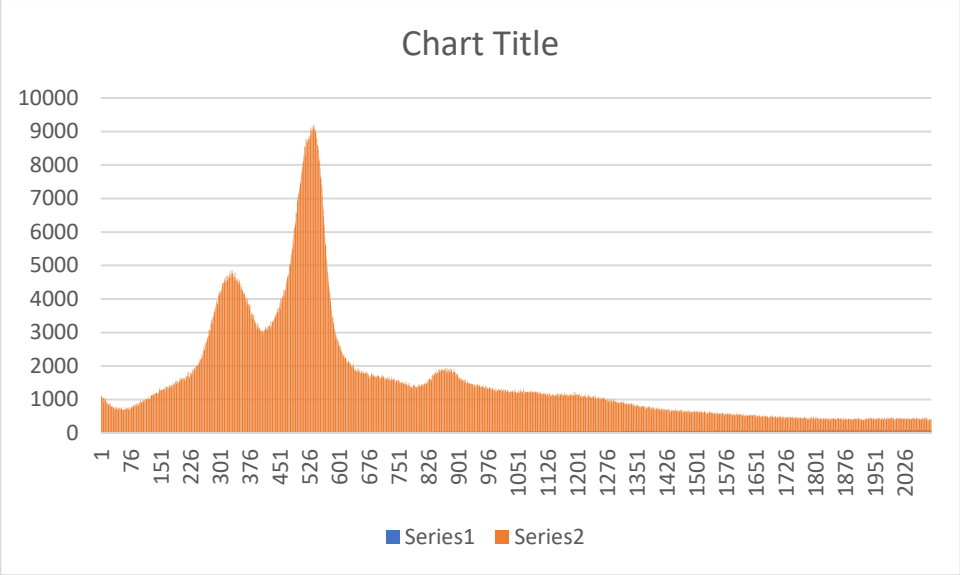



**Figure A.1.3.4 CNC with CNT 0% at PH7 (1 Tempo)**

## A.1.4 TEM

CNC 1Tempo at PH10

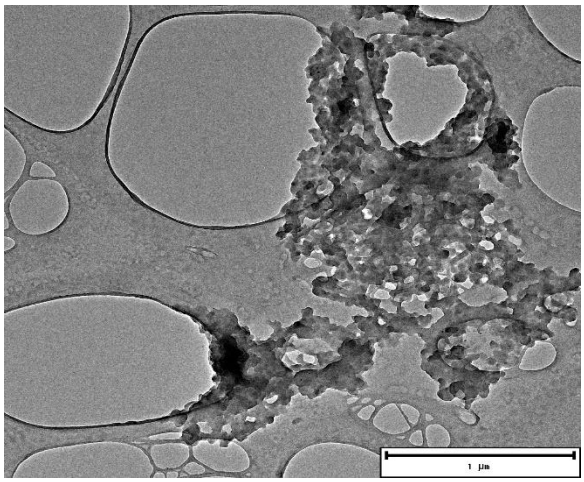


**Figure A.1.4.1 Image of CNC with CNT 0%**

CNC Tempo 1.5 at PH10

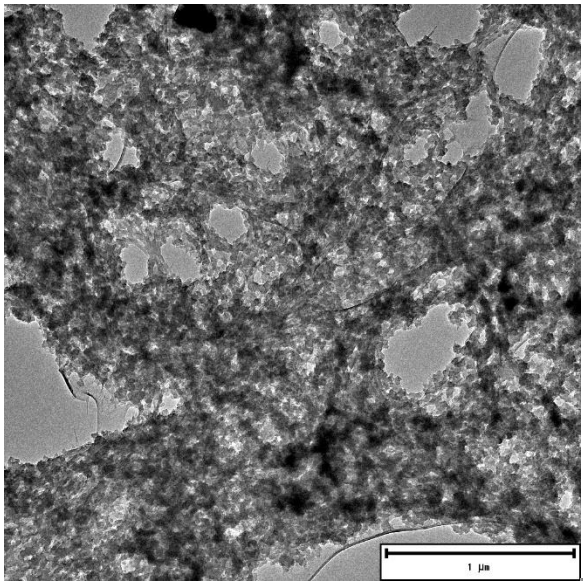



**Figure A.1.4.2 Image of CNC 1.5 Tempo at PH10**

CNC 1Tempo at PH7

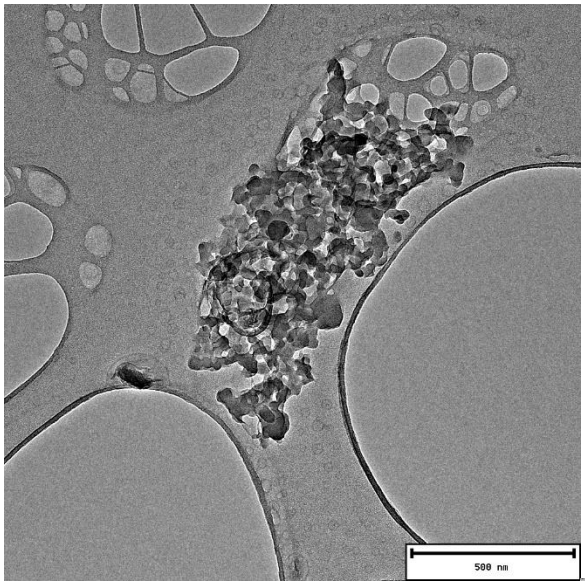



**Figure A.1.4.3 Image of CNC 1 Tempo at PH7**

## A.1.5 SEM

CNC PH7

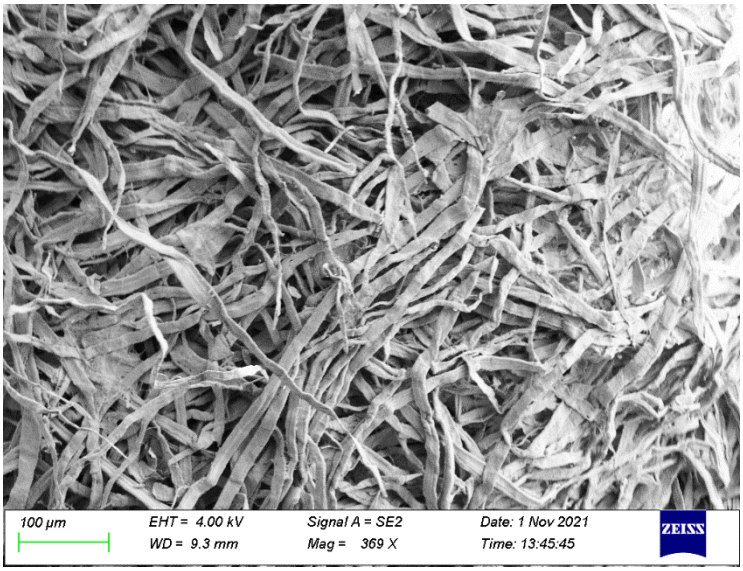



**Figure A.1.5.1 Image of CNC with 1 Tempo at PH7**

CNC Tempo 0.5

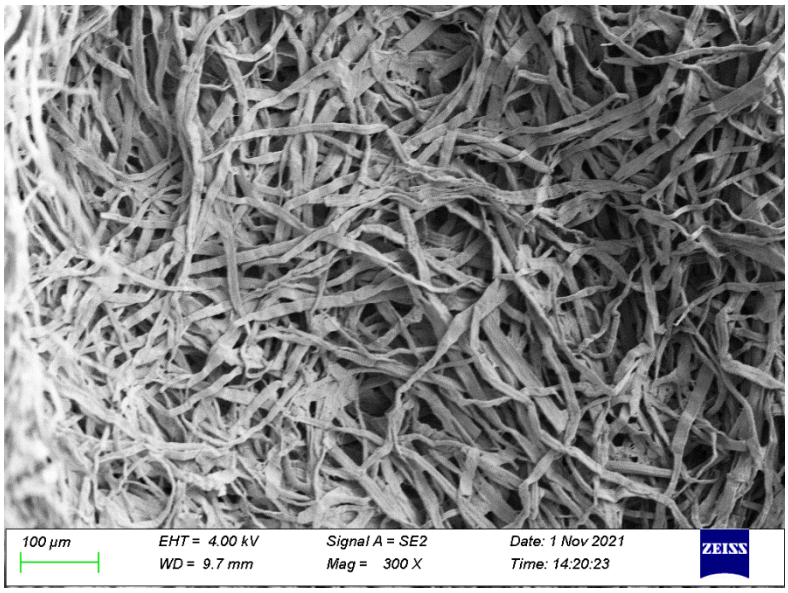



**Figure A.1.5.2 Image of CNC with 0.5 Tempo at PH10**

CNC Tempo 1

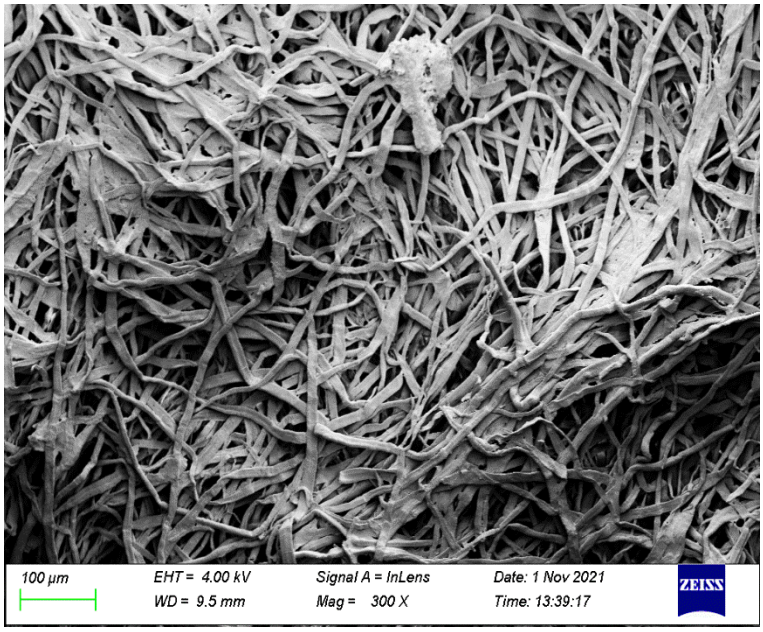



**Figure A.1.5.3 Image of CNC with 1 Tempo at PH10**

CNC Tempo 1.5

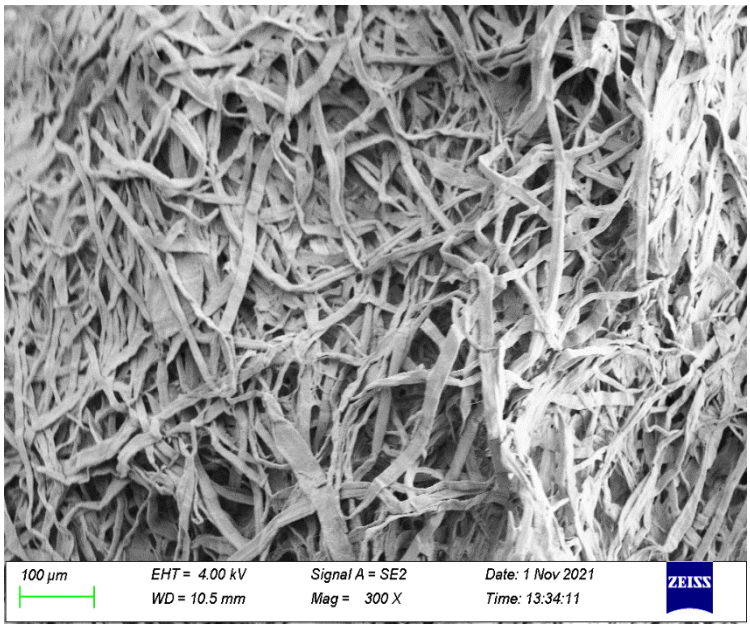



**Figure A.1.5.4 Image of CNC with 1.5 Tempo at PH10**

CNC Tempo 1.25

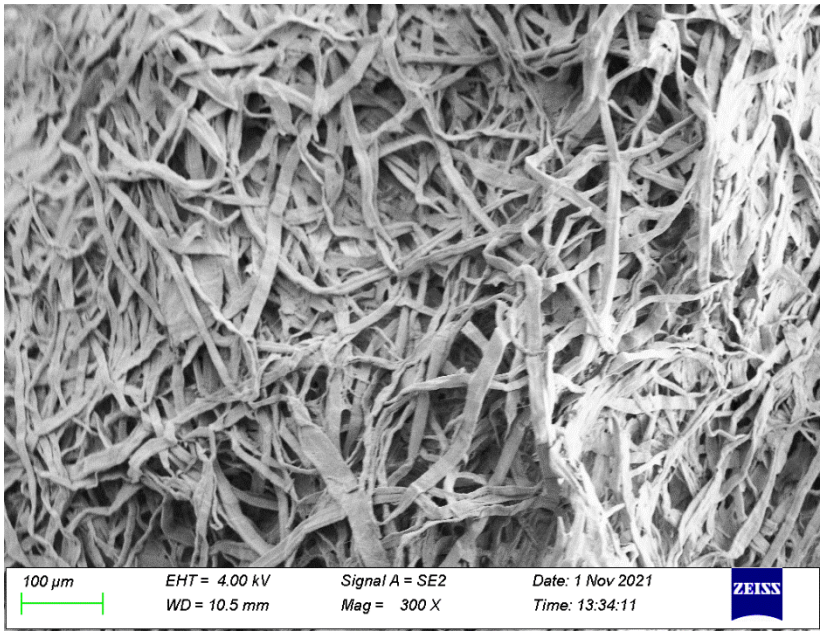



**Figure A.1.5.5 Image of CNC with 1.25 Tempo at PH10**

# A.2 CNT

## A.2.1 SEM

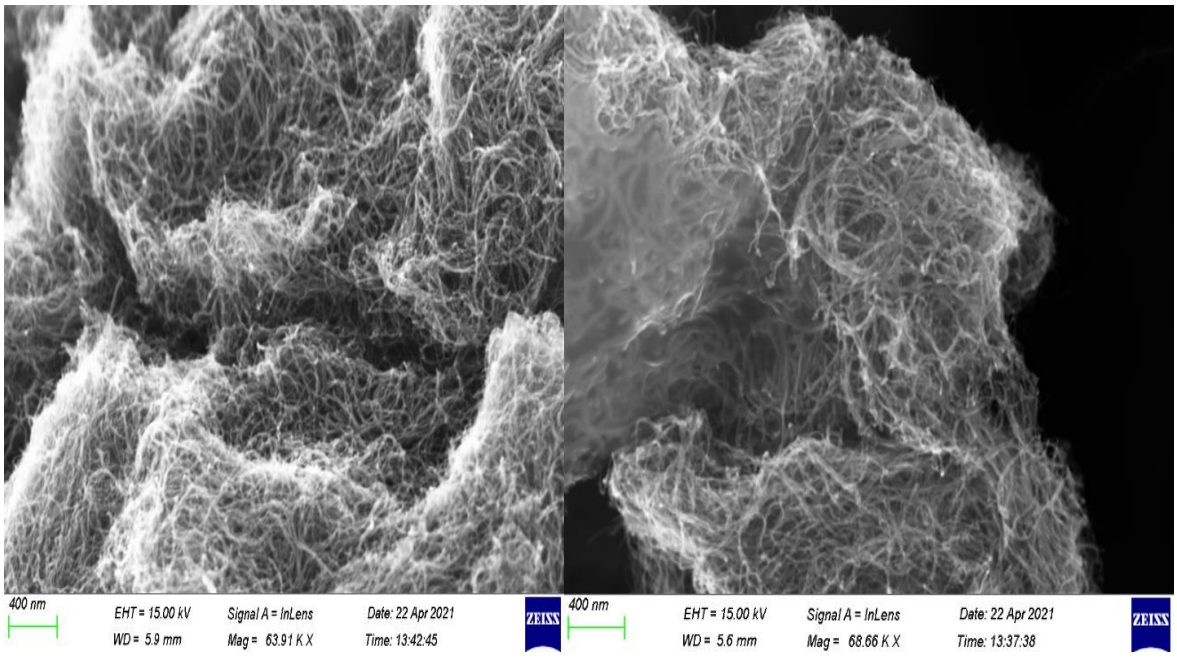



**Figure A.2.1.1 CNT (03) and (02)**

# A.3 CNC doped with CNT in Wt%

## A.3.1 Raman

CNC-CNT 0.05 %

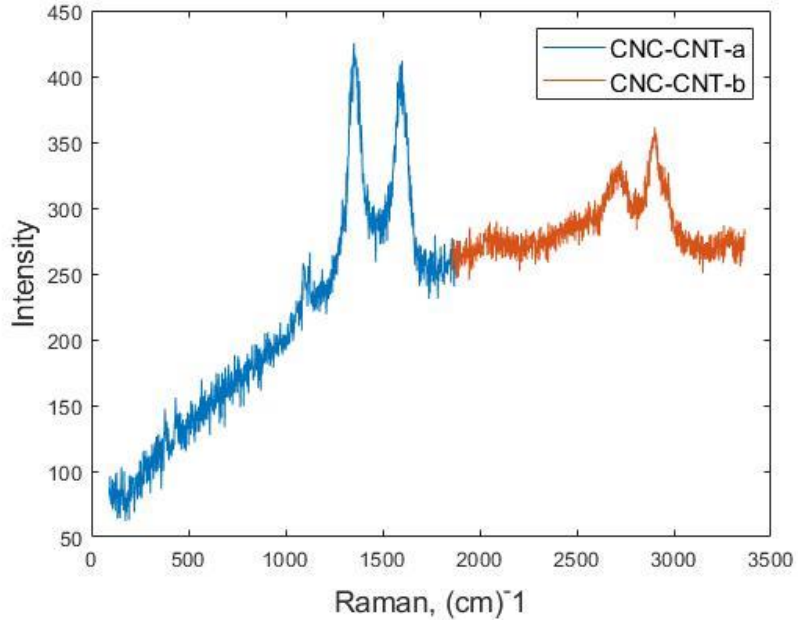



**Figure A.3.1.1.a CNC with CNT O.05% a-b range**

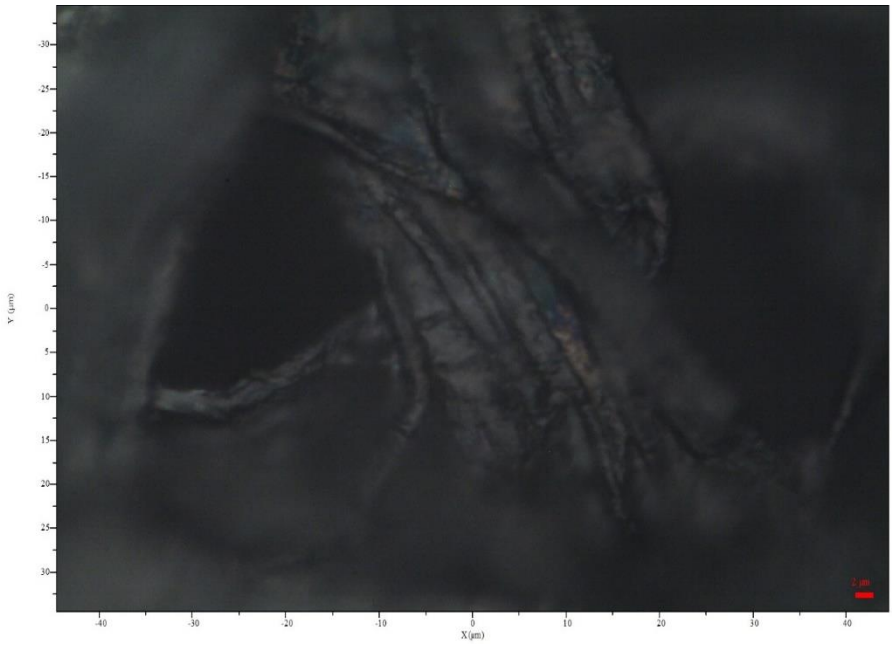


**Figure A.3.1.1.b Image of CNC with CNT O.05% a-b range**

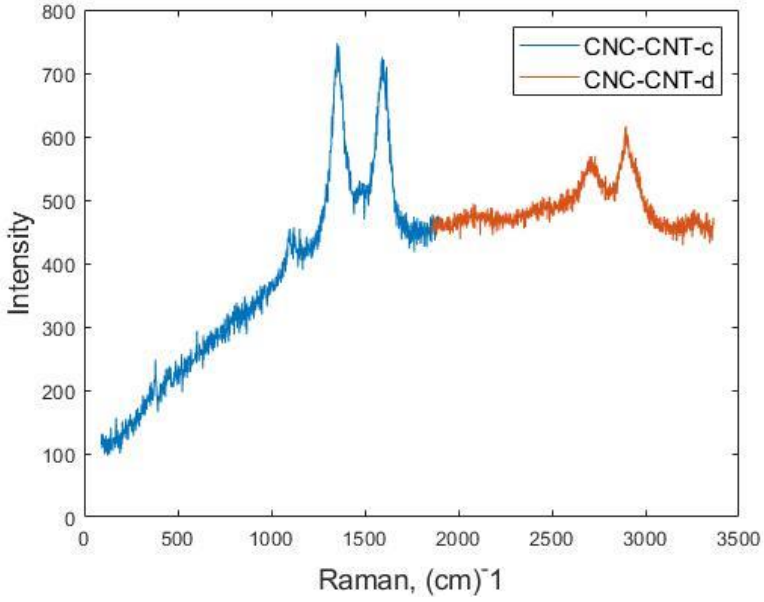



**Figure A.3.1.1.c CNC with CNT O.05% c-d**

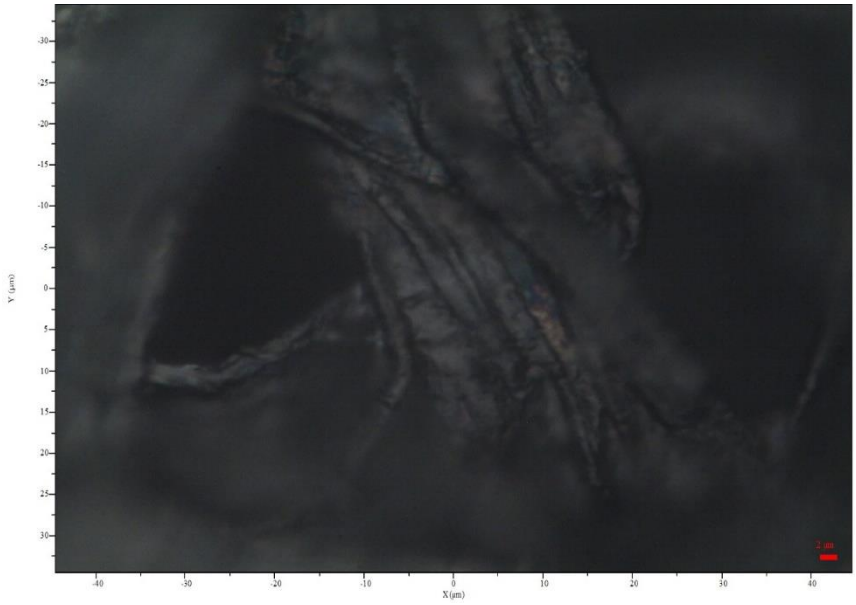


**Figure A.3.1.1.d Image of CNC with CNT O.05% c-d**

CNC-CNT 0.075 %

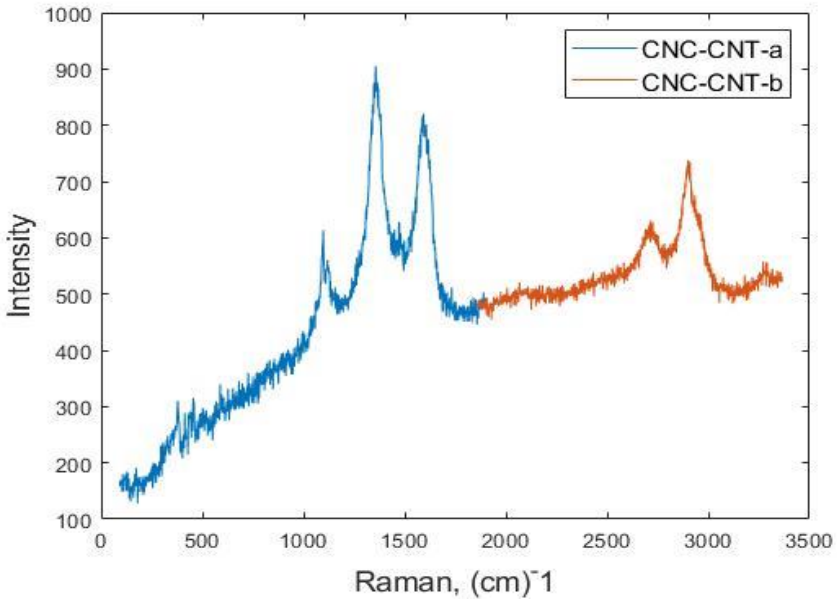



**Figure A.3.1.2.a CNC with CNT O.075% a-b**

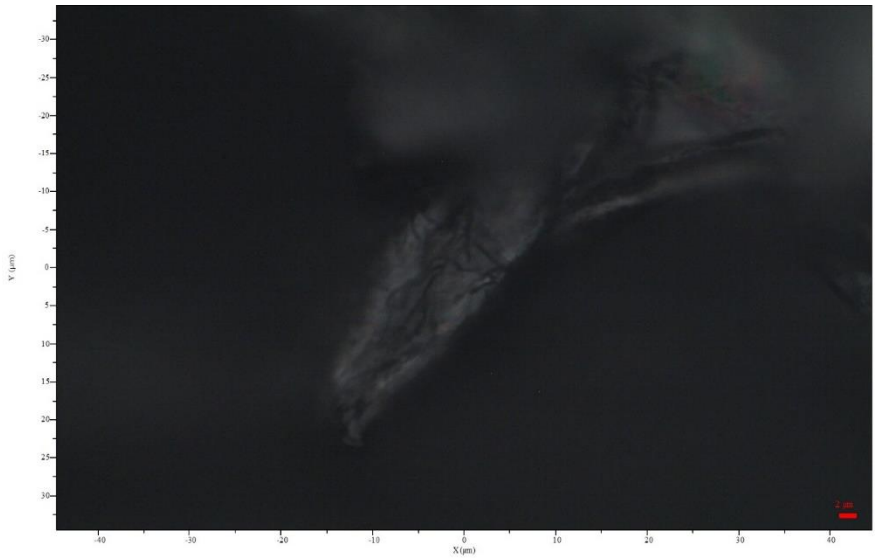


**Figure A.3.1.2.b Image of CNC with CNT O.075% a-b**

CNC-CNT 0.14 %

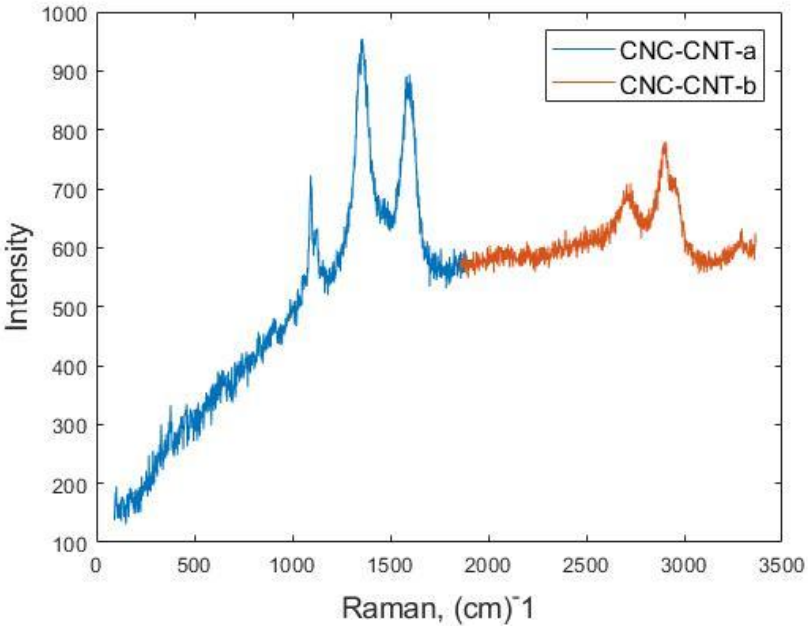



**Figure A.3.1.3.a CNC with CNT O.14% a-b**

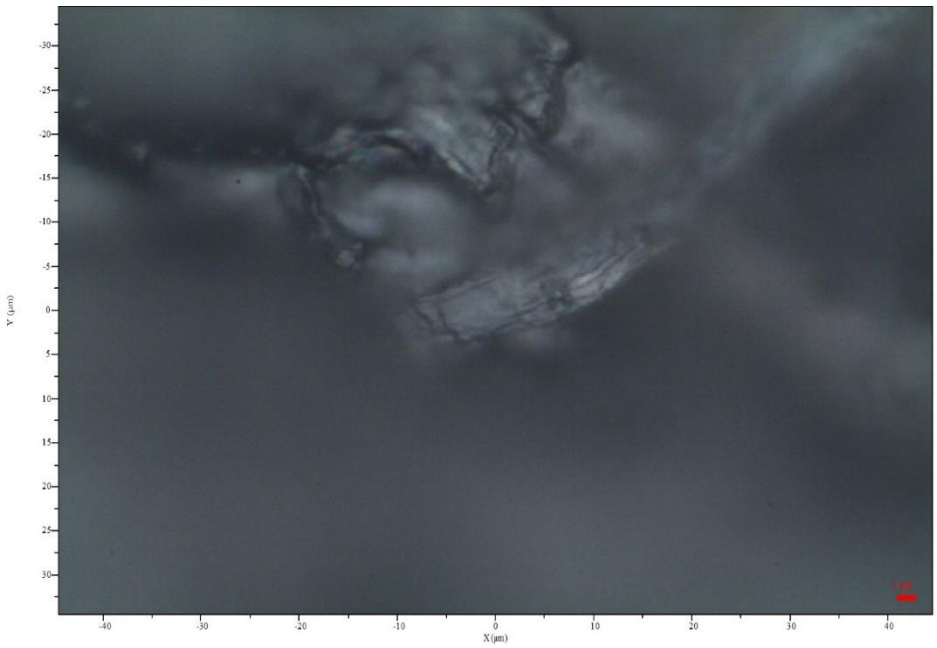


**Figure A.3.1.3.b Image of CNC with CNT O.14% a-b**

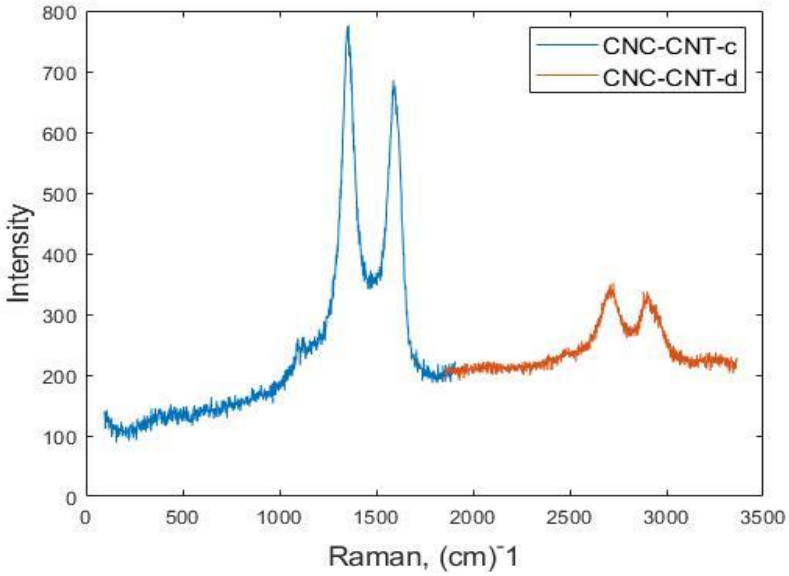



**Figure A.3.1.3.c CNC with CNT O.14% c-d**

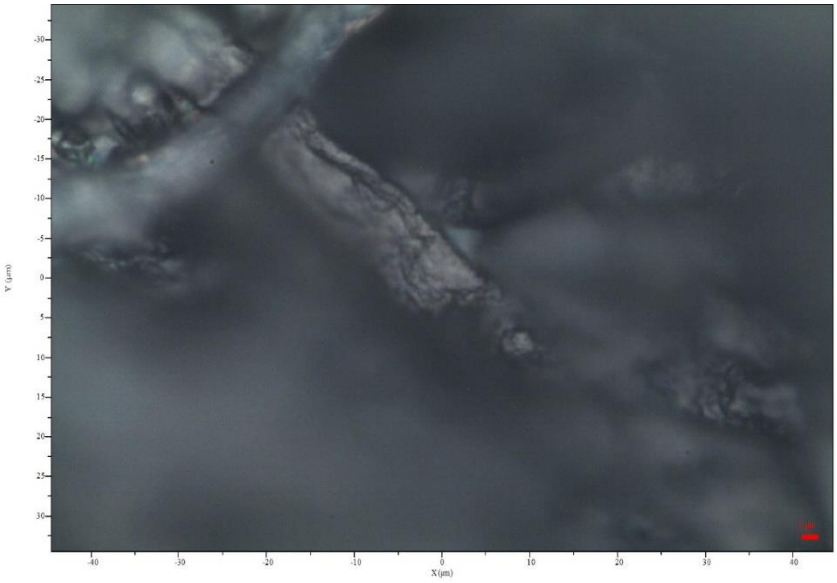


**Figure A.3.1.3.d Image of CNC with CNT O.14% c-d**

CNC-CNT 0.25 %

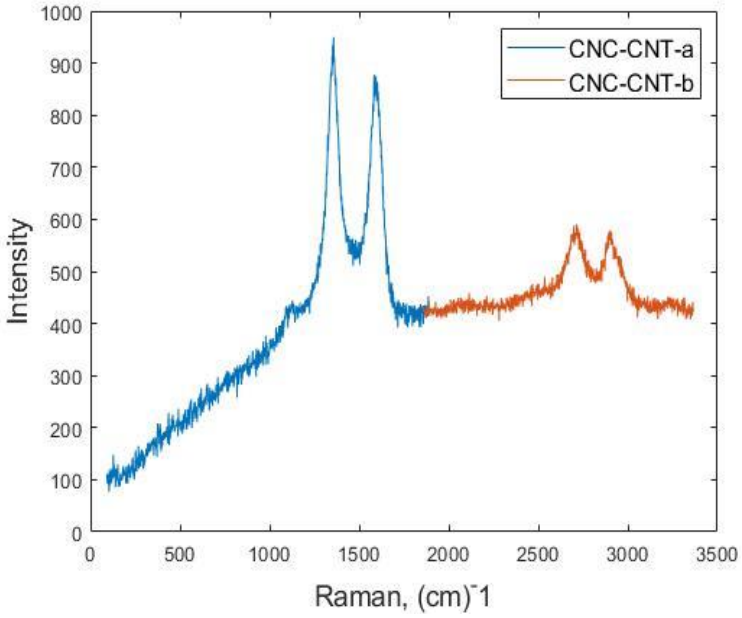



**Figure A.3.1.4.a CNC with CNT O.25% a-b**

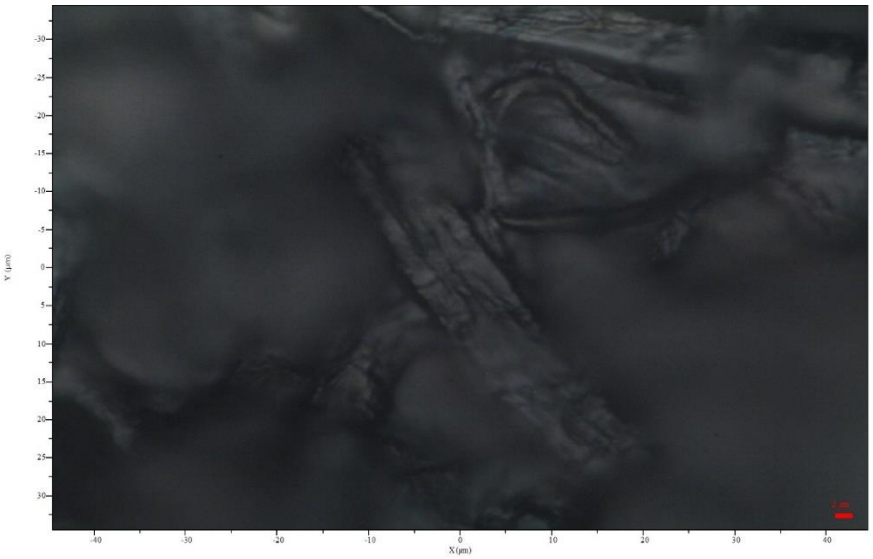


**Figure A.3.1.4.b Image of CNC with CNT O.25% a-b**

CNC-CNT 0.5 %

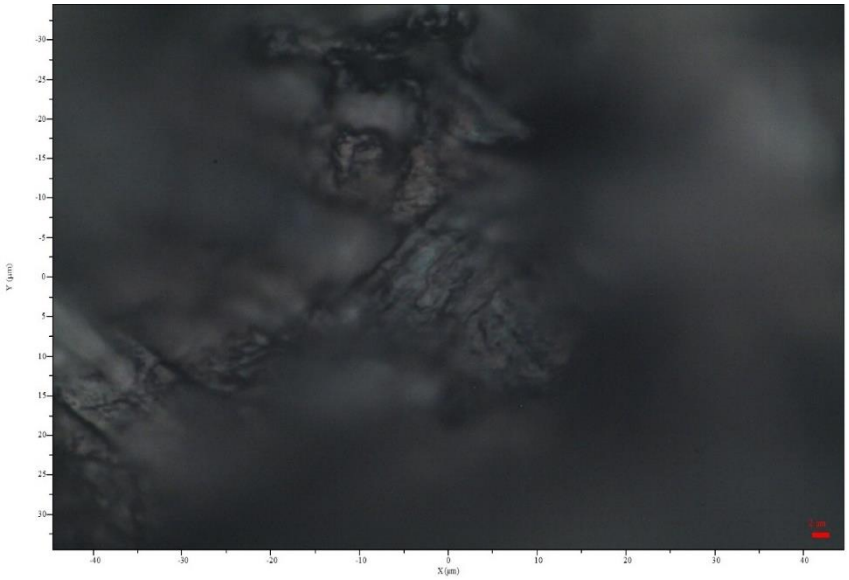


**Figure A.3.1.5 Image of CNC with CNT O.5% a-b**

CNC-CNT 0.75 %

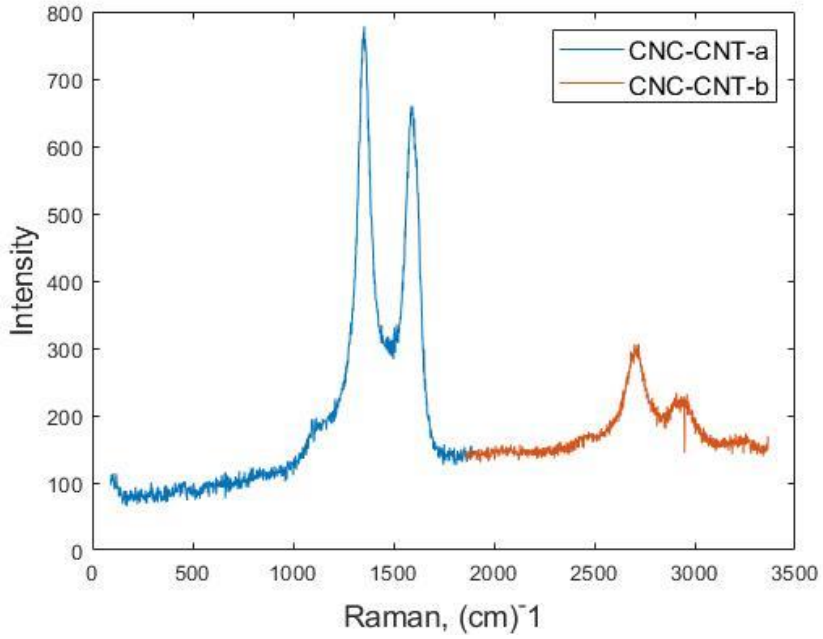



**Figure A.3.1.6.a CNC with CNT O.75% a-b**

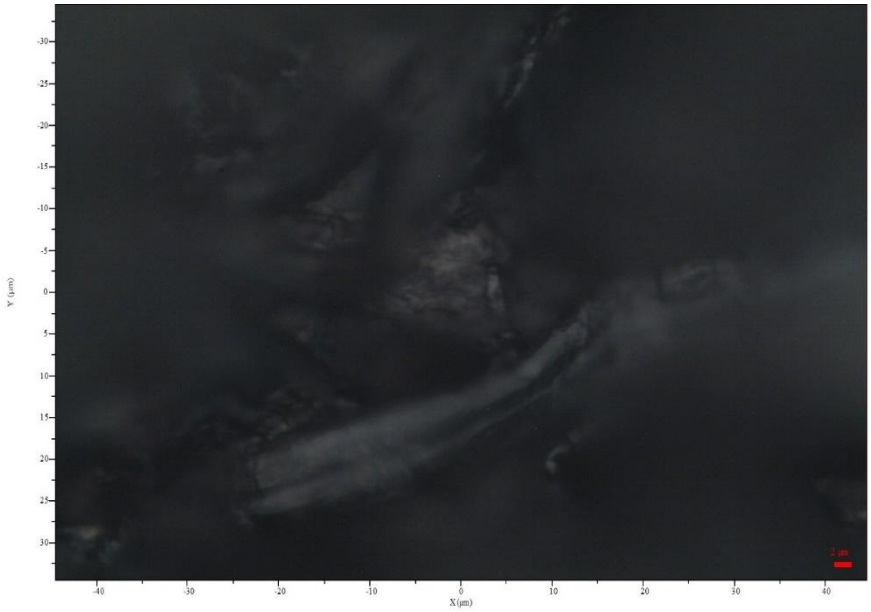


**Figure A.3.1.6.b Image of CNC with CNT O.75% a-b**

CNC-CNT 1 %

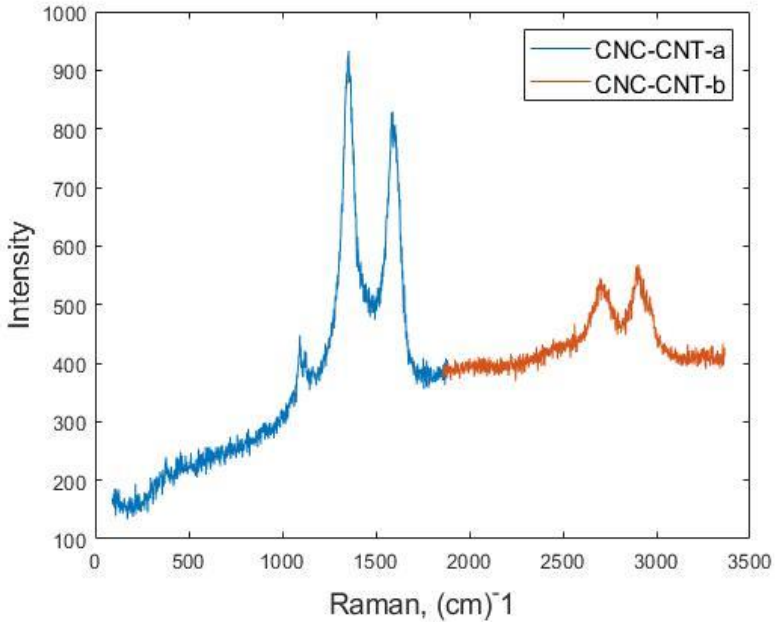



**Figure A.3.1.7.a CNC with CNT 1% a-b**

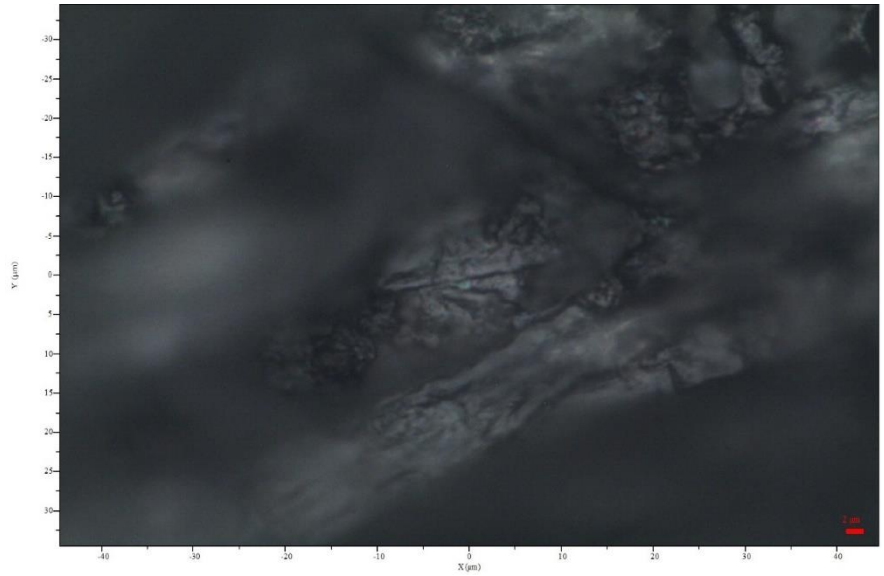


**Figure A.3.1.7.b Image of CNC with CNT 1% a-b**

CNC-CNT 1.5 %

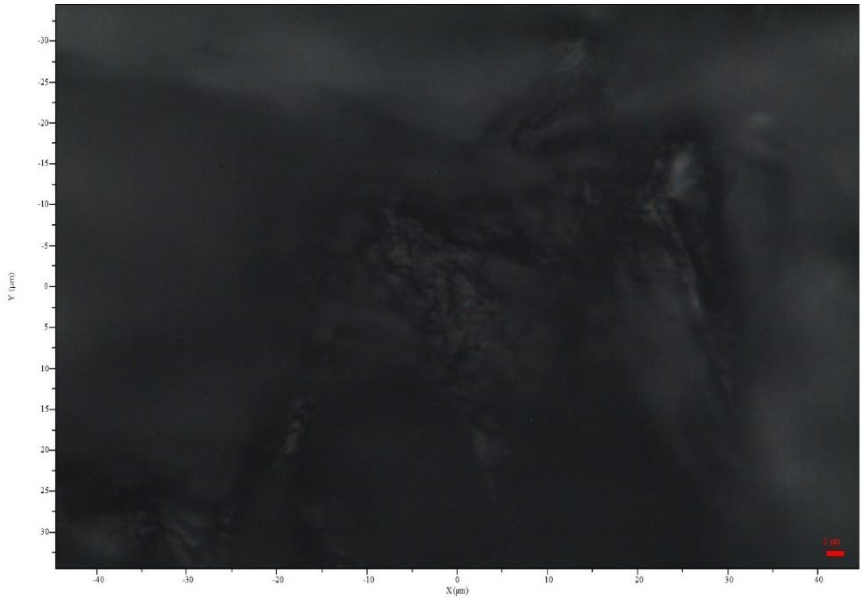


**Figure A.3.1.8 Image of CNC with CNT 1.5% a-b**

CNC-CNT 2 %

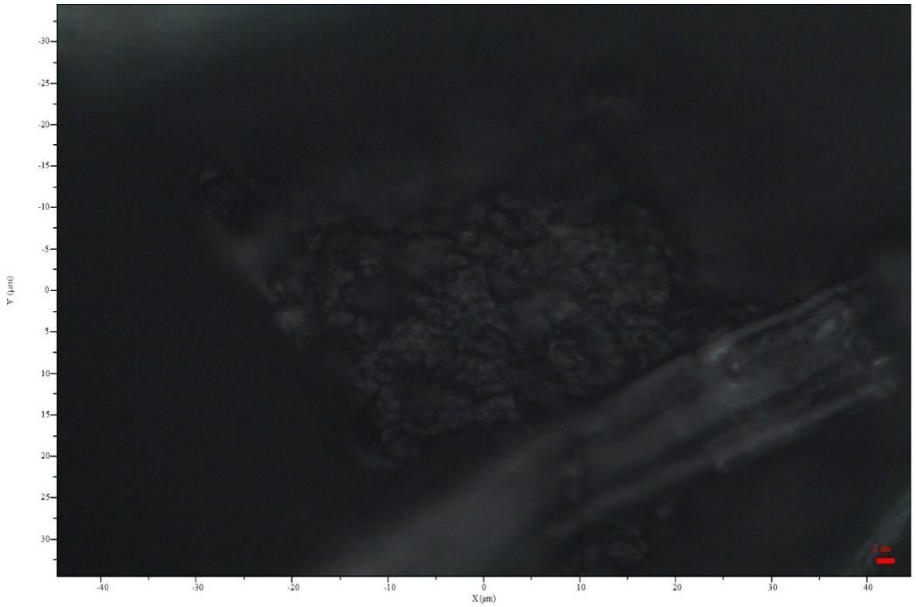


**Figure A.3.1.9.a Image of CNC with CNT 2% a-b**

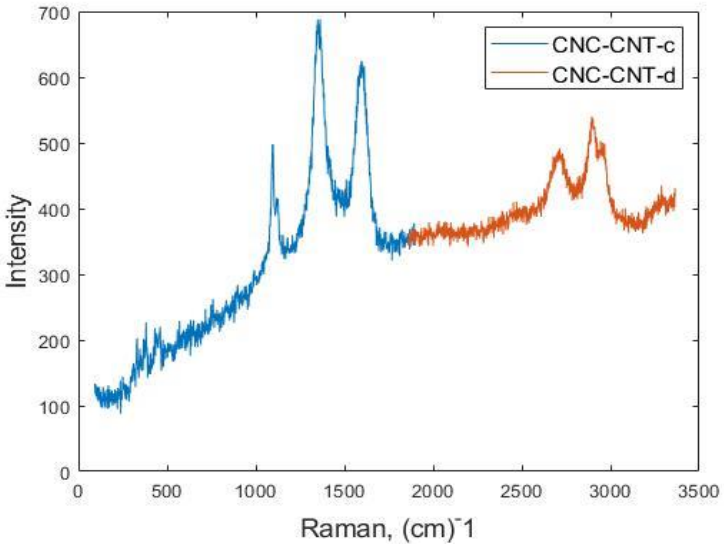



**Figure A.3.1.9.b CNC with CNT 2% c-d**

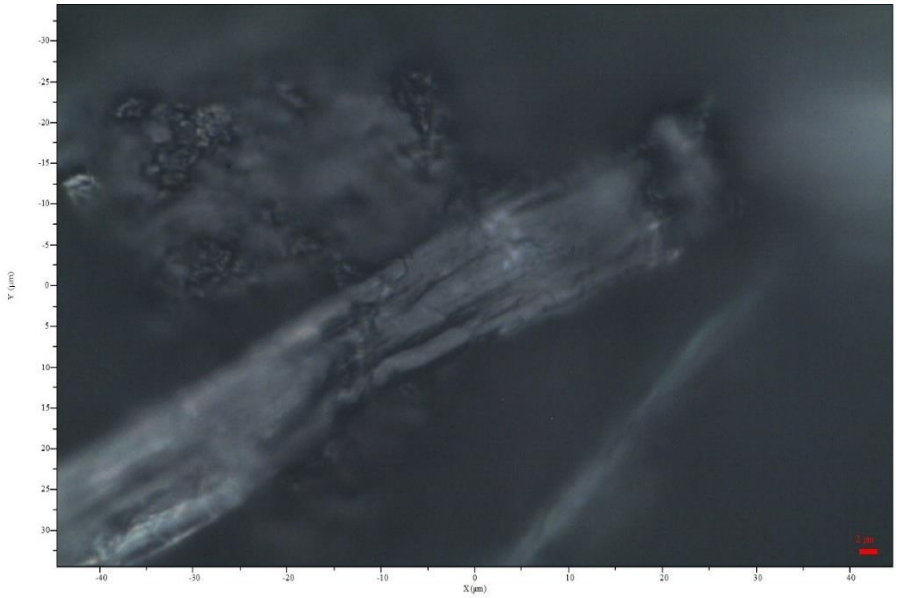


**Figure A.3.1.9.c Image of CNC with CNT 2% c-d range**

CNC-CNT 2.5 %

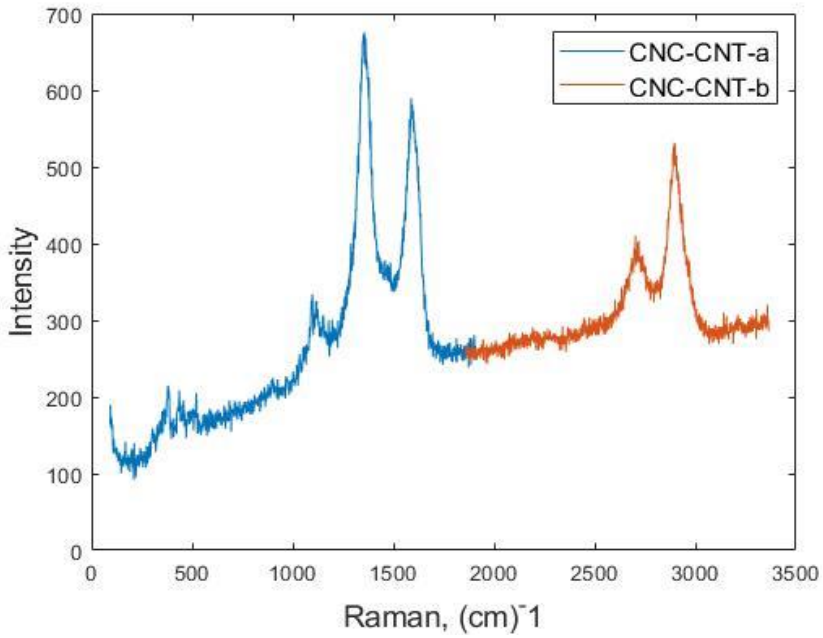



**Figure A.3.1.10.a CNC with CNT 2.5% a-b range**

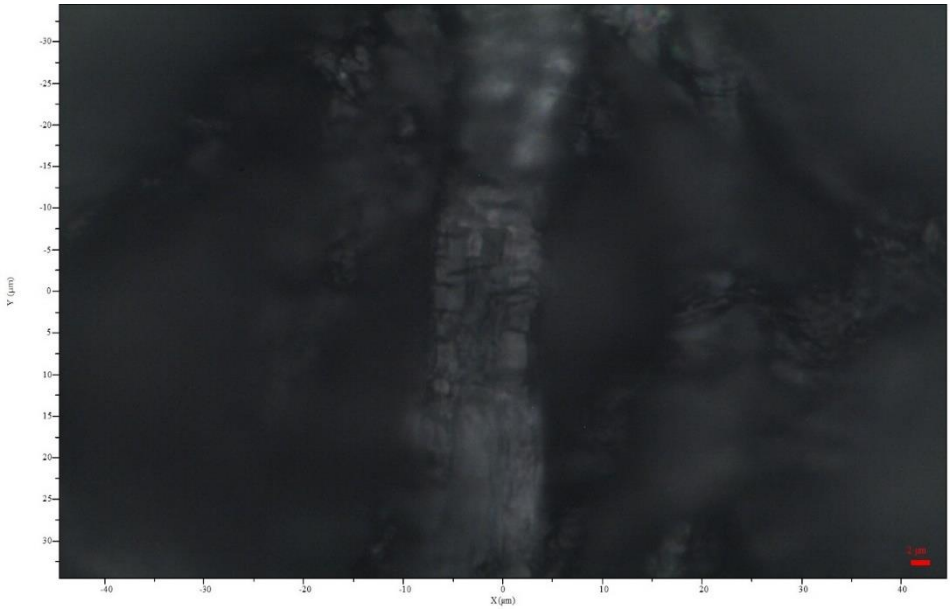


**Figure A.3.1.10.b Image of CNC with CNT 2.5% a-b range**

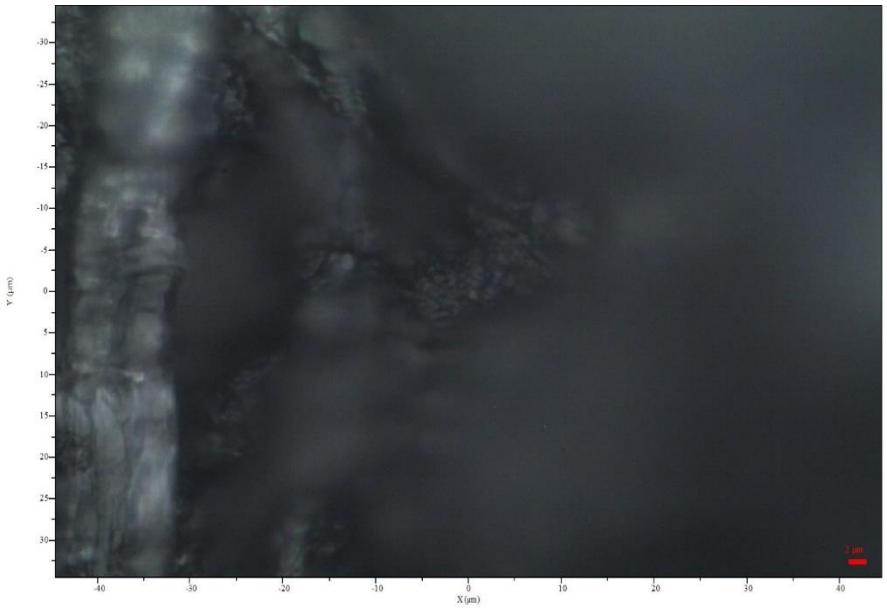


**Figure A.3.1.10.c Image of CNC with CNT 2.5% c-d range**

## A3.2 FTIR

Sample 2 CNC-CNT 0.05%

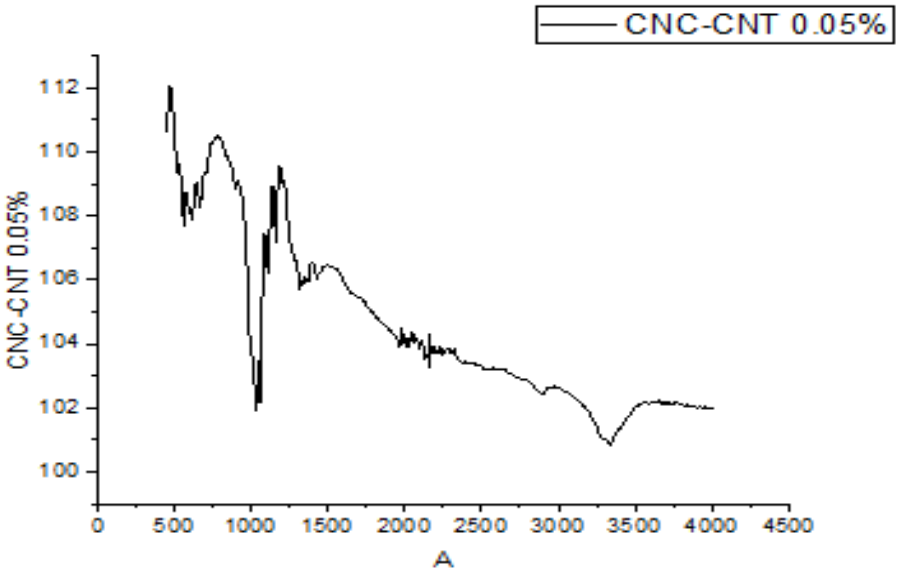



**Figure A.3.2.1 CNC with CNT 0.05 % at PH10**

Sample 3 CNC-CNT 0.075%

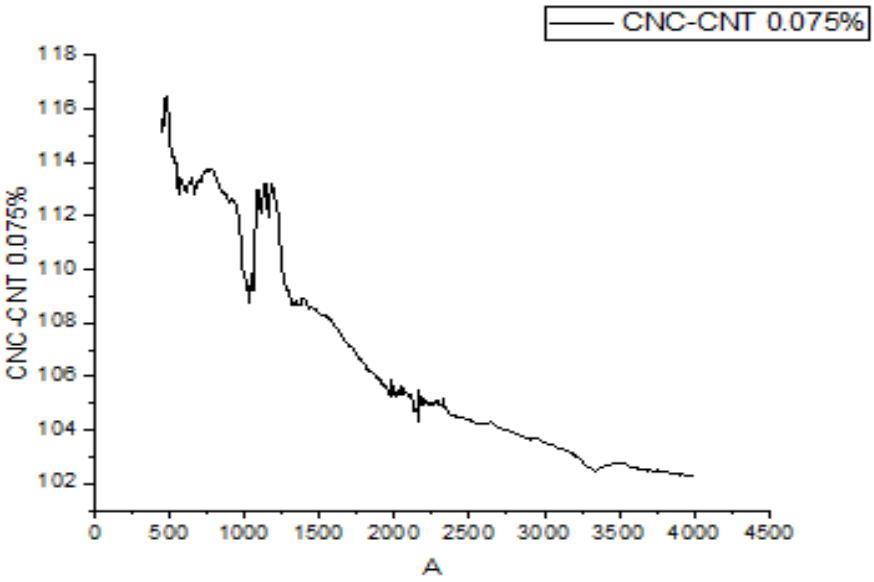



**Figure A.3.2.2 CNC with CNT 0.075 % at PH10**

Sample 4 CNC-CNT 0.14%

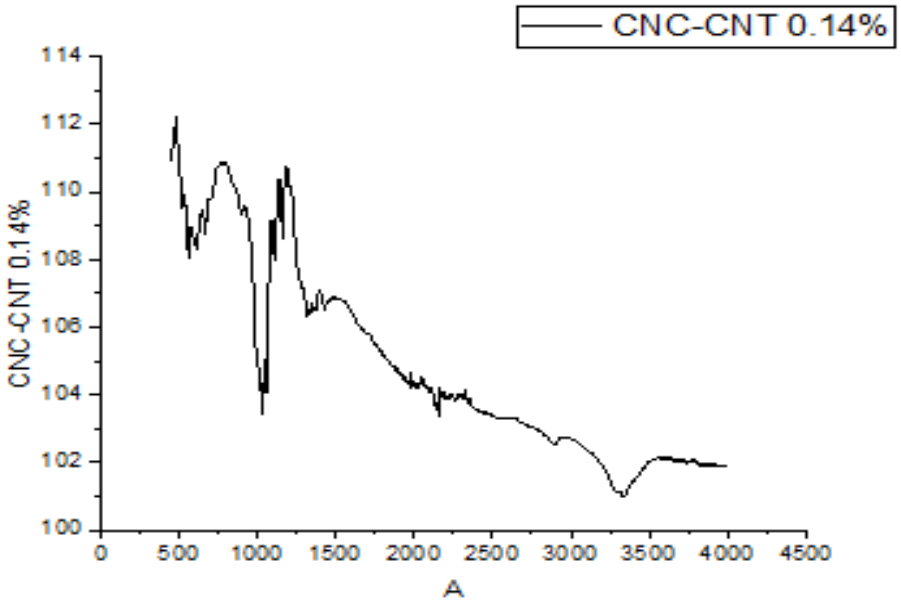



**Figure A.3.2.3 CNC with CNT 0.14 % CNC at PH10**

Sample 5 CNC-CNT 0.25 %

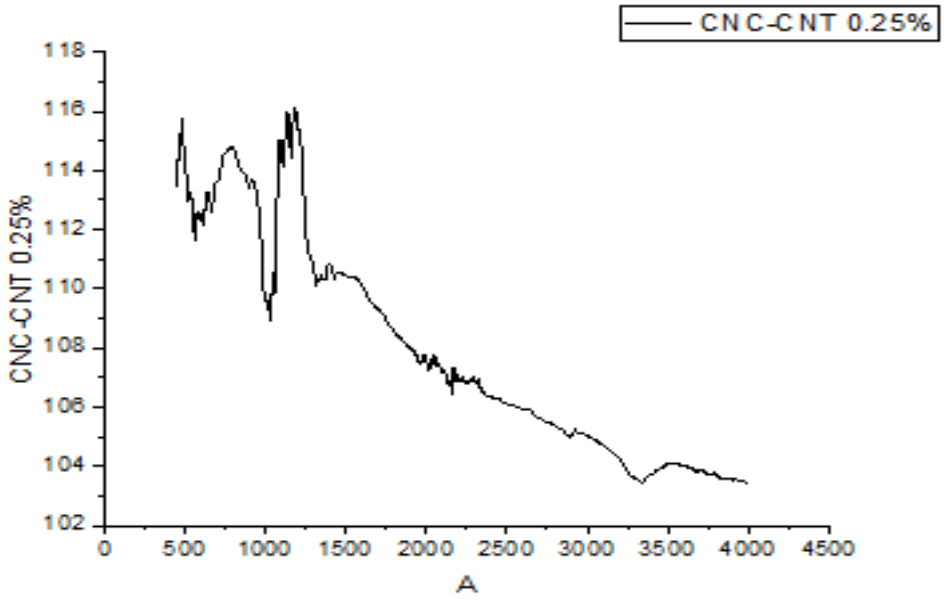



**Figure A.3.2.4 CNC with CNT 0.25 % CNC at PH10**

Sample 7 CNC-CNT 0.75% at PH10

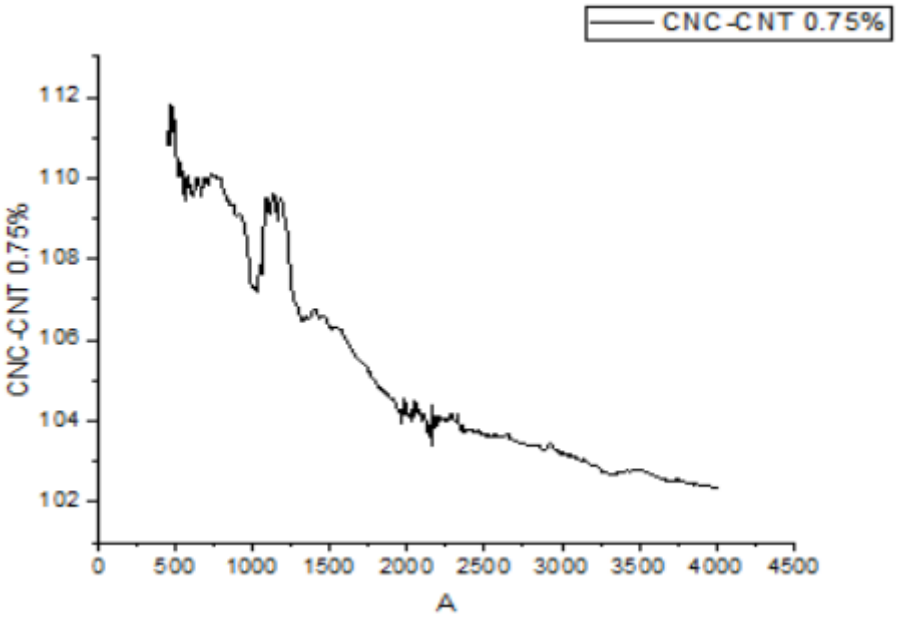



**Figure A.3.2.5 CNC with CNT 0.75 %  CNC at PH10**

## A.3.3 XRD

CNC with doped CNT 0.05% at PH10

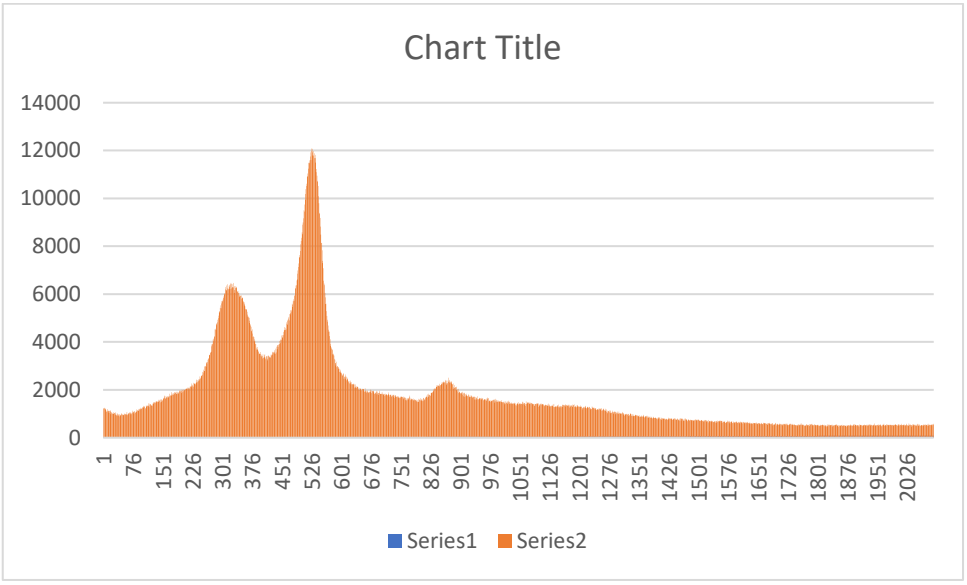



**Figure A.3.3.1 CNC with CNT 0.05 % at PH10**

CNC with doped CNT 0.075% at PH10

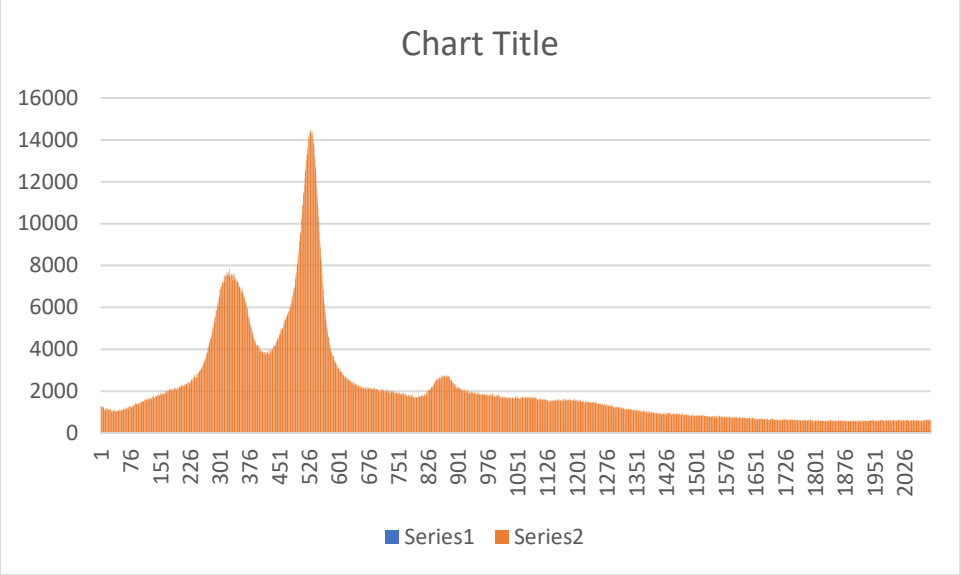



**Figure A.3.3.2 CNC with CNT 0.075 % at PH10**

CNC with doped CNT 0.14%

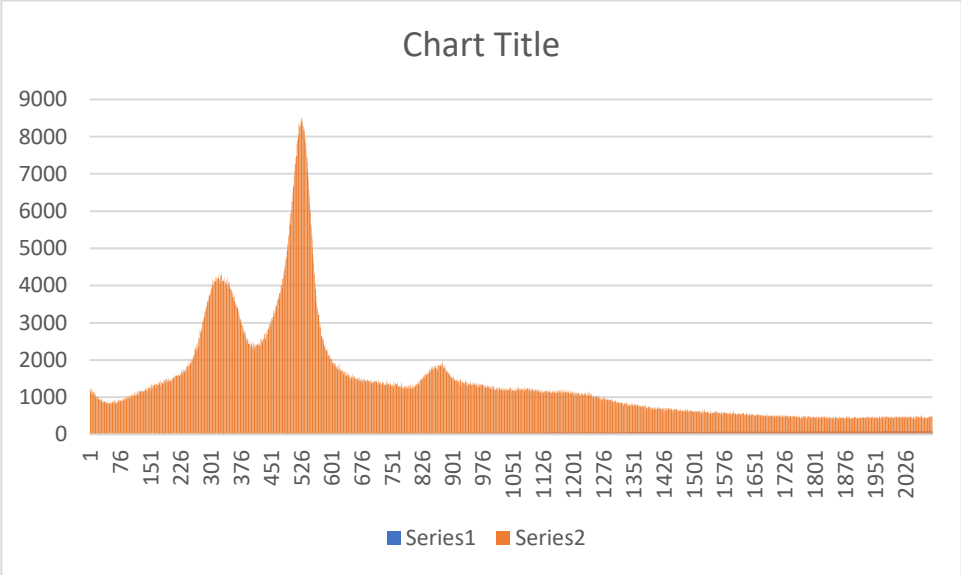



**Figure A.3.3.3 CNC with CNT 0.14 % at PH10**

CNC with CNT 0.25% at PH10

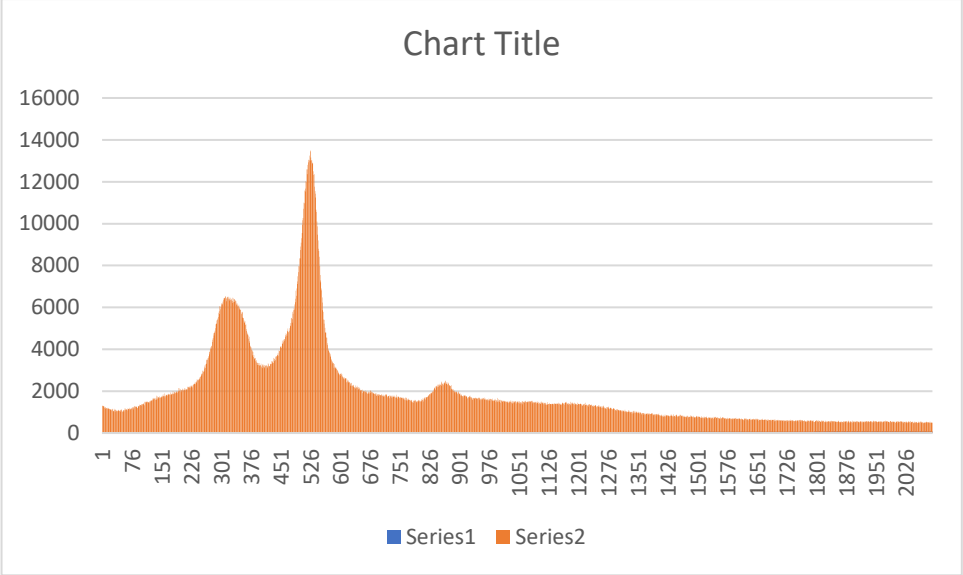



**Figure A.3.3.4 CNC with CNT 0.25 % at PH10**

CNC with doped CNT 0.75% at PH 10

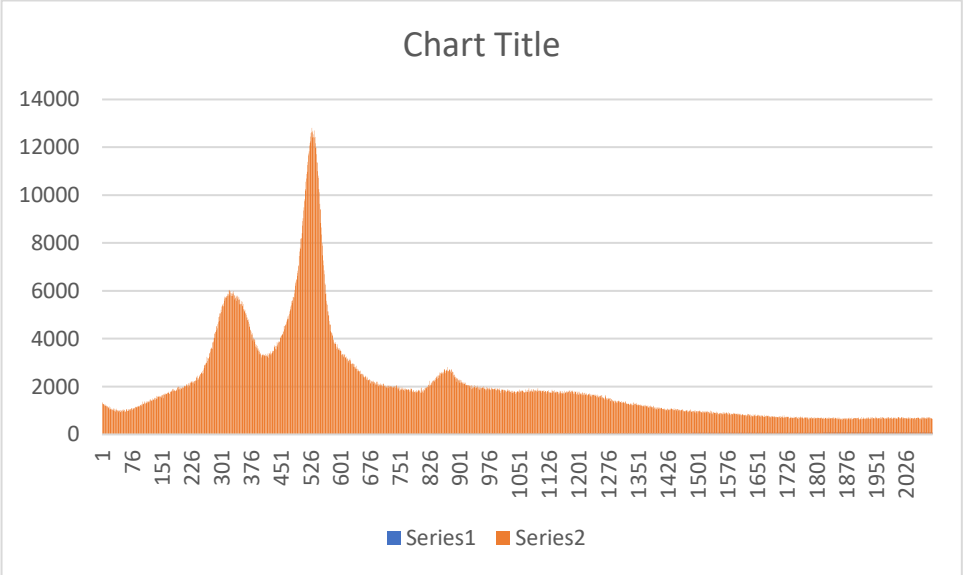



**Figure A.3.3.5 CNC with CNT 0.75 %, CNC at PH10**

## A.3.4 TGA and DTA

Sample CNC-CNT 0.075%

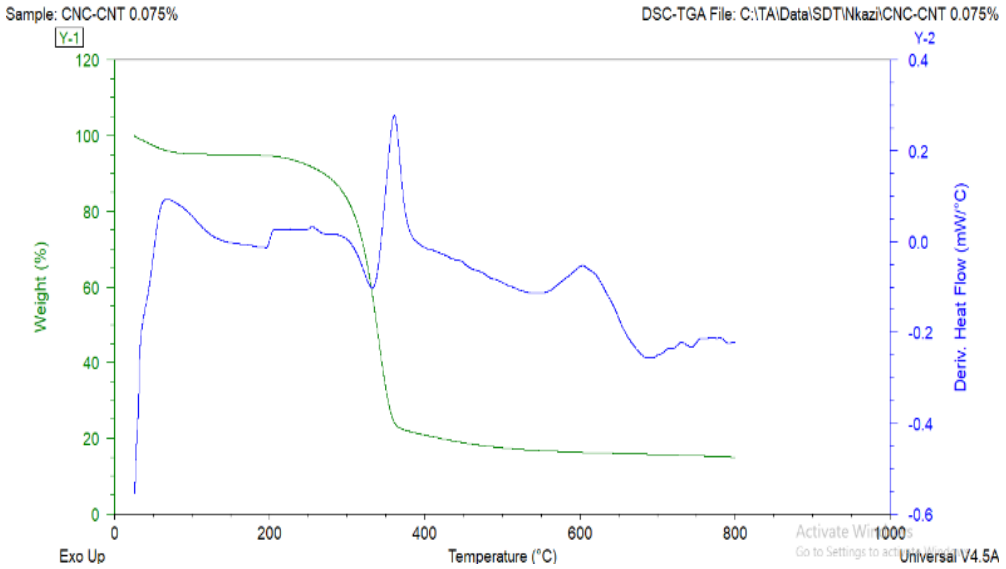



**Figure A.3.4.1 Sample CNC-CNT 0.075%**

Sample CNC-CNT 0.14%

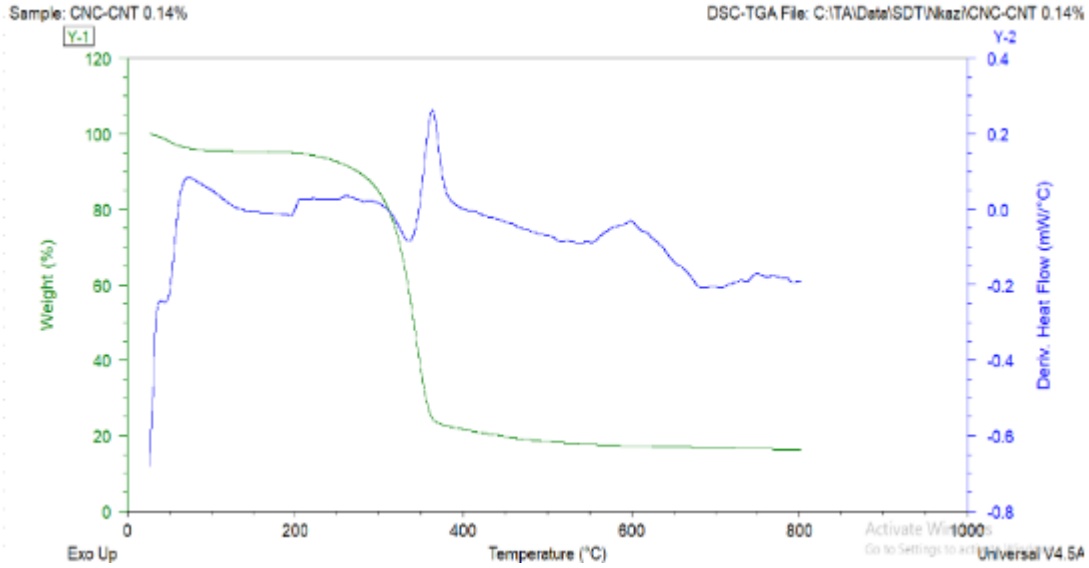



**Figure A.3.4.2 Sample CNC-CNT 0.14%**

Sample CNC-CNT 0.25%

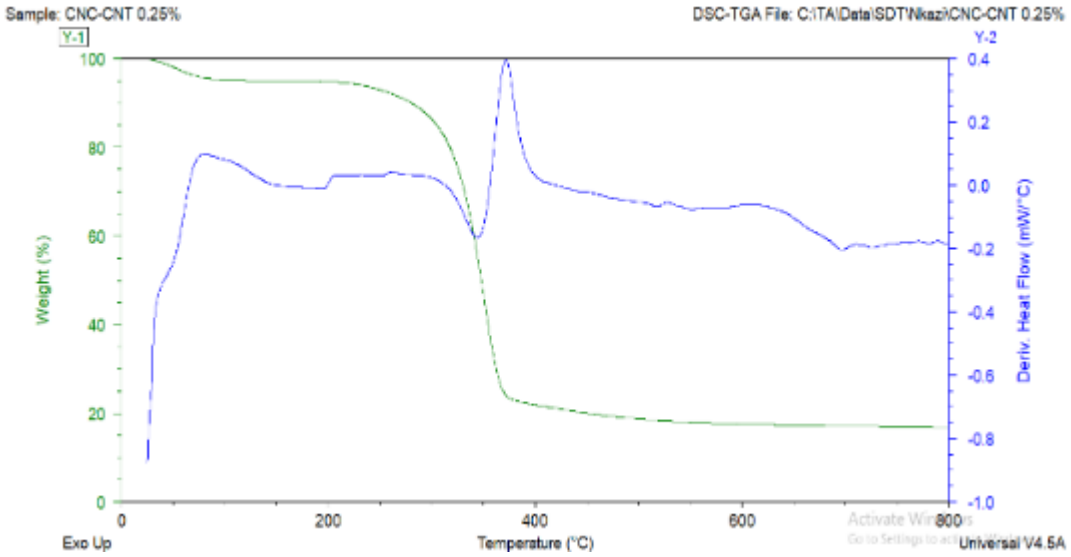



**Figure A.3.4.3 Sample CNC-CNT 0.25%**

Sample CNC-CNT 0.75%

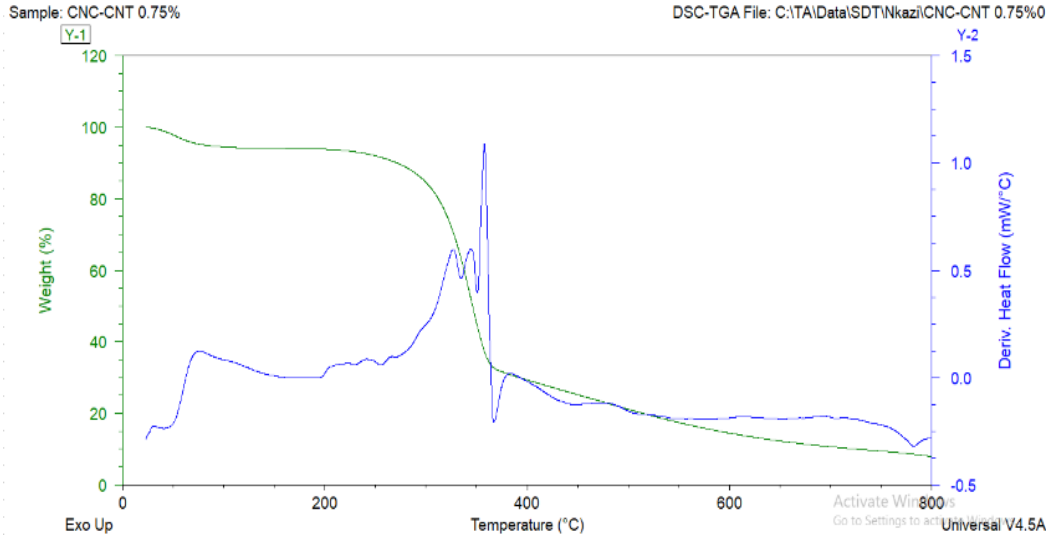



**Figure A.3.4.4 Sample CNC-CNT 0.75%**

## A.3.5 TEM

CNC CNT 0.05%

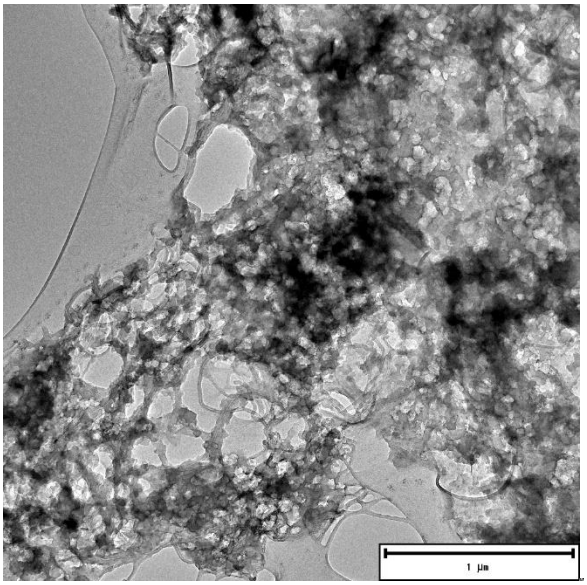



**Figure A.3.5.1 Image of CNC with CNT 0.05%**

CNC CNT 0.075%

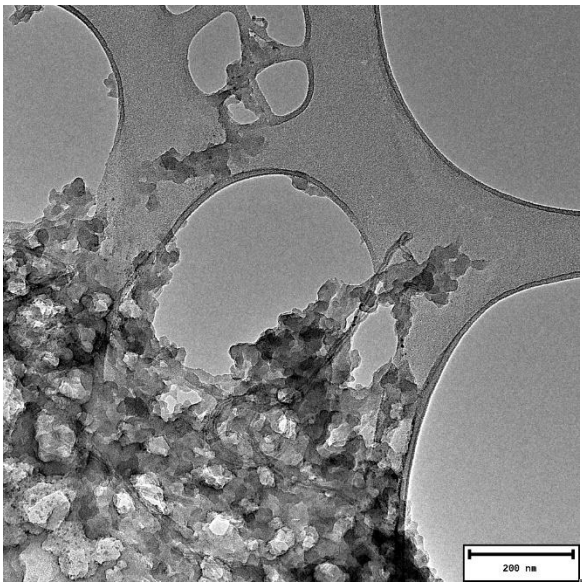



**Figure A.3.5.2 Image of CNC with CNT 0.075%**

CNC CNT 0.14%

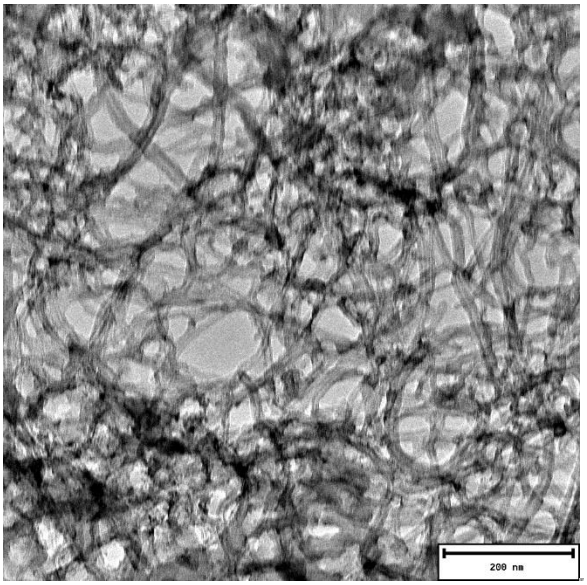



**Figure A.3.5.3 Image of CNC with CNT 0.14%**

CNC CNT 0.25%

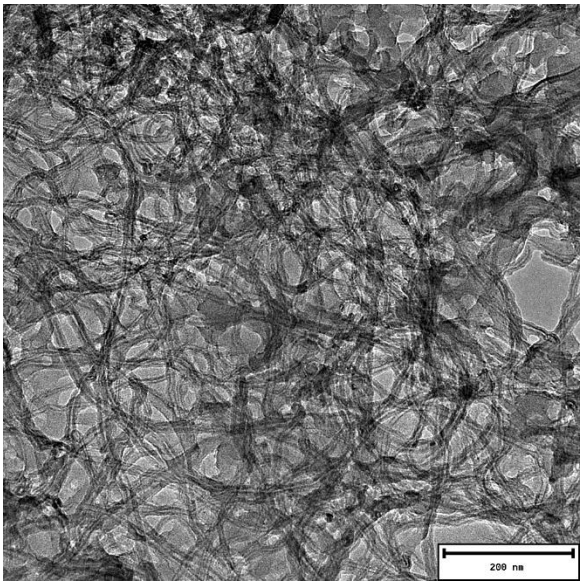



**Figure A.3.5.4 Image of CNC with CNT 0.25%**

CNC CNT 0.75%

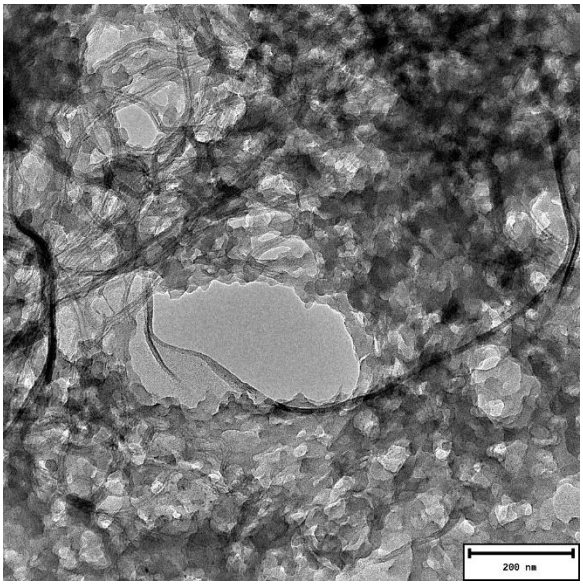



**Figure A.3.5.5 Image of CNC with CNT 0.75%**

## A.3.6 SEM

CNC-CNT 0.05 %

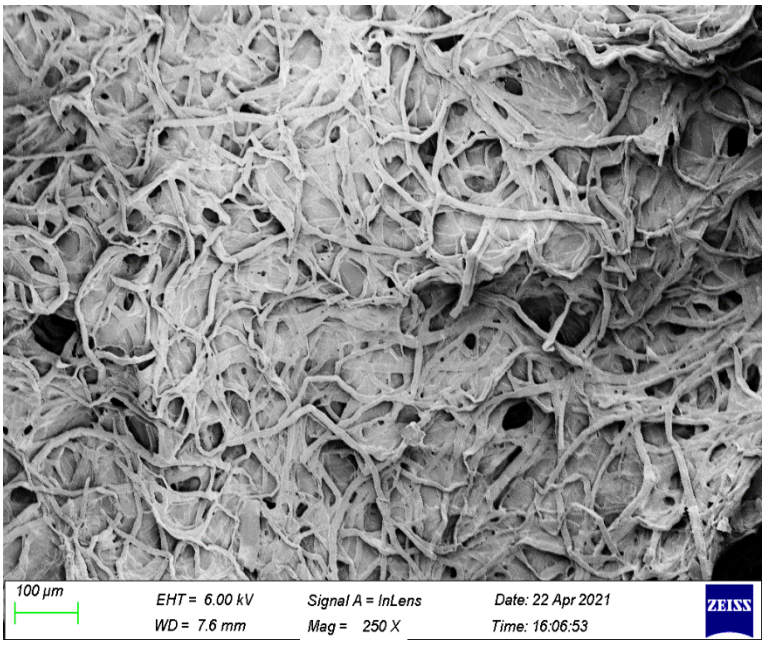



**Figure A.3.6.1 Image of CNC with 0.05% CNT**

CNC-CNT 0.075%

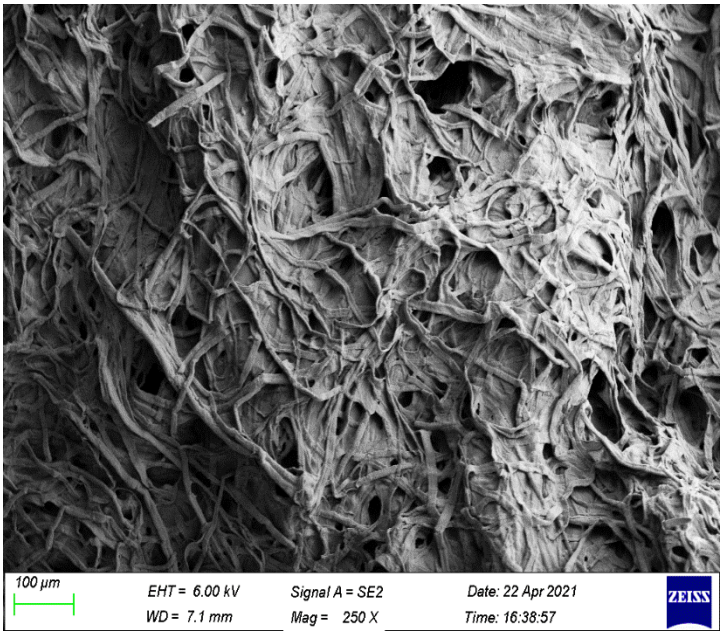



**Figure A.3.6.2 Image of CNC with 0.075% CNT**

CNC-CNT 0.14 %

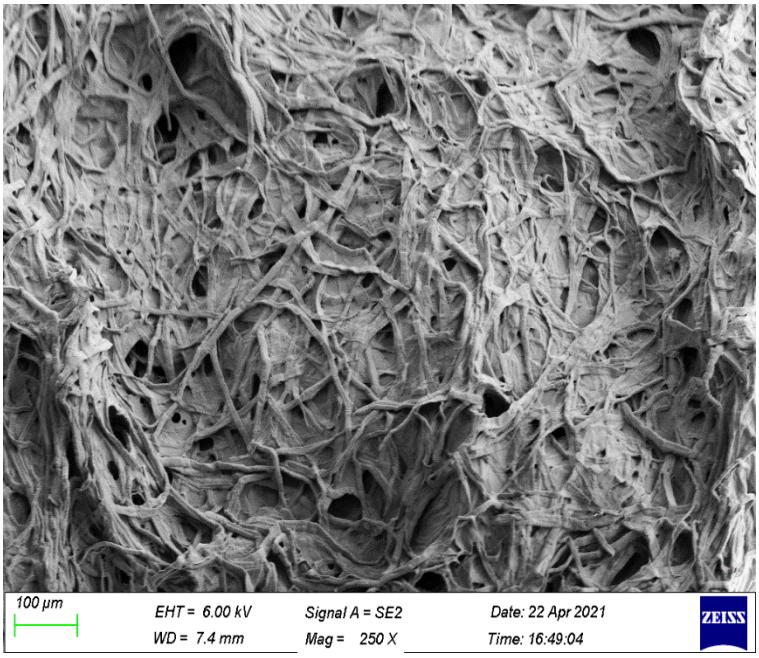



**Figure A.3.6.3 Image of CNC with 0.14% CNT**

CNC-CNT 0.25 %

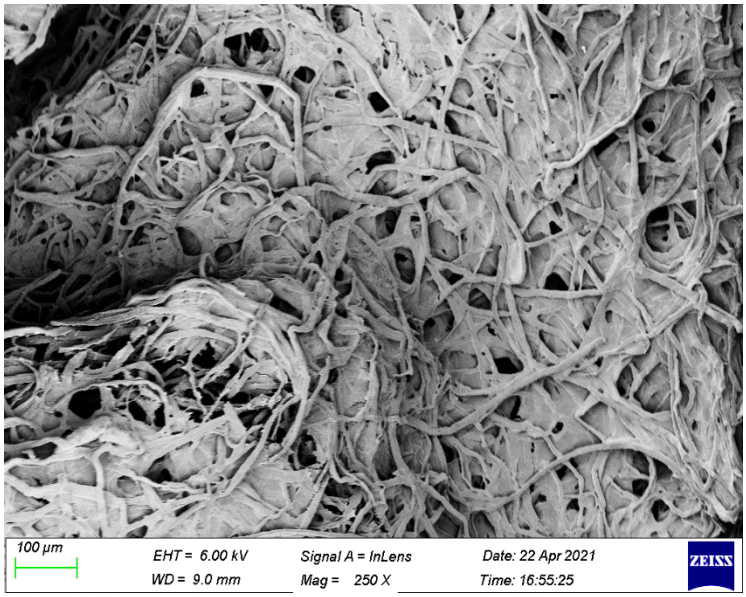



**Figure A.3.6.4 Image of CNC with 0.25% CNT**

CNC-CNT 0.75%

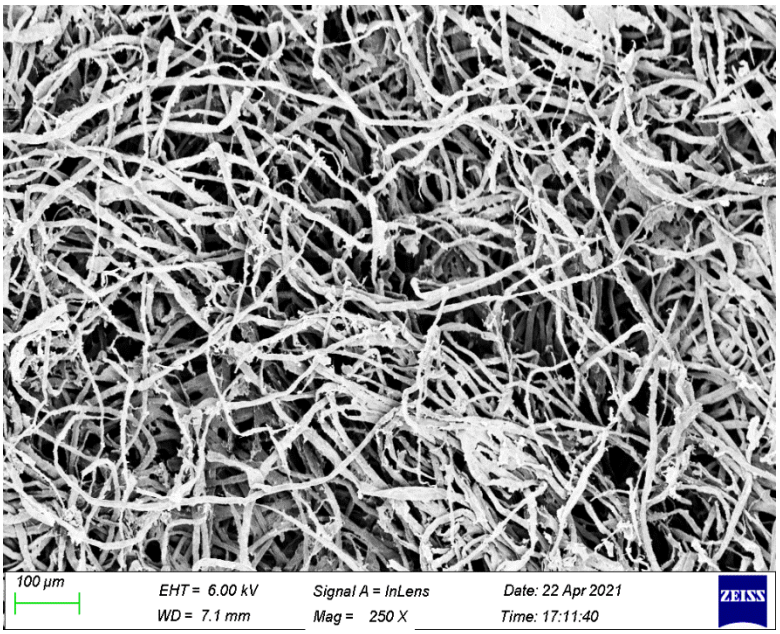



**Figure A.3.6.5 Image of CNC with 0.75% CNT**